CAPITAL UNIVERSITY OF SCIENCE AND TECHNOLOGY, ISLAMABAD

Assessment of Dam Breach Parameters Under Climate Change - A Case Study in Balochistan

by

Muhammad Umer Zia

A thesis submitted in partial fulfillment for the degree of Master of Science

in the

Faculty of Engineering
Department of Civil Engineering

2025

I dedicate this thesis to my beloved family, whose unwavering love, encouragement, and support have been the foundation of my strength and perseverance throughout this journey. To my professors and mentors, whose invaluable guidance, knowledge, and belief in my potential have profoundly shaped my academic and personal growth, thank you for inspiring me to strive for excellence.

This work is also dedicated to the cause of building a brighter future, one driven by knowledge, innovation, and the shared hope of creating a better world for generations to come. May this effort serve as a small step toward that vision.

CERTIFICATE OF APPROVAL

Assessment of Dam Breach Parameters Under Climate Change - A Case Study in Balochistan

by

Muhammad Umer Zia

Registration No: (MCE223003)

THESIS EXAMINING COMMITTEE

S. No.	Examiner	Name	Organization
(a)	External Examiner	Dr. Naeem Ejaz	UET, Taxila
(b)	Internal Examiner	Dr. M. Usman Farooqi	CUST, Islamabad
(c)	Supervisor	Dr. Ishtiaq Hassan	CUST, Islamabad

Dr. Ishtiaq Hassan
Thesis Supervisor
July, 2025

Dr. Majid Ali
Head
Dept. of Civil Engineering
July, 2025

Dr. Imtiaz Ahmad Taj
Dean
Faculty of Engineering
July, 2025

Author's Declaration

I, **Muhammad Umer Zia,** hereby state that my MS thesis titled **Assessment of Dam Breach Parameters Under Climate Change - A Case Study in Balochistan** is my own work and has not been submitted previously by me for taking any degree from Capital University of Science and Technology, Islamabad or anywhere else in the country/abroad.

At any time if my statement is found to be incorrect even after my graduation, the University has the right to withdraw my MS Degree.

(Muhammad Umer Zia)

Registration No: (MCE223003)

Plagiarism Undertaking

I solemnly declare that research work presented in this thesis titled **Assessment of Dam Breach Parameters Under Climate Change - A Case Study in Balochistan** is exclusively my research work with no remarkable contribution from any other individual. Small contribution/help wherever taken has been acknowledged and that complete thesis has been written by me.

I understand the zero tolerance policy of the Higher Education Commission and CUST towards plagiarism. Therefore, I as an author of the above titled thesis declare that no part of my thesis has been plagiarized and any material used as reference is properly cited.

I undertake that if I am found guilty of any formal plagiarism in the above titled thesis even after award of MS Degree, the University reserves the right to withdraw/revoke my MS degree and that HEC and the University have the right to publish my name on the HEC/University website on which names of students are placed who submitted plagiarized work.

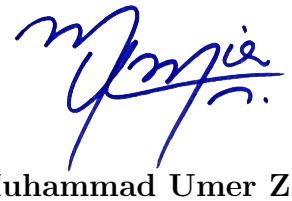

(Muhammad Umer Zia)

Registration No: (MCE223003)

Acknowledgement

I would like to express my deepest gratitude to all those who made this thesis possible. First and foremost, I extend my heartfelt thanks to my family especially my Father, **Mr. Zia-Ul Haq Dar** for their endless encouragement, patience, and unwavering belief in me. Their emotional support and constant motivation have been pivotal in overcoming the challenges faced during this journey.

I am profoundly grateful to my professors and mentors, whose expert guidance, thoughtful feedback, and encouragement have provided clarity and direction in my research. Their dedication to academic excellence and their willingness to share knowledge have greatly enriched my learning experience. Special thanks to **Engr. Prof. Dr. Ishtiaq Hassan**, whose insightful suggestions and personal guidance were essential in shaping the final outcome of this study.

I also wish to acknowledge the invaluable support of my friends and colleagues, who provided both intellectual stimulation and moments of much-needed relief. Their camaraderie and willingness to lend a helping hand during difficult times made the process more manageable.

Additionally, I extend my sincere appreciation to the staff and administrative personnel who facilitated access to essential resources and ensured the smooth progression of my research work. Without their assistance, many logistical hurdles would have remained insurmountable.

Finally, I am deeply thankful to every individual, directly or indirectly, who contributed to this thesis. Whether through inspiring conversations, technical support, or simply offering words of encouragement, your contributions have left an indelible mark on my work. This thesis stands as a testament to the collective effort, support, and belief of all those who accompanied me on this journey.

Muhammad Umer Zia

Abstract

Global warming has significantly intensified climate change across the globe, leading to more frequent and severe hydrometeorological events. Pakistan, due to its diverse topography and shifting climatic patterns, has become increasingly susceptible to extreme flooding, including riverine, flash, and urban floods. These recurrent flood events have resulted in substantial damage to agricultural lands, infrastructure, and human settlements, causing economic losses worth billions of rupees annually. The escalating trend in flood frequency and magnitude underscores the urgent need for comprehensive flood risk assessment and climate-resilient water infrastructure planning.

Overtopping of dams, especially in earthen dams, is a major dam failure resulting in dam breach and devastation in the downstream side of the dam. The problem is more severe because of climate changes resulting in extreme weather events followed by flash flood more than the design considerations. In case of absence of climate and flow data, GCMs are considered as an appropriate tool for doing analysis but they also need to be validated through statistical methods such as Delta method. Selection of GCMs is based on certain directions e.g., their resolution or their capabilities to represent the climate conditions. Gumbel method is applied to perform frequency analysis based on annual peaks and once frequency data is available, flows could be determined using tools such as HEC-HMS. In order to do breach analysis, HEC-RAS has the capability to model the scenarios (present or future).

Balochistan is one of the main provinces of Pakistan where dams are built to fulfil agriculture and domestic needs. This study assesses dam breach risks under historical and future climate scenarios using GCMs data downscaled using nearest-neigbour method and validation done by Delta method. Two scenarios i.e., SSP 2-4.5 and SSP 5-8.5, have been applied to simulate flows for 100 and 200-year return periods, using HEC-HMS. Whereas HEC-RAS is used for breach modeling.

Rainfall frequency analysis reveals increased precipitation in future climates. Under SSP2-4.5, rainfall ranges from 4.18 inches (100-year) to 4.68 inches (200-year),

while SSP 5-8.5 projects 4.50-5.01 inches. Corresponding peak inflows rise significantly: 47,464.6 and 57,039 cusecs (SSP2-4.5), and 56,130.0 and 66,998.9 cusecs (SSP5-8.5), compared to historical values.

Before the breach, both water levels stay steady. Once the breach begins, they rise quicklyshowing fast emptying of the reservoir and the start of a flood wave. In historical cases, the headwater peaks at 1711.7 m (100-year) and 1713.03 m (200-year), while tailwater reaches 1705.27 m and 1705.61 m. In future scenarios, these levels rise higher: SSP2-4.5 reaches 1713.39 m (100-year), while SSP5-8.5 reaches 1713.7 m (100-year) and 1714.87 m (200-year). Tailwater levels also increase under future climate conditions.

Simulations indicate a more rapid development of breach under future climate scenarios. During the 2022 flood event, the observed breach width reached 151 meters over an unknown time span (not one hour and may be after many hours). In projected scenarios, carried out during 1st hour, breach widths expand significantly reaching 94.56 meters and 136.64 meters under SSP2-4.5, and 104.64 meters and 155 meters under SSP 5-8.5 highlighting the increased risk of rapid dam failure associated with intensified flooding due to climate change. Peak breach velocities also increase from 2.24 - 2.41 m/s (historical) to 2.47 - 2.75 m/s (SSP 2-4.5), and up to 3.22 - 3.81 m/s (SSP 5-8.5) indicating more energetic flood waves. Similarly, breach discharges, for 100- and 200-year return period respectively, rise from 848.22 and 1,034.93 cumec (historical) to 1,301.78 and 1,368.32 cumec (SSP 2-4.5), and 1,335.82 and 1,597.86 cumec (SSP 5-8.5).

Downstream flood risk projections show increasing village inundation due to dam breach under future climate scenarios. For the 100-year return period, 13 villages will be inundated under SSP2-4.5 (flood depths: 0.15-6.70 m), 16 villages under SSP5-8.5 (0.19-6.91 m), and 8 villages under historic conditions. For the 200-year return period, 16 villages will be affected under SSP2-4.5, 18 under SSP5-8.5, and 10 under historic conditions. The highest projected flood depth is 6.81 m at Muhammad Qadir village under SSP2-4.5 (200-year return), indicating escalating flood hazards with climate change.

This study highlights the intensifying risk of dam failures under climate change, calling for climate-resilient spillway designs, reinforced embankments, and robust early warning systems. The integrated modeling approach offers critical guidance for improving dam safety and flood management in Balochistan.

Keywords: Climate Change, Global Warming, Dam breach, climate change, SSP 2-4.5, SSP 5-8.5, HEC-RAS, HEC-HMS, Breach width, peak discharge, flood risk, Balochistan, Headwater, Tailwater

Contents

List of Figures

List of Tables

Abbreviations and Symbols

1-D	One Dimensional
2-D	Two Dimensional
CMS	Cubic Meter Per Second
CN	Curve Number
CMIP-6	Coupled Model Intercomparison Project Phase 6
DEM	Digital Elevation Model
EAP	Emergency Action Plan
FFA	Flood Frequency Analysis
FEMA	Federal Emergency Management Agency
GEV	Generalized Extreme Value
GHG	Greenhouse Gases
GIS	Geographical Information System
GCM	Global Climate Model
HD	Height of Dam
HEC-HMS	Hydrologic Engineering Center Hydrologic Modeling System
HEC-RAS	Hydrologic Engineering Center River Analysis System
HW	Head Water
ICOLD	International Commission on Large Dams
IPCC	Intergovernmental Panel on Climate Change
LP(III)	Log-Pearson Type 3
NWS	National Weather Service
PAR	Population at Risk

PCRA	Probabilistic Risk Assessment
PMP	Probable Maximum Precipitation
PMD	Pakistan Meteorological Department
PMF	Probable Maximum Flood
PVC	Polyvinyl Chloride
RCP	Representative Concentration Pathways
SCS	Soil Conservation Service
SRTM	Shuttle Radar Topography Mission
SSP	Shared Socioeconomic Pathways
TC	Time-of-Concentration
TW	Tailwater
UAVs	Unmanned Aerial Vehicles
USACE	United States Army Corps of Engineers
USBR	United States Bureau of Reclamation
USDA	United States Department of Agriculture
UTM	Universal Transverse Mercator
VW	Reservoir Volume
WGS	World Geodetic System

Chapter 1

Introduction

1.1 General

Pakistan is a flood-prone country and one of the ten countries most affected by climate change worldwide. In April-June 2022, it suffered an unprecedented intense heat wave followed by a long monsoon that lasted until September and dumped a record amount of rain across the country. Pakistan is experiencing its worst floods in a century, with glacial lake bursting, river-breaking banks, flash flooding, and landslides. In the wake of rising prices at the global level, Pakistan faced significant economic challenges even before recent floods. These devastating floods have caused further economic hardships in the country. More than half of all districts in the country have officially declared calamity. As a result of these floods, 1,731 people died, 12,867 were injured, and over 2 million houses were destroyed or damaged, affecting the lives of 33 million people across the country. The provinces of Sindh and Balochistan experienced unprecedented monsoon rainfall during the summer of 2022, leading to catastrophic flooding. In July 2022, Sindh received 625% more rainfall than its 30-year average, while Balochistan saw a 501% increase. In August 2022, the rainfall further exceeded the climatological mean, with Sindh experiencing a 726% increase and Balochistan a 590% rise. These extreme rainfall events resulted in widespread flooding, affecting over 80% of the total area in both provinces causing substantial damage to the lives, infrastructure, and livelihoods of the affected population. The floods cause damage to

hundred thousand acres of fertile agricultural lands and standing crops and affect adjoining populations with monetary loss in billions of rupees almost every year. Major direct flood damage is caused to agricultural lands, standing crops, urban and rural populations, besides, other private and public property located near the banks of rivers [1], [2], [3], [4], [5], [6], [7].

The 2022 floods in Pakistan, exacerbated by climate change, led to a severe humanitarian crisis. Over 33 million people were affected, with 1,739 fatalities reported between June and November. The disaster caused significant damage to housing, with 897,014 houses fully destroyed and 1.391 million partially damaged, leaving over 2.1 million people home. Livelihoods were heavily impacted, as more than 1,164,270 livestock perished, a critical source of sustenance for many families [2], [4], [8].

Historically, from 1950 to 2022, Pakistan has experienced 28 significant flood events, leading to major economic and human losses. The total direct losses from these floods are estimated at USD 68.169 billion, with 15,200 lives lost.nThese flooding events broke the previous records not only for rainfall and discharge but also for damage to life and property. This alarming situation reveals that it may continue in the coming years with more severity. The key factor of flooding is intense rainfall (Cloud Burst) and rapid glacier melting during the summer season due to climatic change conditions in the region. Considering this disastrous situation, it is crucial to give attention to flood risk management [1], [3], [9].

Dams are hydraulic infrastructure that have several purposes, such as irrigation, hydropower, water supply, flood control, recreation, fish breeding and navigation. However, their failure or malfunctioning can pose a threat to downstream communities, and thus, their safety is paramount to public protection and economic security. The construction of dams is perhaps the best method for safeguarding sustainable water supply and overcoming the growing populations rising water demand. Embankment dams are subject to possible failure from either overtopping or piping which erodes a breach through the dam. The breach formation is gradual with respect to time and width. The majority of embankment dam

failures are generally the result of inadequate design, poor construction methods, deteriorated pipe, Hydraulic fractures, or significant environmental occurrence [10], [11], [12], [13].

A breach in a dam can be defined as any opening in a dam that leads the dam to fail and water behind the dam to propagate downstream rapidly. The flood hydrograph resulting from a breach differs significantly from that produced by rainfall, attaining a higher peak discharge and shorter time to peak [14], [15].

The Malgagai Dam was constructed in 2016, with its spillway designed to handle a discharge of 544 cubic meters per second (19,200 cusecs) and a width of 36.58 meters (120 feet). However, during the 2022 flood, the flow reached approximately 1,330.90 cubic meters per second (47,000 cusecs), far exceeding the dam's design capacity. This led to significant damage to both the spillway structure and the dam body. Additionally, residents had constructed several bunds upstream of the dam, which were also breached during the 2022 flooding, which had further intensified the flood discharge on the dam [16], [17].

FIGURE 1.1: Breached Section of the Malgagai dam

The salient features of the existing Dam are as follows:

TABLE 1.1: Salient features of existing dam and spillway. Source: (Irrigation Department, Balochistan)

General Information	
Dam Body	
Type	Modified Homogeneous Earthfill Dam
Length	1517 m (4978 ft)
Top Width	6.096 m (20.0 ft)
Maximum Height	14.3 m (47 ft)
Upstream Slope	3 H: 1 V
Downstream Slope	2.5 H: 1 V
Upstream Slope Protection Thickness	0.45 m (1.476 ft)
Downstream Slope Protection Thickness	0.30 m (0.984 ft)
Component 2: Spillway and Stilling Basin	
A. Spillway and Reservoir	
Type of Spillway	Sloping baffled Apron
Side Walls Height	5.20 m (17.06 ft)
Location	left side abutment
Design Capacity	544 cumecs (19,200 cusecs) for 100 years R. P
Width of Spillway	36.58 m (120 ft)
B. Outlet Structure	
Intake type and size	Sump arrangement with vertical perforated pipe shrouded in coarse aggregates
Outlet Conduit	PVC Pipe (Dia 0.137 m) (0.45 ft)
Energy Dissipation	Main hole and Valve Arrangement

1.2 Problem Statement

Global warming is accelerating climate change, leading to a noticeable rise in extreme weather events worldwide, particularly floods and droughts. One of the most pressing consequences of climate change is the increased intensity and frequency of floods, which are affecting vulnerable regions across the globe. In Pakistan, especially in the province of Balochistan, the impacts of climate change have become increasingly evident in recent years. The region has experienced recurrent episodes of extreme flash floods, which have not only devastated communities and agricultural lands but also placed enormous pressure on the regions hydraulic infrastructure. Among these, earthen dams which are widely used for irrigation, water storage, and flood control have proven particularly susceptible to damage and failure.

Earthen dams are inherently more vulnerable to hydrological stresses due to their construction materials and design. Unlike concrete or composite structures, earthen

dams rely on compacted soil and rock, which can be quickly eroded or destabilized during overtopping or internal seepage. Overtopping, in particular, is a leading cause of dam failure and is directly influenced by extreme rainfall and inadequate spillway capacity. In the context of Balochistan, where rainfall patterns have become more erratic and intense, the design assumptions based on historical climate data are no longer sufficient to ensure dam safety.

Therefore, there is a pressing need to reassess the structural and operational safety of earthen dams in light of climate change induced flood hazards. Understanding how extreme precipitation and flood magnitudes are likely to evolve is essential for designing effective risk mitigation strategies. This includes evaluating potential breach parameters, simulating dam failure scenarios and analyzing downstream flood propagation using reliable hydrological and hydraulic modeling techniques. Such assessments are vital not only for enhancing dam safety but also for protecting downstream populations and ensuring sustainable water management in vulnerable regions like Balochistan.

"Balochistan is dependent on dams to meet its agriculture and other daily needs and has developed a network of dams. Majority of dams have been experiencing issues such as dam breaches due to intensified rainfall causing flash floods. Hence, there is need to do hydraulic modelling based on future projections to mitigate dam breach issues to ensure safe operations during the 21st century."

1.3 Research Questions

Following are the research questions which are to be answered in this research study:

- What were the key breach characteristics of an Earthen dam during its 2022 overtopping failure in Balochistan?
- How did the overtopping event influence the water surface profile in the downstream channel under unsteady flow conditions?

- How do the actual breach parameters of Earthen Dam compared with those recommended in standard dam design manuals?
- Can breach parameters be adapted to better reflect the specific geographical, hydrological, and flood conditions of Balochistan?

1.4 Research Gap

- No prior dam breach analysis has been conducted in study area, despite recent failures in 2022.
- This research fills the gap by analyzing an actual dam failure event, but under certain limitations, and then assessing climate-adaptive breach parameters for minimizing the severity of flood risks in the region.

1.5 Objectives of Research

To assess impact of Climate change on breach of an earthen dam by using GCMs data and standard design procedures in the study area experiencing flash floods

1.6 Scope of Study

The research focuses on dam breach analysis for an earthen dam under a single mode of failure such as overtopping, which is a common issue in embankment dams. The scope of study for this research study comprises of :

- Selection of suitable Global Climate Models (GCMs) and climate change scenarios based on the IPCCs 6th Assessment report.
- Bias correction and analysis of simulated future climate data under SSP 2-4.5 and SSP 5-8.5 scenarios.
- Developing a flood frequency model using HEC-HMS to simulate flood risks under both current and future conditions.

- Developing a hydraulic model using HEC-RAS for Dam breach analysis and downstream flood risk assessment to analyze the potential impacts of dam failure on downstream areas.

1.7 Study Limitations

- This study is specific to an earthen dam in Balochistan and its associated flood risks. The findings and recommendations may not be directly applicable to other dams.
- Variations in dam design, topography, and local climate conditions could result in different risk profiles and breach dynamics for other dams. Therefore, while the methodology and models used in this study provide valuable insights, they must be tailored to the unique characteristics of each dam for broader applicability.
- This study is purely based on GCMs data, and no gauge data (of discharge) is available.
- Only one Climate Station data i.e. Muslim Bagh climate station was used in this research study and no other station data is available.
- The baseline period for the MET and GCM data is 1990-2014. Despite efforts, meteorological department data was not available during 2015 - 2024. Future projections are divided into three 25-year time periods: 2025-2050, 2051-2075, and 2076-2100.

1.8 Thesis Outline

The thesis contains five chapters. These are:

Chapter 1: This chapter provides an overview of the Malgagai Dam, outlining its significance in water resource management and flood control. It defines the problem statement, focusing on dam safety concerns and potential breach scenarios.

The research objectives are clearly stated, aiming to assess dam break parameters and downstream flood risks. The scope of the study establishes its geographical and methodological framework, while the significance highlights its contribution to dam safety, flood risk mitigation, and climate change adaptation strategies

Chapter 2: This chapter presents a comprehensive review of existing studies on earthen dams, focusing on failure mechanisms and historical dam breach events. It examines past and recent research on dam breaches, emphasizing the influence of climate change on failure probabilities. Various probabilistic methods for estimating dam breach parameters are explored, along with the application of HEC-RAS for breach modeling. Additionally, the chapter discusses hazard classification systems and their categories, providing a foundation for assessing dam failure risks and flood impacts

Chapter 3: This chapter outlines the study area, data sources, and research methodology. It provides a concise overview of the approach, including data collection, watershed characteristics, and hydrological modeling using HEC-HMS. Various dam break methods and breach parameter estimation techniques are explored, followed by a detailed methodology for HEC-RAS modeling. The chapter concludes with a summary of key findings, setting the foundation for subsequent analysis and results

Chapter 4: This chapter presents the findings and analysis of the research, covering key aspects such as rainfall frequency results, inflow hydrographs, and breach width evaluation across different return periods and climate scenarios. It further includes breach velocity and flow analysis, water surface elevation trends, and total flow variations under different conditions. Additionally, the downstream flood risk assessment is conducted for both 100-year and 200-year return periods across multiple scenarios, with a specialized assessment using the Froehlich formula to evaluate breach dynamics and flood impact.

Chapter 5: This chapter provides a comprehensive summary of the studys key findings, highlighting the major conclusions drawn from the analysis. It also addresses the limitations encountered during the research, including data constraints, modeling assumptions, and uncertainties associated with dam breach simulations.

Additionally, the chapter discusses the broader benefits of the study, emphasizing its significance in flood risk management, dam safety assessment, and climate change adaptation. Finally, future recommendations are proposed to enhance dam breach modeling, improve flood mitigation strategies, and guide further research in the field of dam safety and hydrological modeling.

Chapter 2

Literature Review

2.1 General

Dams play a vital role in water resource management by providing numerous benefits, including a reliable water supply for drinking, irrigation, industrial use, and recreation. Additionally, dams are essential for flood control, hydropower generation, and in some cases, facilitating navigation. However, to ensure continued service and safety, dams require regular maintenance, monitoring, and rehabilitation when necessary [18], [19].

Dams are engineered structures designed to store, control, or divert water by creating an upstream reservoir. While they offer significant advantages, the failure of a dam can lead to catastrophic consequences. Dam failures can manifest in different forms, such as structural collapse or breaches, and often result in downstream flooding that poses a serious threat to lives, infrastructure, and the environment. The risk of dam failure is elevated when large volumes of water are stored, and the failure mechanisms are typically linked to several factors [20], [21].

2.2 Types of Embankment Dam

The two principal types of embankment dams are earth and rockfill dams. Depending on the predominant fill material used. Some generalized sections of earth

dams showing typical zoning for different types and quantities of fill materials and various methods for controlling seepage are presented. When practically only one impervious material is available and the height of the dam is relatively low, a homogeneous dam with internal drain may be used [22], [23], [24]. The inclined drain serves to prevent the downstream slope from becoming saturated and susceptible to piping and/or slope failure and to intercept and prevent piping through any horizontal cracks traversing the width of the embankment. Earth dams with impervious cores, are constructed when local borrow materials do not provide adequate quantities of impervious material [25]. A vertical core located near the center of the dam is preferred over an inclined upstream core because the former provides higher contact pressure between the core and foundation to prevent leakage, greater stability under earthquake loading, and better access for remedial seepage control [26], [27]. An inclined upstream core allows the downstream portion of the embankment to be placed first and the core later and reduces the possibility of hydraulic fracturing. However, for high dams in steepwalled canyons the overriding consideration is the abutment topography. The objective is to fit the core to the topography in such a way to avoid divergence, abrupt topographic discontinuities, and serious geologic defects [28], [29]. In Pervious foundations, seepage control is necessary to prevent excessive uplift pressures and piping through the foundation. The methods for control of under seepage in dam foundations are horizontal drains, cutoffs (compacted backfill trenches, slurry walls, and concrete walls), upstream impervious blankets, downstream seepage berms, toe drains, and relief wells. Rockfill dams may be economical due to large quantities of rock available from required excavation and/or nearby borrow sources, wet climate and/or short construction season prevail, ability to place rock fill in freezing climates, and ability to conduct foundation grouting with simultaneous placement of rock fill for sloping core and decked dams [22], [23], [27], [30].

2.3 Consequences of Dam Breaks

In the event of a dam break, the energy stored in the reservoir can be rapidly released, causing sudden and severe downstream flooding. Such flooding is often unpredictable and can lead to significant loss of life, extensive property damage, and

the disruption of essential infrastructure. The magnitude of these impacts underscores the critical importance of proper dam design, maintenance, and emergency preparedness [31], [32], [33].

This research on Earthen Dam highlights the need to assess potential dam breach scenarios, focusing on overtopping as a primary mode of failure. By evaluating flood risks downstream and identifying critical failure thresholds, this study aims to contribute to the development of effective risk mitigation strategies, including emergency action plans and early warning systems tailored to the specific conditions of Balochistan [34], [35].

2.4 Dam Failure

Between 1946 and 1955, a total of 12 major dam failures were recorded, coinciding with the construction of over 2,000 dams worldwide. Similarly, from 1956 to 1965, 24 dam failures were documented, during which more than 2,500 new dams were constructed globally. While dam failures are not uncommon, the mode of failure varies depending on the dam type and design characteristics. Understanding these failure mechanisms is critical for improving dam safety and mitigating potential risks associated with future dam operations [36], [37], [38].

2.4.1 Cause of Failure of Earth Dam

Earth dams are subjected to mainly three ways of failures hydraulic failure may occur due to one or more of the following causes: overtopping, erosion of the upstream face, erosion of the downstream face, erosion of the downstream toe, and frost action. Seepage failure can happen due to piping through the dam, piping through the foundation, conduit leakage, or sloughing of the downstream toe. Structural failures are generally shear failures leading to sliding of the embankment or the foundation, and they consist of slides in the embankment, foundation slides, liquefaction slides, failure by spreading, failure due to earthquakes, failure due to holes caused by burrowing animals, and failure due to holes caused by the leaching of water-soluble salts [39].

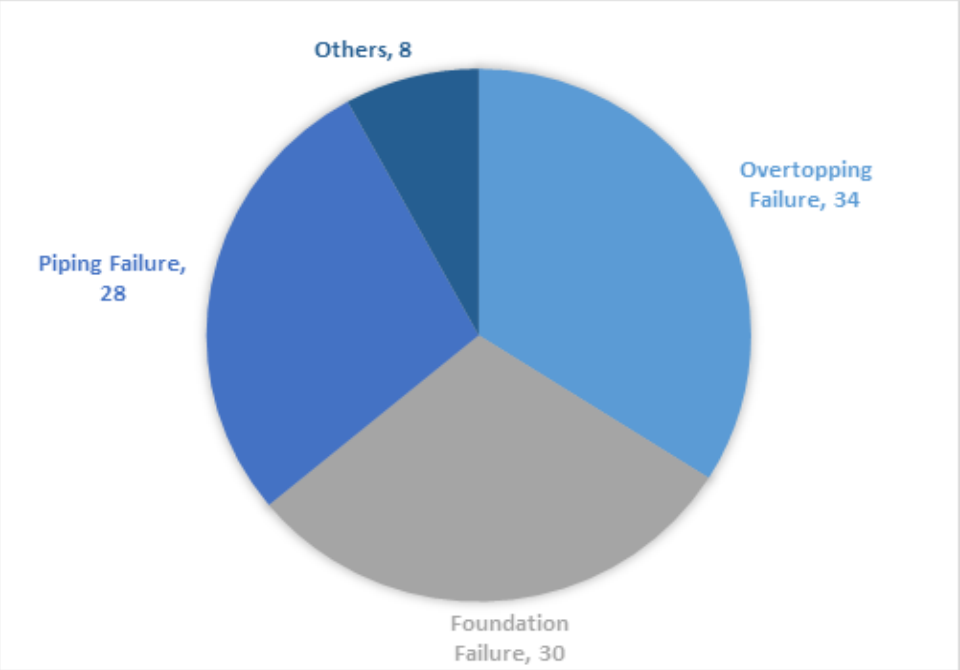

FIGURE 2.1: Modes of failure in percentage [41]

The pie chart illustrates the distribution of dam failure causes based on recorded data. It categorizes the failures into four primary modes: overtopping, foundation failure, piping, and other causes. The percentages indicate the proportion of dam failures attributed to each specific mode [41].

I. Overtopping (34%) Overtopping is the leading cause of dam failures, accounting for 34% of the cases. This typically occurs when the water level in the reservoir exceeds the dam's capacity due to inadequate spillway design or extreme inflow events, leading to overflow and subsequent erosion of the dam crest and downstream slope [40].

II. Foundation Failure (30%) Foundation failure contributes to 30% of dam failures. It arises when the foundation material beneath the dam is unable to support the load, resulting in instability or collapse. Common causes include weak geological formations, seepage, and inadequate compaction during construction [41].

III. Piping Failure (28%) Piping accounts for 28% of the recorded failures. This mode of failure involves internal erosion caused by seepage through the dam or its foundation. Over time, the seepage can enlarge voids, eventually leading to structural collapse [39], [41].

IV. Other Causes (8%) The remaining 8% of failures fall under miscellaneous causes, including factors such as seismic activity, operational errors, and extreme weather conditions. Although less frequent, these causes can have severe consequences depending on the dams design and location [39], [40], [41].

2.5 Historical and Recent Case Studies of Dam Breaches

Case studies of dam failures, particularly those caused by overtopping and piping, provide important insights into the vulnerabilities of dams under extreme conditions. Both overtopping and piping are significant failure mechanisms that are often exacerbated by extreme rainfall, poor maintenance, or improper design. Here, we present some notable case studies that highlight the consequences of these failure mechanisms and lessons learned from the events [42], [43].

2.5.1 Banqiao Dam Collapse (1975) - Overtopping and Structural Failure

The Banqiao Dam, located in China, is one of the most devastating dam failures in history, and its collapse was due to a combination of overtopping and structural failure. The dam was overwhelmed by a massive flood caused by Typhoon Nina, which led to its overtopping. The intense floodwaters eroded the dams embankment, triggering the catastrophic breach. Despite the failure of the dam's spillway, it was the inability of the dam to cope with the extreme water flow that led to the breach. The flood that followed caused tens of thousands of deaths and widespread devastation [44].

2.5.2 Teton Dam Failure (1976) - Overtopping Failure

Although the primary cause of the Teton Dam failure was seepage and piping, overtopping also played a role in exacerbating the breach. The Teton Dam, located in Idaho, USA, failed after heavy rainfall caused the reservoir to overflow.

The spillway design was inadequate to handle the massive inflow, which led to overtopping. As the dam began to erode, the structure's integrity was further compromised, contributing to the eventual breach. The flood caused by the failure resulted in extensive damage downstream [45].

2.5.3 Sardar Sarovar Dam (2006) - Overtopping Incident

In India, the Sardar Sarovar Dam faced significant overtopping risk in 2006 after a period of excessive rainfall. The spillway, designed to manage overflow, was insufficient for the massive volume of water, leading to a dangerous situation. Although the dam did not breach, the incident highlighted the importance of ensuring that spillways are designed to handle extreme weather events and the necessity of implementing more stringent monitoring during high-flow conditions [46].

2.5.4 Piedras Negras Dam (2007) - Overtopping and Erosion

In 2007, the Piedras Negras Dam in Mexico experienced overtopping during a period of extreme rainfall. The dam, designed to regulate water levels for agriculture, was not equipped to handle such intense events. The overtopping led to erosion of the dam's embankment, and eventually, a breach occurred. This failure was a critical event for dam safety officials, highlighting the importance of maintaining appropriate freeboard and spillway capacity to manage extreme flood conditions. Recent studies have pointed to the need for better flood routing and hazard assessment in similar dams [47].

2.5.5 Lower Walnut Creek Dam Failure (2008)

The Lower Walnut Creek Dam in Texas, USA, failed in 2008, causing significant flooding in downstream areas. [48] revisited this breach to better understand the

role of internal erosion and seepage in dam failures. Their findings underscored the need for continuous monitoring of internal dam conditions, particularly in older embankment dams. The study also demonstrated the value of using real-time sensors to detect seepage and prevent potential failures before they escalate. The use of advanced computational models to simulate the breach event helped refine the understanding of breach progression and flood propagation [48].

2.5.6 Felizbiri Dam (2014) - Overtopping and Structural Damage

The Felizbiri Dam in Brazil failed after overtopping during an intense storm event. The dam, built on a river with seasonal high flows, was not designed to cope with the extreme rainfall of 2014. Overtopping caused significant erosion, and although the dam was not completely breached, the resulting damage led to a partial collapse of the spillway [49].

2.5.7 Dahuofang Dam (2016) - Piping and Seepage

The Dahuofang Dam, located in China, suffered significant piping issues in 2016, leading to concerns over its stability. During heavy rainfall, seepage water from the dams foundation eroded the soil, creating a channel that gradually enlarged and posed a serious threat to the dams integrity. Researches emphasized the role of dam foundation conditions and the need for continuous monitoring of seepage. Their study also proposed strategies for improving dam safety through early detection technologies [50].

2.5.8 Oroville Dam Spillway Crisis (2017) - Overtopping and Spillway Failure

The Oroville Dam crisis in California, while not a breach per se, was caused by the failure of the main spillway due to overtopping. The situation was exacerbated by heavy rainfall during the winter of 2017, which resulted in a rapid increase in

water levels. The spillway was damaged as a result of extreme flows, leading to the temporary evacuation of nearly 200,000 people [51].

2.5.9 Whaley Bridge Dam Failure (2019) - Piping and Overtopping Threat

In the UK, the 2019 near-failure of the Whaley Bridge Dam due to heavy rainfall and erosion of the spillway brought dam safety concerns to the forefront. Researchers have assessed the failure mechanisms and highlighted the role of emergency response efforts, which were critical in preventing a disaster. Their study focused on rapid response systems, such as the emergency evacuation of nearby residents and the monitoring of dam integrity through drones and satellite imagery, setting an example for future dam breach risk management practices [52].

2.5.10 Xinfengjiang Dam Breach Simulation (2020)

In China, the Xinfengjiang Dam was studied by Zhang et al. (2020) to model a hypothetical breach under extreme rainfall scenarios. The researchers used advanced breach modeling tools like HEC-RAS and LISFLOOD-FP to simulate flood inundation patterns. This study provided valuable insights into flood propagation and the downstream consequences of dam failures in densely populated regions, highlighting the critical importance of floodplain mapping and emergency response planning in mitigating disaster impacts [53], [54].

2.5.11 San Vicente Dam Seepage Incident (2021)

The San Vicente Dam in California experienced significant seepage problems in 2021, raising concerns about the potential for failure. Researchers analyzed the incident, focusing on the interplay between seepage and the dams structural integrity. Their findings emphasize the need for a combination of monitoring tools and rapid intervention systems to prevent similar incidents in the future. Their work also demonstrates the importance of geotechnical studies in identifying potential weaknesses before they escalate into major problems [55].

2.5.12 Pidekso Dam Break Risk Analysis and Mitigation, Wonogiri Regency, Central Java, Indonesia

The study on Pidekso Dam in Central Java, Indonesia, analyzed dam safety and flood risk management using HEC-HMS and HEC-RAS. Two failure scenarios, piping and overtopping, were modeled, with overtopping producing a higher peak discharge of 14,821 m/s compared to 8,314 m/s for piping. HEC-HMS simulated rainfall-runoff processes using precipitation data and the SCS Curve Number method, while HEC-RAS modeled downstream flood propagation to create flood inundation maps and classify affected villages into risk zones [56].

2.5.13 Dam Break Analysis: Case Study of Phukot Karnali (480 Mw) Hydroelectric Project in Nepal

The case study of the Phukot Karnali Hydroelectric Project (PKHEP) in Nepal provides critical insights into dam breach analysis and flood risk management in high-altitude regions. The 109-meter-high concrete gravity dam, with a reservoir volume of 37.00 Mm, was analyzed for potential breach scenarios using HEC-RAS and GIS tools. Two breach scenarios, complete and partial failure, were simulated using 1D unsteady flow equations, with input parameters such as breach geometry and formation time derived from guidelines by the National Weather Service (NWS), Federal Energy Regulatory Commission (FERC), and U.S. Army Corps of Engineers (USACE). The complete breach scenario resulted in a peak discharge of 91,418.15 m/s, with the flood wave traveling 232.95 km downstream, reaching critical locations like Rakham valley within 50 minutes, posing severe risks to lives and infrastructure due to velocities exceeding 10 m/s and depths over 10.5 m [57].

Flood inundation maps generated from the simulations identified high-risk zones, prioritizing areas for evacuation and emergency planning. Settlements near Rakham valley were marked for immediate evacuation due to limited escape time. The study proposed a comprehensive Emergency Action Plan (EAP), including early warning systems, evacuation plans, and relocation of settlements in high-risk areas.

It also emphasized protecting critical infrastructure such as roads and hospitals while recommending structural improvements to the dam and non-structural measures like community awareness programs [58], [59].

The findings underscore the utility of HEC-RAS and GIS tools in dam breach analysis, highlighting the importance of combining robust structural design with proactive emergency preparedness. This research provides valuable guidance for policymakers and engineers to enhance dam safety and mitigate flood risks in vulnerable regions [60], [61].

2.5.14 Dam Break Analysis Using HEC-RAS and HEC-GeoRAS: A Case Study of Hidkal Dam, Karnataka State, India

The case study of the Hidkal Dam in Karnataka, India, demonstrates a comprehensive analysis of dam breach scenarios using HEC-RAS and HEC-GeoRAS tools to predict potential downstream impacts. The study involved the simulation of breach scenarios under two failure modes: piping and overtopping. Utilizing Cartosat-1 Digital Elevation Model (DEM) data, the authors extracted river geometry and generated inundation maps to identify affected areas and populations [60], [62].

The HEC-RAS model simulated unsteady flow conditions, incorporating Probable Maximum Flood (PMF) hydrographs provided by dam authorities. For dam breach parameter estimation, empirical equations such as Froehlich (1995, 2008) and MacDonald and Langridge-Monopolis (1984) were applied. The breach parameters, including breach width, depth, and formation time, were evaluated for their sensitivity to flood hydrograph characteristics. The sensitivity analysis revealed that peak flow is significantly influenced by breach width and depth, while less sensitivity was noted for side slopes. The overtopping failure mode was found to have a greater impact compared to piping failure, with higher peak discharge (78,454.82 m/s) and inundation area (79.205 km), posing significant risks to downstream region [63], [64].
Floodplain mapping indicated that 20 downstream villages, including agricultural lands and infrastructure, would be severely affected in the event of a dam breach.

The study emphasized the importance of proper reservoir management to mitigate overtopping risks and proposed that HEC-RAS is a reliable tool for dam breach analysis and emergency response planning [65], [66].

This research highlights the critical need for detailed hydraulic modeling in dam safety assessments and underscores the importance of generating inundation maps to support disaster management strategies [67], [68].

2.5.15 Dam Break Analysis and Flood Inundation Mapping: The Case Study of Sefid Roud Dam, Iran

The case study of the Sefid-Roud Dam in Iran analyzed dam breach risks and downstream flood impacts using HEC-RAS and HEC-GeoRAS (USACE, 1997 [63], [67]. The study examined two failure scenarios: overtopping due to extreme inflow and piping from internal erosion. Breach parameters, such as width and formation time, were estimated using the Froehlich method and USACE guidelines. The overtopping scenario produced a higher peak discharge and larger inundation area compared to piping, posing significant risks to downstream communities and infrastructure [63].

Flood inundation maps identified high-risk zones and estimated damage to agricultural land, residential areas, and critical facilities. The findings emphasized the importance of early warning systems, evacuation plans, and proactive maintenance to mitigate risks. This research highlights the effectiveness of combining HEC-RAS with GIS-based tools for dam breach analysis and flood risk management, providing valuable insights for improving disaster preparedness and policy-making [69], [70].

2.6 Summary of Dam Break Case Studies: Emphasizing Climate Change Impacts

The review of various dam failure case studies highlights that overtopping is the most common cause of dam breaches. Many of these failures occurred due to extreme rainfall events, which exceeded the design capacities of spillways and

reservoirs [71], [72], [73]. The Banqiao Dam collapse (1975), one of the deadliest dam failures, was triggered by an unprecedented flood caused by Typhoon Nina, overwhelming the dams spillway and leading to a catastrophic breach [74]. Similarly, the Teton Dam failure (1976), while primarily caused by internal erosion, saw overtopping contribution to the severity of the failure due to inadequate spillway capacity [45].

The Oroville Dam Spillway Crisis (2017) in California serves as a modern example of overtopping-induced structural failure, where severe rainfall caused spillway damage, leading to a mass evacuation. The Felizbiri Dam (2014) in Brazil also suffered partial collapse due to overtopping from intense storms, highlighting the vulnerability of dams in regions experiencing changing precipitation patterns due to climate change [75], [76].

Beyond overtopping, other failures, such as the Dahuofang Dam (2016) and Whaley Bridge Dam (2019), were linked to piping and seepage, showing that internal erosion remains a secondary but significant concern (Li et al., 2020; Glover et al., 2021). However, even in these cases, heavy rainfall played a role in accelerating dam deterioration, reinforcing the argument that climate variability is increasing dam failure risks globally [77].

Recent studies, including the Pidekso Dam (2020) in Indonesia and the Phukot Karnali Hydroelectric Project (2020) in Nepal, have emphasized the role of advanced modeling tools such as HEC-RAS and HEC-HMS in simulating dam breaches and flood propagation (Morris & Fan, 1998; Froehlich, 2016). These studies underline the importance of accurate dam break analysis to assess potential inundation areas and enhance emergency response planning. The Hidkal Dam (2021) in India and the Sefid-Roud Dam (Iran) have also demonstrated the effectiveness of HEC-RAS in predicting breach evolution and flood hazard mapping, further confirming its role as a reliable tool for flood risk assessment [42], [43], [76], [77], [78], [79].

A critical pattern emerges from these case studiesthe underestimation of climate change impacts is a major factor in overtopping-related failures. Many historical dam designs do not account for the increasing intensity and frequency of extreme weather events, leading to spillway inadequacy, increased reservoir pressure, and

embankment erosion. This review demonstrates that climate change-driven extreme rainfall is a key driver of modern dam failures [80], [81].

Unlike previous research, my study specifically integrates climate change scenarios (SSP2-4.5 and SSP5-8.5) into dam break modeling, making it a unique and significant contribution to the field. By incorporating future precipitation projections into HEC-RAS simulations, my research aims to bridge the gap between traditional flood risk assessment and climate-adaptive dam safety planning. This approach will provide a more realistic and proactive strategy for managing dam failures under evolving climate conditions, ensuring that future dam infrastructure is resilient and prepared for extreme hydrological events [60], [63], [82], [83].

2.7 Impact of Climate Change on Dam Failures

Climate change is having profound and far-reaching impacts on hydrological cycles, which significantly increases the risks of dam failures. Rising global temperatures, changing precipitation patterns, and more frequent and intense extreme weather events exacerbate the vulnerabilities of dam structures and their operations. These impacts necessitate urgent action to re-evaluate and enhance dam design, maintenance, and management practices to adapt to these evolving challenges [82], [84].

One of the most evident consequences of climate change is the increased frequency and intensity of extreme rainfall events, which can overwhelm the capacity of dams and lead to overtopping. According to [85] future rainfall projections under various climate scenarios suggest a significant rise in the likelihood of dam overtopping and subsequent failure. Similarly, the Intergovernmental Panel on Climate Change (IPCC, 2021) has noted that the intensification of extreme rainfall events is directly linked to a warmer atmosphere's capacity to hold more moisture. This increased risk requires an urgent reassessment of spillway designs and flood storage capacities in reservoirs to prevent catastrophic failures during unprecedented rainfall events. Additionally, [86] highlighted that in regions prone to monsoons, such as South and Southeast Asia, the intensification of monsoon rainfall could further increase stress on aging dams, leading to higher risks of overtopping [87].

The changing timing of snowmelt, driven by rising global temperatures, is another critical factor influencing dam safety. [88] demonstrated that earlier and more rapid snowmelt events, a direct consequence of warming temperatures, can cause sudden and significant increases in reservoir inflows. This sudden surge can strain reservoir capacity, increasing the risk of overtopping and structural failure. Furthermore, [89] highlighted that these altered snowmelt patterns, combined with reduced predictability in seasonal inflows, pose severe challenges for flood management strategies, particularly for regions dependent on snow-fed river systems. These findings emphasize the need for updated hydrological models that incorporate changing snowmelt dynamics and climate variability into reservoir operation protocols [90].

Temperature rise also directly affects the structural integrity of dams particularly older ones not designed to withstand the stresses imposed by modern climatic conditions [91]. [92] found that higher temperatures accelerate the degradation of construction materials, leading to increased occurrences of internal erosion, seepage, and cracking in dam structures. Moreover, [93] pointed out that thermal stress can exacerbate the aging process of concrete and earthen dams, weakening their resilience to extreme hydrological events. Thus, adapting dam rehabilitation and maintenance programs to account for temperature-induced wear and tear is critical for ensuring the long-term safety and functionality of dams [94].

In addition to physical vulnerabilities, climate change also introduces uncertainties in operational decision-making for dam managers. [95] emphasized that traditional flood management practices often rely on historical hydrological data, which may no longer be valid in a rapidly changing climate. This disconnect can lead to suboptimal decision-making, further increasing the risks associated with dam operations. The need for real-time monitoring, predictive modeling, and flexible management strategies is now more critical than ever to mitigate these risks effectively [96].

In summary, the impacts of climate change on dam failures are multi-faceted, encompassing increased risks of overtopping due to extreme rainfall, altered snowmelt patterns leading to sudden inflows, and temperature-induced material degradation that compromises structural integrity [97]. Addressing these challenges requires a combination of updated engineering designs, advanced hydrological modeling,

real-time monitoring systems, and proactive adaptation strategies. By integrating climate-resilient approaches into dam safety and management practices, it is possible to mitigate these risks and ensure the safety of downstream communities and ecosystems [98], [99].

2.8 Dam Breach Risk Assessment Using Probabilistic Methods

Assessing the risk of dam breaches involves analyzing the likelihood of failure and the potential consequences. Probabilistic methods are widely used for this purpose, as they rely on statistical techniques to evaluate the probability of dam failure under different scenarios [100]. These methods account for various failure mechanisms, such as overtopping, internal erosion, and seepage, and calculate the likelihood of these events occurring. By combining the probabilities of multiple failure modes, probabilistic models help identify the most vulnerable dams and prioritize them for preventive measures [101], [102].

Probabilistic methods are particularly useful because they incorporate uncertainty and variability in dam failure mechanisms. For example, factors such as the intensity and duration of extreme rainfall events, reservoir water levels, and the condition of dam materials are all considered when estimating the probability of failure. This allows for a more comprehensive and realistic understanding of risks compared to deterministic approaches. Additionally, these models are often integrated with consequence assessments to provide a complete picture of dam breach risks, enabling better decision-making for emergency planning and resource allocation [103], [104], [105].

By focusing exclusively on probabilistic approaches, dam safety professionals can use these tools to develop robust risk management strategies that are adaptable to uncertain and evolving climate conditions. These methods provide valuable insights for prioritizing dam rehabilitation projects, designing emergency response plans, and reducing the likelihood of catastrophic failures [82], [84].

2.9 Dam Breach Modelling Techniques Using Hec-Ras

Dam breach modeling is a critical component of flood risk assessment, helping to predict the behavior of floodwaters following dam failure. Among the various computational tools available, HEC-RAS (Hydrologic Engineering Centers River Analysis System) is the most widely used and adaptable model for dam breach analysis, flood hazard assessment, and emergency planning. Developed by the U.S. Army Corps of Engineers (2016), HEC-RAS is specifically designed to simulate water flow through rivers, reservoirs, and floodplains during dam failure events. The model provides essential insights into flood propagation, peak discharges, flow velocities, and inundation extents, making it invaluable for risk assessments and decision-making in dam safety [103], [104], [105].

HEC-RAS incorporates both one-dimensional (1D) and two-dimensional (2D) hydraulic modeling to assess dam breaches under various failure mechanisms, including overtopping, piping failure, and structural collapse. The model requires defining key breach parameters such as breach width, depth, side slopes, and formation time, which can be derived from empirical equations, historical dam failures, or site-specific assessments. Once the breach characteristics are established, HEC-RAS simulates flood wave propagation downstream, considering factors such as terrain elevation, channel geometry, and hydraulic structures [106], [107].

In dam breach modeling, HEC-RAS is frequently used in combination with other flood simulation models to improve accuracy and reliability. Models like FLO-2D and LISFLOOD-FP complement HEC-RAS by providing detailed floodplain dynamics and overland flow assessments. FLO-2D is particularly effective in simulating urban flood inundation, while LISFLOOD-FP enhances large-scale flood modeling. By integrating multiple models, researchers can gain a more comprehensive understanding of flood behavior, improving flood risk mitigation strategies [108], [109], [110].

One of the major challenges in dam breach modeling is uncertainty in breach development and flood propagation. Factors such as breach formation time, erosion processes, and dam material properties can significantly influence flood severity. HEC-RAS allows researchers to account for these uncertainties using Monte

Carlo simulations, where multiple breach scenarios are simulated to evaluate the sensitivity of different parameters. [109] demonstrated that varying breach width and formation time in HEC-RAS significantly altered flood wave characteristics, highlighting the importance of incorporating uncertainty analysis in dam breach studies [111].

HEC-RAS has also been widely used for climate impact assessments on dam failures, particularly under different climate change scenarios. With increasing precipitation intensities and changing hydrological patterns, future dam breach studies must consider extreme weather events and their impact on flood magnitude. Researchers have emphasized the importance of integrating climate projections into dam safety assessments, ensuring that flood risk models accurately reflect future hydrological conditions. By simulating different precipitation scenarios and return periods, HEC-RAS helps engineers and decision-makers design dams and spillways that can withstand extreme flood events [112], [113].

The practical applications of HEC-RAS in dam breach modeling are extensive, from designing flood control structures and spillways to preparing emergency response plans and evacuation strategies. Flood inundation maps generated from HEC-RAS simulations provide crucial information for identifying high-risk areas, infrastructure vulnerabilities, and necessary flood mitigation measures. The flexibility of the model allows for customized breach scenarios, making it adaptable for a wide range of dam types, terrains, and hydrological conditions [114], [115].

In conclusion, HEC-RAS remains the most widely used and reliable tool for dam breach modeling, offering a comprehensive approach to simulating dam failures, flood wave propagation, and downstream flood risks. Its ability to incorporate uncertainty analysis, integrate climate projections, and work alongside other flood models makes it indispensable for dam safety assessments, emergency preparedness, and flood mitigation planning. As climate variability and extreme weather events continue to challenge dam safety, HEC-RAS will play an increasingly critical role in ensuring resilient water infrastructure and minimizing the risks associated with dam failure [60], [62], [63], [114]. The reviewed literature collectively advances the field of dam breach analysis and flood inundation modeling using sophisticated hydrologic and hydraulic tools. [116] utilized HEC-RAS for detailed dam break

analysis, establishing a foundational framework for simulating post-failure flood dynamics. [117] expanded upon this by incorporating a probabilistic approach in HEC-RAS to quantify parametric uncertainties in dam breach processes, addressing variability in breach characteristics and downstream flood propagation. The study on Dire Dam [118] further integrated HEC-HMS and HEC-RAS, demonstrating the advantages of coupled hydrologic and hydraulic modeling in capturing complex interactions during dam failures. [119] applied dam-break flood simulations combined with GIS mapping to assess multiple potential scenarios for a proposed dam on the River Yamuna, emphasizing spatial flood hazard visualization. Finally, [120] highlighted the significance of these tools in disaster risk management by leveraging HEC-RAS and GIS for effective dam breach analysis and flood inundation mapping. Collectively, these studies illustrate a progressive shift toward integrating uncertainty analysis, multi-model coupling, and spatial mapping to enhance predictive capabilities and support robust flood mitigation strategies.

2.10 Climate Change Induced Vulnerability in Dam Safety

The safety and stability of dams are critical considerations during their design, construction, and operation due to the immense risks associated with retaining large volumes of water. A dam failure can lead to catastrophic consequences, including significant loss of life, widespread destruction of property, and severe economic damage in downstream areas. These potential impacts make dam safety a priority in civil engineering and water resource management [77], [79], [121]. For earth-fill dams, ensuring safety involves addressing both structural and operational aspects. Structural safety is achieved through a detailed focus on design and construction. This includes selecting appropriate materials for components such as the dams core, filters, and shells to ensure durability and stability. The design must account for external forces like floods, seismic activity, and seepage pressures, which

can compromise the dam's integrity. For example, designing robust core and incorporating drainage systems helps prevent seepage-induced erosion, while ensuring adequate freeboard minimizes the risk of overtopping during extreme rainfall events. Guidelines such as those provided by the International Commission on Large Dams (ICOLD) emphasize the importance of proper material selection and adherence to modern engineering standards to reduce the likelihood of structural failures [122], [123].

Operational safety is equally important for maintaining a dams long-term functionality and stability. This involves regular monitoring, inspections, and maintenance activities to identify and address potential issues before they escalate. For example, seepage control measures, such as installing piezometers and monitoring devices, help detect abnormal seepage patterns that could indicate internal erosion or piping. Spillway operation and maintenance are also crucial to ensure that floodwaters can be safely discharged without overtopping the dam. Moreover, emergency preparedness plans, including early warning systems and evacuation protocols, are critical for mitigating the impacts of potential failures. These operational measures are supported by advancements in technology, such as remote sensing, unmanned aerial vehicles (UAVs), and real-time monitoring systems, which enhance the ability to detect and respond to safety concerns efficiently [27], [77], [124].

Earth-fill dams are more vulnerable to specific failure mechanisms like overtopping, piping, and seismic activity, which necessitate additional precautions. Overtopping, often caused by inadequate spillway capacity or extreme rainfall, remains one of the leading causes of dam failures. To address this, spillways must be designed to handle probable maximum floods (PMF), as outlined in the United States Bureau of Reclamation (USBR) guidelines [125]. Similarly, piping process where water flows through the dam or its foundation, eroding the material and forming voidsrequires robust internal drainage systems and regular seepage monitoring. Seismic activity also poses a significant risk, as vibrations can destabilize the dam structure. Advanced seismic analysis and the use of resilient materials, such as compacted earth with appropriate filters, are vital to ensure stability during earthquakes [104].

By addressing both structural and operational aspects comprehensively, the risks associated with dam failure can be significantly reduced. This dual-phase approach ensures the dam's long-term functionality and safety while protecting lives, property, and ecosystems in downstream areas. Furthermore, ongoing research and innovations in dam engineering, monitoring systems, and risk management strategies continue to enhance the safety standards of dams worldwide, ensuring their resilience against evolving environmental and operational challenges [126], [127]. Existing dams may not be equipped to handle the intensified hydrological events associated with climate change. A review by [128] emphasizes the need to integrate climate change projections into dam safety assessments, particularly concerning hydrological loads such as floods. This integration could involve structural modifications, such as enhancing spillway capacities to manage increased flood risks, and operational changes, including the adoption of real-time monitoring systems to improve response times during extreme weather events. The CSA Group (2022) highlights that in Canada, existing dam safety guidelines do not specifically address climate change adaptation, underscoring the need for updated standards that incorporate future climate scenarios [129].

Conducting detailed vulnerability assessments is crucial for understanding how climate-induced changes affect dam safety. [128] a quantitative assessment of a Spanish dam, revealing a progressive deterioration in dam failure risk due to alterations in the hydrological regime caused by climate change. Such assessments should be regularly updated using the latest climate models to ensure that dam infrastructure can withstand future conditions. The CSA Group (2022) also notes that in Canada, there is a lack of specific guidelines addressing climate change adaptation for dams, indicating a gap in current vulnerability assessments [114].

Adapting dam safety protocols to address climate change impacts requires the development of comprehensive risk management strategies and supportive policies. Implementing robust monitoring and early warning systems can help detect potential structural issues before they lead to failures. Additionally, policies should mandate regular reviews of dam safety standards to align with evolving climate data, ensuring that both new and existing dams are capable of withstanding anticipated environmental stresses. The CSA Group (2022) points out that existing

dam safety and operations guidelines in Canada do not specifically address climate change adaptation, highlighting the need for updated policies that incorporate climate resilience [130], [131], [132].

2.11 Hazard Classification

The hazard potential classification system for dams is designed to assess the risks posed by dam failure based on three primary criteria: the probable loss of human life, the potential economic losses, and the environmental damage or disruption of critical infrastructure (lifelines) that may result from an uncontrolled release of stored water. This system emphasizes that even small dams or water-retaining structures can pose significant risks to downstream areas, especially in scenarios where failure leads to uncontrolled water discharge. The classification underscores the importance of evaluating the potential consequences of dam failure, regardless of the dams size or capacity [133].

Dams are categorized into different hazard potential classes low, significant, and high classes. Based on the severity of potential downstream impacts. A high-hazard potential dam is one where failure is expected to result in extensive loss of life and severe economic damage, whereas low-hazard potential dams are those where failure would lead to minimal or no loss of life and limited economic impacts [134].

2.11.1 Modern Developments in Hazard Classification

Recent advancements in dam safety emphasize the integration of probabilistic risk assessment (PRA) methods alongside traditional deterministic approaches. These methods account for uncertainty in hydrological events, structural performance, and potential downstream consequences, providing a more comprehensive understanding of dam safety risks [135].

Moreover, with the increasing frequency and intensity of extreme weather events driven by climate change, hazard classification now incorporates future climate

projections to evaluate potential risks. This ensures that spillway design and dam safety measures are adequate for handling more severe flood scenarios [136], [137].

2.11.2 Types of Hazards in Dam Safety

Hazards associated with dams can be broadly categorized into the following types:

2.11.2.1 Structural Hazards

Structural hazards in dams arise from design flaws, material deficiencies, or deterioration over time, potentially leading to failure and uncontrolled water release. Seismic activity can cause cracking, while poor construction and aging infrastructure may lead to seepage and piping, weakening the dam's integrity. Additionally, erosion of the dam face or spillway due to water flow or extreme events further increases failure risk. Regular inspections, maintenance, and reinforcement are crucial for mitigating these hazards and ensuring dam safety [138].

2.11.2.2 Hydraulic Hazards

Hydraulic hazards arise when a dam is unable to manage incoming water flows effectively, leading to potential overtopping, which is a primary cause of dam failure. Inadequate spillway capacity prevents the controlled release of excess water, increasing the risk of overflow during extreme rainfall events. Additionally, floods exceeding the dams design capacity, such as 100-year or probable maximum floods (PMF), can overwhelm the structure, resulting in structural instability and failure. Furthermore, wave action and wind-driven run-up can erode the upstream face of the dam, weakening its stability over time. Addressing these hazards through enhanced spillway design, flood forecasting, and protective measures is crucial for maintaining dam resilience and preventing catastrophic failures [139], [140].

2.11.2.3 Seismic Hazards

Seismic hazards occur when earthquakes trigger ground shaking, deformation, or liquefaction in a dams foundation or embankment, compromising its stability and

increasing the risk of failure. Seismic forces can cause cracking or sliding of the dam embankment, weakening its structural integrity. Additionally, liquefaction of foundation materials in earthen dams can lead to a loss of strength, making the dam more vulnerable to collapse. The presence of active fault lines beneath or near the dam site further amplifies the risk of sudden structural failure. To mitigate these risks, seismic hazard assessments, advanced engineering designs, and reinforcement measures are essential for ensuring dam safety in earthquake-prone regions [139], [141].

2.11.2.4 Hydrological Hazards

Hydrological hazards arise from extreme weather events and climate variability, impacting water inflow and reservoir storage, and posing significant risks to dam safety. Prolonged heavy rainfall can lead to severe flooding, overwhelming the dams capacity and increasing the likelihood of overtopping. Similarly, rapid snowmelt in upstream catchments can cause sudden inflow surges, straining the dams structural integrity. Additionally, shifting rainfall patterns due to climate change may result in the underestimation of flood magnitudes, leading to inadequate design considerations and increased flood risks. Addressing these hazards requires improved hydrological modeling, climate-adaptive reservoir management, and robust flood mitigation strategies to enhance dam resilience in changing climatic conditions [142].

2.11.2.5 Operational Hazards

Operational hazards arise from human error, insufficient maintenance, or inadequate management of the dam and its associated structures, which can compromise its safety and functionality. Improper gate operation during high inflow periods can lead to uncontrolled water release or excessive reservoir pressure, increasing failure risks (Bowles et al., 2016). Additionally, failure to clear debris or vegetation from spillways can obstruct water flow, reducing the dams capacity to manage floods effectively. Furthermore, lack of routine inspections and maintenance can

allow minor structural issues to escalate into critical failures over time. To mitigate these risks, implementing regular monitoring, well-defined operational protocols, and proper maintenance strategies is essential for ensuring long-term dam safety and performance [139], [141].

2.11.2.6 Environmental Hazards

Environmental hazards arise from dam failure or improper operation, significantly impacting the surrounding ecosystem and natural resources. Sudden water release can disrupt aquatic ecosystems, leading to habitat destruction and loss of biodiversity (Singh, 1996). Additionally, erosion of downstream riverbanks and increased sediment deposition can alter river morphology, affecting water quality and aquatic life. Furthermore, dam failure can result in the spread of pollutants from industrial or agricultural runoff, contaminating water sources and posing risks to human and environmental health. Implementing sustainable dam management practices, environmental monitoring, and ecological restoration strategies is essential to mitigate these risks and ensure long-term environmental stability [143].

2.11.2.7 Socioeconomic Hazards

Socioeconomic hazards arise from dam failure, leading to loss of life, economic damage, and disruptions to infrastructure and livelihoods. The displacement of downstream communities is a significant consequence, as floods triggered by dam failure can force residents to evacuate, leading to long-term socio-economic challenges. Additionally, damage to critical infrastructure, such as bridges, roads, and farmlands, can severely impact transportation, trade, and agricultural productivity. Furthermore, the loss of water supply for domestic, industrial, and agricultural use can create severe shortages, affecting both local populations and economic activities. Effective risk assessment, emergency planning, and resilient infrastructure development are essential for minimizing the socioeconomic impacts of dam failures [144].

2.12 Flood Frequency Analysis Using Statistical Methods in Pakistan

Flood frequency analysis (FFA) is a vital statistical tool used in hydrology to estimate the likelihood of flood events for specific return periods. This analysis plays a critical role in designing and managing hydraulic structures, such as dams and spillways, to ensure their safety during extreme flood events. In Pakistan, various statistical distributions have been applied to model flood frequencies, with the Gumbel Extreme Value Type I distribution being widely utilized due to its simplicity and effectiveness [145], [144].

The Gumbel distribution is particularly useful for modelling extreme events, such as annual maximum flood peaks. Its application has been demonstrated in several studies across Pakistan. For instance, research conducted on the River Chenab used the Gumbel distribution to estimate maximum discharges for different return periods, helping to predict flood-prone areas and supporting the design of flood management strategies. Similarly, a study on the River Swat at Chakdara Station applied the Gumbel distribution to calculate flood magnitudes for return periods ranging from 2 to 10,000 years. The study highlighted the Gumbel method's effectiveness in analyzing flood risks in regions prone to seasonal flooding [146].

Another study at the Guddu Barrage on the Indus River employed the Gumbel distribution to assess flood risks and predict future flood events. The results emphasized the importance of statistical modelling for improving flood preparedness and reducing the impacts of extreme events on critical infrastructure. These studies demonstrate that the Gumbel distribution is a reliable tool for FFA in Pakistan, particularly in areas with stable long-term flood records.

In summary, FFA using statistical methods, particularly the Gumbel distribution, is critical for understanding and mitigating flood risks in Pakistan. The application of these methods in various studies underscores their importance in flood risk management, hydraulic structure design, and disaster preparedness. By adopting robust statistical approaches, researchers and planners in Pakistan continue to

enhance flood prediction capabilities and reduce the vulnerabilities associated with extreme hydrological events [78], [145], [146], [147].

2.13 Climate Change Scenarios as per IPCC

The Intergovernmental Panel on Climate Change (IPCC), in its Sixth Assessment Report (AR6), provides a framework of climate change scenarios combining Shared Socioeconomic Pathways (SSPs) and Representative Concentration Pathways (RCPs) to assess future climate and socio-economic trajectories. These scenarios offer insights into the range of possible radiative forcing levels (expressed in watts per square meter) and their associated impacts on global temperatures by 2100. The SSP framework defines socio-economic futures based on variables like population growth, energy use, technological advancement, and land-use change, while the RCPs describe the resulting levels of greenhouse gas (GHG) emissions and climate forcing. Together, these pathways enable researchers to evaluate the consequences of varying mitigation and adaptation efforts across different socio-economic contexts [148], [149].

Among the key IPCC scenarios, SSP 1-1.9 represents a sustainable future where aggressive global mitigation efforts limit radiative forcing to 1.9 W/m, resulting in a global temperature rise of approximately 1.5C above pre-industrial levels. This scenario assumes rapid decarbonization, significant use of renewable energy, and global efforts to reduce inequality. In contrast, SSP 2-4.5 depicts an intermediate pathway where socio-economic and technological trends follow historical patterns, resulting in moderate mitigation efforts. Radiative forcing stabilizes at 4.5 W/m, leading to a temperature rise of approximately 2.7C by 2100. This scenario assumes a gradual energy transition with fossil fuels remaining a part of the energy mix until mid-century [150], [151].

The SSP 3-7.0 scenario describes a fragmented world with limited international cooperation and persistent reliance on fossil fuels, leading to radiative forcing of

7.0 W/m^2 and a temperature rise of over 3.6°C. This pathway projects significant climate impacts, including biodiversity loss, food and water insecurity, and heightened vulnerability to extreme weather events (Popp et al., 2017). On the higher end, SSP 5-8.5 represents a fossil-fueled development pathway with limited climate policies and rapid economic growth, resulting in radiative forcing of 8.5 W/m^2 and temperature increases exceeding 4°C. This scenario projects severe impacts, including accelerated sea-level rise, extreme heatwaves, and irreversible ecological damage [152], [153], [154].

2.14 Flood Estimation Approach Using HEC-HMS

Proper spillway design is critical for dam safety, as inadequate capacity is a leading cause of dam failures, contributing to overtopping events that are particularly catastrophic for earthen dams (ICOLD, 2013). Estimating design floods, such as 100-year and 200-year return period floods, is essential to ensure spillways can handle extreme hydrological events. The Hydrologic Engineering Centers Hydrologic Modeling System (HEC-HMS) is a widely used tool for simulating rainfall-runoff processes and generating inflow hydrographs, making it a standard method for flood estimation and spillway design [155], [156], [157].

In this study, the Soil Conservation Service Curve Number (SCS-CN) method, integrated within HEC-HMS, was employed to estimate runoff from rainfall events. The SCS-CN method is an empirical technique used to estimate rainfall-runoff volume from precipitation in small watersheds, with the Curve Number (CN) being an empirically derived parameter that depends on soil type, land use, and land cover (USDA, 1986). This method has been effectively applied in various regions, including Pakistan.

HEC-HMS, combined with the SCS-CN method, has been successfully utilized in semi-arid regions for flood estimation. Many Researches have focused on flood modeling in the Chenab River basin using HEC-HMS and emphasized its effectiveness in predicting peak discharges. Some have applied HEC-HMS to simulate flash floods in the Swat River basin, underscoring the importance of integrating catchment-specific parameters such as rainfall intensity and land-use patterns.

The integration of site-specific parameters enhances the reliability of runoff and flood predictions using this method [158], [159].

In this research, HEC-HMS, with the SCS-CN method was used to estimate peak discharges for 100-year and 200-year return periods. The results provide critical insights into flood magnitudes, aiding in the design of spillways capable of withstanding extreme hydrological events and preventing overtopping. While alternative empirical methods, such as the Creager curve and Snyders unit hydrograph, are available for flood estimation [160], the ability of HEC-HMS to incorporate the SCS-CN method and account for site-specific factors makes it the preferred tool for detailed flood analysis and spillway design.

Chapter 3

Study Area, Data, and Methodology

3.1 Study Area

Malgagai Dam is located in the Balochistan province of Pakistan, a region characterized by an arid to semi-arid climate, rugged terrain, and limited water resources. The dam plays a crucial role in water storage, irrigation, and flood mitigation for nearby communities that rely heavily on its supply. It is situated in a remote area surrounded by steep hills and narrow valleys, which significantly influence the region's hydrology. The local geology consists mainly of sedimentary rock formations, with loose soil deposits in the valleys that are prone to erosion during heavy rainfall. Seasonal variations, particularly during the monsoon period, can lead to rapid inflows into the reservoir, increasing the risk of overtopping. The downstream region includes sparsely populated villages, agricultural lands, and essential infrastructure such as roads and small bridges, all of which are vulnerable to flooding. The area experiences erratic and infrequent rainfall, mostly occurring between July and September, with an annual average ranging from 100 mm to 250 mm. However, localized storms can produce intense downpours, triggering flash floods. These climatic and geological factors make Dam, an essential yet potentially high-risk structure in the region [161], [162], [163].

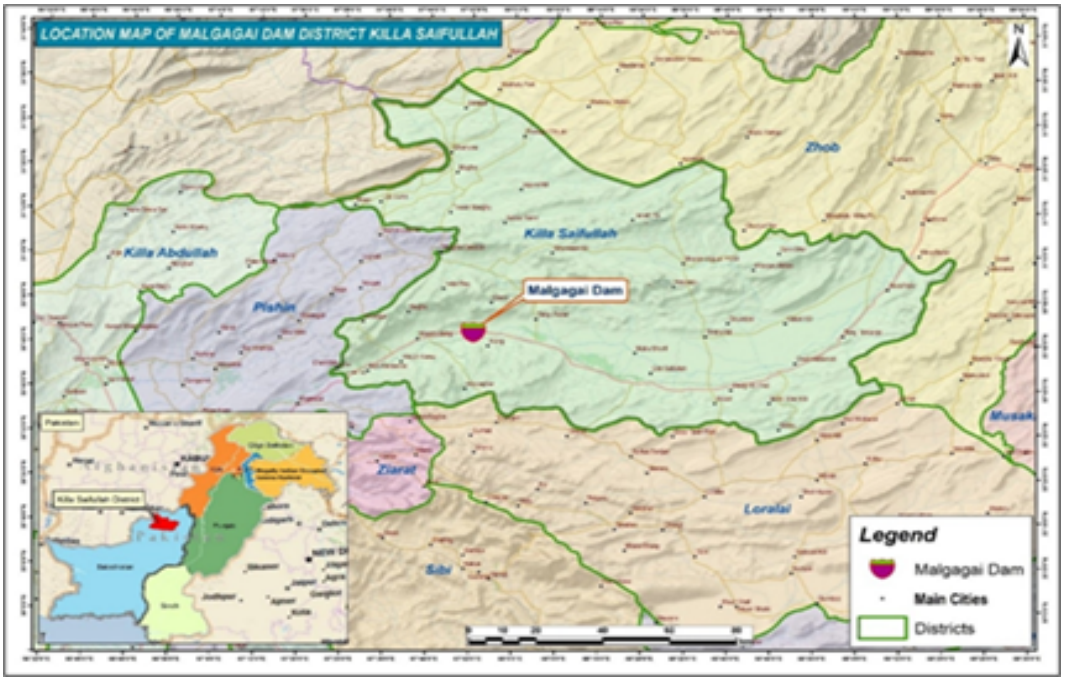

FIGURE 3.1: The location map of the study site

3.2 Significance of Study

Given the socio-economic dependence of local communities on the Dam, ensuring its safety and functionality is critical. The results of this dam break analysis will not only help in identifying potential risks but also provide actionable insights for disaster risk management. By developing detailed inundation maps and risk mitigation strategies, this study will contribute to enhancing the resilience of communities living downstream of the dam. Furthermore, the methodology employed in this research can serve as a model for similar dam break analyses in other arid and semi-arid regions. The integration of erosion rate estimation, hydraulic modeling, and risk assessment provides a comprehensive framework for assessing dam safety and planning for potential failure scenarios.

3.3 Brief Methodology

The methodology for this study was structured to evaluate hydrological patterns, flood risks, and the structural performance of the dam under historical and future climate conditions. The research began with the collection of precipitation data

for Muslim Bagh (1985-2014) and Global Climate Model (GCM) outputs for the same period, focusing on future climate scenarios under SSP 2-4.5 and SSP 5-8.5. To estimate peak discharges for 100-year and 200-year return periods, frequency analysis was applied to both historical and future datasets. The delta method was used to correct the precipitation and temperature data, ensuring consistency with observed historical records. Bias correction involved calculating a delta factor and applying it to future time slices 2026-2050, 2051-2075, 2076-2100 for both precipitation and temperature data.

After bias correction, hydrological modeling was performed using HEC-HMS. The SCS Curve Number method was employed to estimate runoff, incorporating precipitation, land use, and soil characteristics of the catchment. This step provided flood hydrographs and peak discharge estimates under both historical and projected scenarios. These outputs served as critical inputs for the dam breach analysis.

The HEC-RAS software was used for detailed dam breach analysis. Field data related to breach width, side slopes, and other structural parameters were collected from the dam site and thoroughly evaluated. Breach parameters were adopted as per actual Breach scenario occurred during the flood event 2022, ensuring that they reflected the dam's topography and structural characteristics. These parameters were optimized to simulate potential breach scenarios, and the findings were used to establish standardized breach parameters for Balochistan. These benchmarks are particularly useful for designing and analyzing new dams in similar hydrological and topographical conditions across the region.

Following the dam break analysis, a detailed risk assessment was conducted to evaluate the downstream impacts of a potential breach. Inundation maps were developed using HEC-RAS outputs, highlighting areas at risk of flooding, including infrastructure, agricultural lands, and residential zones. The total flooded area was calculated, and critical zones were prioritized for intervention. Based on this risk assessment, flood risk adaptation and management strategies were proposed. These included the implementation of early warning systems to alert downstream communities in case of a breach, strengthening the dams spillway to handle extreme discharge events, and developing evacuation plans for high-risk

areas. Structural measures such as reinforcing embankments and non-structural measures like community awareness programs and land use zoning were also recommended.

This comprehensive methodology ensured a robust evaluation of Dams hydrological and structural behavior. By integrating hydrological modeling, dam breach analysis, risk assessment, and adaptive management strategies, the study not only evaluated the safety and performance of the dam but also established breach parameter benchmarks for Balochistan. These benchmarks provide a standardized approach for future dam projects, ensuring proactive flood risk management and enhancing the resilience of dams under changing climatic and hydrological conditions. The findings offer critical insights for policymakers and engineers to improve dam safety and implement sustainable water resource management strategies.

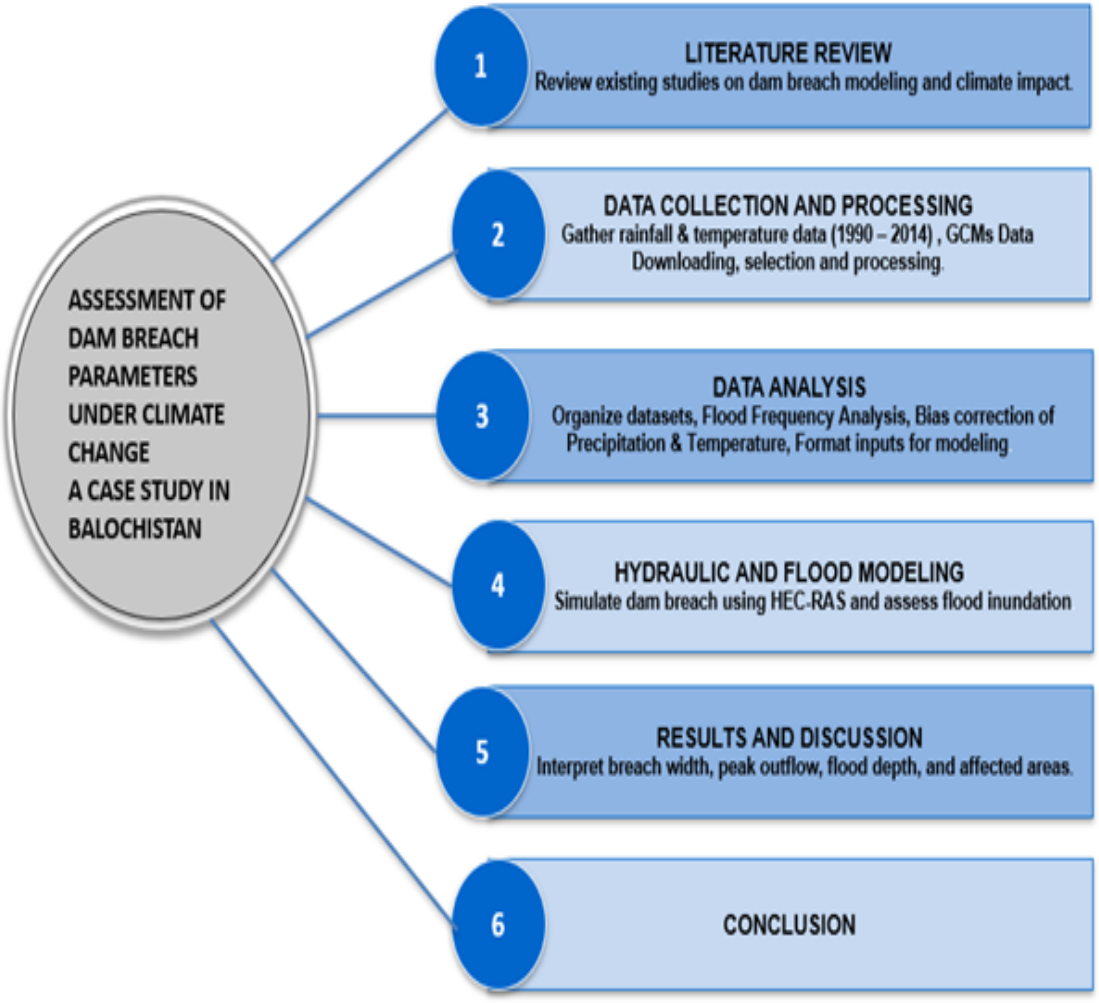

FIGURE 3.2: Methodology of thesis

3.4 Data Collection

The data collection process for this research focused on obtaining accurate and region-specific datasets to support hydrological modelling, flood estimation, and climate impact assessments. Meteorological data, including daily precipitation and temperature records, was acquired from the Pakistan Meteorological Department (PMD) for the period 1985-2014, ensuring the inclusion of long-term historical trends. This data was crucial for understanding the climatic variability and hydrological patterns influencing the dam's catchment area.

For topographical and hydrological analysis, SRTM DEM (Shuttle Radar Topography Mission Digital Elevation Model) was utilized to delineate the catchment area, generate stream networks, and analyze elevation profiles. This high-resolution elevation data played a key role in accurately defining the watershed and routing runoff during extreme weather events.

3.4.1 Precipitation

The precipitation data for Muslim Bagh Climate Station from 1985 to 2014 shows significant variation in annual and seasonal rainfall. The total yearly rainfall ranged from a maximum of 476.2 mm to a minimum of 116.8 mm. On average, the area receives about 295.15 mm of rainfall each year, but the amount of rainfall changes greatly from one year to another.

Most of the rainfall occurs during the monsoon months of July and August, with average rainfall of 31.01 mm and 27.26 mm, respectively. The winter months, especially January and February, also contribute significantly to the total rainfall, with averages of 32.99 mm in January and 46.7 mm in February, mainly due to westerly weather systems. In contrast, the pre-monsoon summer months, such as May and June, receive less rainfall, averaging 15.29 mm and 15.41 mm, respectively.

This variability shows the region's vulnerability to both low rainfall and extreme weather events. Table 3.1 shows mean monthly Precipitation of Muslim Bagh Climate station (mm). The data highlights the importance of effective water management to handle both dry periods and heavy rainfall. Seasonal rains are

crucial for agriculture and water resources, making it essential to plan for irregular rainfall patterns in the future.

TABLE 3.1: Mean Monthly Precipitation of Muslim Bagh Climate station (mm)

Year	Jan	Feb	Mar	Apr	May	Jun	Jul	Aug	Sep	Oct	Nov	Dec	Total
1985	32.8	9.3	31.5	63.6	10.8	4.8	27.5	12.6	2.1	4.7	2.1	34.3	236.1
1986	32.4	38.8	52.2	6.6	6.6	12.6	30.6	104.5	5.3	9.5	10.7	0.7	310.5
1987	17.4	25	40.9	2.5	6	6.1	6	32.4	8.3	0	0	38.4	183
1988	8.5	4.6	37.7	0.4	2	16.3	24.9	35.4	3.7	2.7	8.4	26.2	170.8
1989	25.2	12.3	78.5	3.4	8	23.9	42.1	24.6	4.6	0	5.5	34.8	262.9
1990	85.2	71.1	21.6	19.4	13.2	12.4	23.6	53.2	15.7	2.7	2.5	28.2	348.8
1991	91	101.1	75	42.2	9.9	2.3	1.4	9.3	11.8	0.5	7.7	18.6	370.8
1992	53	56.7	60.5	118.1	12.5	25.9	19.6	41.5	22.3	12.7	5	48.4	476.2
1993	82.2	19.2	23.6	19.9	2	9.6	45.7	11	15.6	5.9	8.1	47.1	289.9
1994	10.2	74.1	34	20.7	13.3	8.3	90.8	26.9	28.2	0.3	0.6	28.5	335.9
1995	7.1	19.8	19.9	51.8	4.2	5.2	55.2	19.9	5.1	15.6	0.4	67.1	271.3
1996	25.5	25.3	38.2	6	20.6	26.8	11	7.9	2	1.9	0	12.4	177.6
1997	22.3	7.4	58.6	43	20.6	42.3	56.6	24.9	3.1	53.8	23	16.5	372.1
1998	44.4	46.7	70.6	12.6	33.5	8.6	28.3	10.3	8.4	0.9	0	0	264.3
1999	39	58.1	31	0.7	5.9	0.9	14.2	19.7	12.4	0.5	1.8	0.2	184.4
2000	16.7	19.4	3.9	0.6	0.2	1.9	17.3	6.5	3.9	0	5.2	41.3	116.9
2001	1.2	18.1	29.4	22.8	1.5	9.2	49.1	10.9	3.5	0	0.7	5.8	152.2
2002	2.6	49.4	36.6	31.3	5.2	7.4	2.2	14.7	6.4	2.8	18.2	30.6	207.4
2003	28.8	63.5	21.4	14.7	11	2.6	64.8	29.1	6.4	0	9.5	0.9	252.7
2004	58.4	8.8	1	7.6	5.1	8.9	11.7	21.5	10.1	2.7	4.9	35.1	175.8
2005	37.3	146	130	5.8	23.1	3.7	38.9	20.3	16.7	0	0.2	0.5	422.5
2006	14.1	37.9	57.3	9.5	19	9.9	19.4	46.7	12.2	18.2	68.4	106.7	419.3
2007	5.6	120	70.4	13.3	2.5	109.5	30.5	15	6.5	0	2.6	6.9	382.8
2008	86.4	19.4	1.6	23.9	15.1	49.1	50.4	37.9	29	0.3	0.1	42.3	355.5
2009	81.7	57.1	28	60.2	8.4	6.6	43	14.5	3.9	1.5	1.8	56.4	363.1
2010	31.4	33.1	21.1	13.3	9.6	11.4	48.6	70.7	27.1	0.9	0	1.6	268.8
2011	10.9	104.7	59.8	69.1	13.1	6.1	27	28.6	81.1	23	17.7	3.1	444.2
2012	36.2	39.4	44.7	91.6	32.9	14.2	25.2	24.7	63.3	4.7	5.4	31.3	413.6
2013	1.5	119.2	40.3	66.2	6.4	10.1	13.3	34.5	1.8	1.6	17.8	1.8	314.5
2014	0.8	28.2	73.2	33.6	136.5	5.7	11.5	8.2	2.5	0.5	8.2	1.7	310.6
Average	**32.99**	**47.79**	**43.08**	**29.15**	**15.29**	**15.41**	**31.01**	**27.26**	**14.1**	**5.6**	**7.88**	**25.58**	**295.15**

Similarly, the precipitation data derived from five General Circulation Models (GCMs) under the SSP 2-4.5 scenario exhibits notable variations in annual and seasonal rainfall patterns over different years. The total yearly precipitation fluctuates significantly, with the highest recorded annual rainfall reaching 490.2 mm in 2099 and the lowest at 209.3 mm in 2094. The average annual precipitation across the dataset is approximately 335.4 mm, reflecting substantial interannual variability.

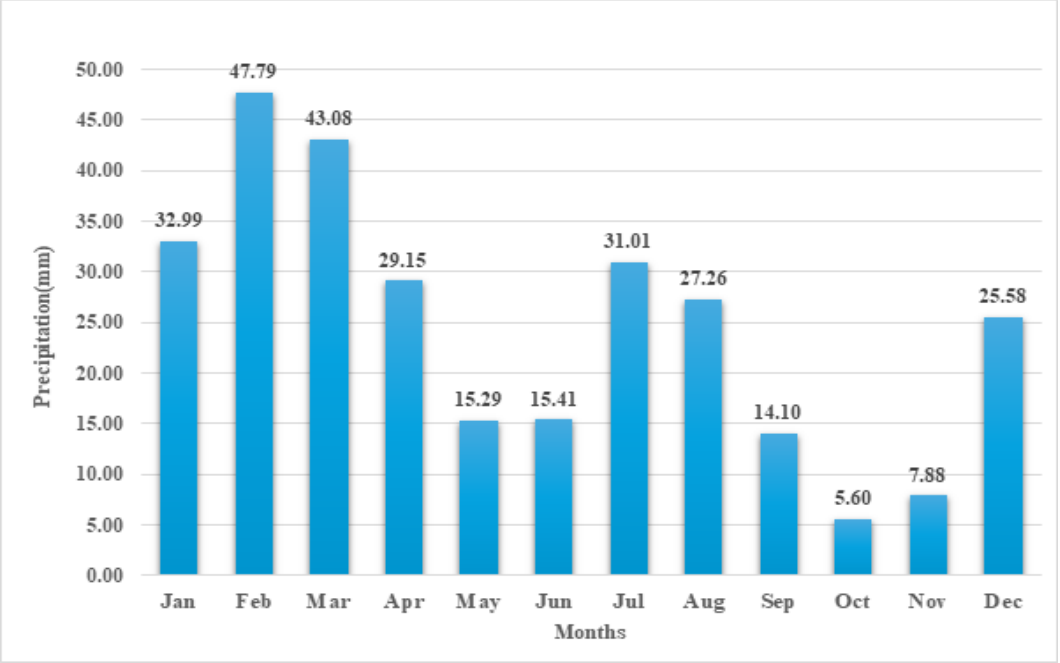

FIGURE 3.3: Mean monthly Precipitation (mm) of Muslim Bagh Climate Station

Seasonally, the highest precipitation levels are generally recorded during the monsoon months of July and August, with average monthly values of 34.8 mm and 38.8 mm, respectively. Winter months, particularly January and February, also contribute significantly to total rainfall, with mean values of 43.8 mm and 42.8 mm. In contrast, the pre-monsoon summer months such as May and June receive relatively lower rainfall, averaging 18.2 mm and 22.3 mm, respectively.

The data highlights years of extreme rainfall, such as 2099 and 2100, where precipitation exceeded 480 mm, indicating periods of heightened flood risk. Conversely, years like 2094 and 2050, with total precipitation below 260 mm, demonstrate potential drought conditions. This variability underscores the susceptibility of the region to climate extremes, emphasizing the need for adaptive water resource management strategies.

Overall, the results suggest that precipitation patterns under SSP 2-4.5 exhibit increasing variability, with some years experiencing significantly higher rainfall than others. These findings play a crucial role in hydrological modeling and flood risk assessments, particularly for earthen dams. Understanding these trends is essential for improving flood forecasting, optimizing reservoir management, and developing effective mitigation strategies against climate-induced hydrological extremes.

TABLE 3.2: Mean Monthly Precipitation of 5GCMS (mm) of SSP 2-4.5

Year	Jan	Feb	Mar	Apr	May	Jun	Jul	Aug	Sep	Oct	Nov	Dec	Total
2017	21.5	59	51.9	28.4	17	11.2	46.5	48.6	5.3	1.6	14.2	60.1	365.3
2018	25.7	17.4	35.1	84.2	27.3	19	28.1	21.4	9.9	11.5	18.7	75.3	373.8
2019	34.7	23.2	53.5	22.7	8	21.8	33.7	67.4	21.1	1.3	17	14.1	318.6
2020	37.6	26	28	31.1	19.4	14.4	18.9	62	3.1	1.7	10.9	40.6	293.5
2021	55	45.9	36.4	64.4	25.2	20.1	26	39.7	4.2	39.4	29.7	41.9	428
2022	28.3	40.6	31.7	30.1	9.1	20	14.8	9.8	19.3	18.5	37.7	21	281.1
2023	35	46.4	27.3	12	33.6	23.4	32	40.6	23.4	7	28.3	37.7	346.6
2024	16.1	41.6	62.2	26.2	23.2	23.2	24.3	22.1	6.1	4.7	13.9	12.4	276
2025	77.3	70.6	20.5	17.8	17.7	43.3	38.3	41.5	16.5	1.7	8	8.9	362
2026	18	20.2	51	26.5	17.1	6.6	21.8	56.8	16.3	2.5	19.7	33.6	290.1
2027	33.9	49.5	79.6	53.3	7.5	62.4	22.6	42.9	19	4.4	8.6	36	419.7
2028	74.9	58.8	19.9	58.5	7.3	6.6	27.2	34.3	2.5	3.1	6.8	10.1	309.9
2029	33.9	45.9	38	41.4	19.2	4.4	12.3	41.5	4.6	11.5	6.5	17.2	276.2
2030	36.3	45.4	31.3	28.9	43.7	13.2	27.1	19.3	11.2	10.5	9	26.9	302.9
2031	68.7	73.5	32.1	23.2	21.2	12.1	53.3	86.6	7.9	14.5	3.5	33.1	429.7
2032	34.8	13.5	27.1	25.2	44.4	8.4	30.1	20.9	3.8	15.4	30.7	19.9	274.2
2033	59.2	20.3	45	65.8	16.2	16.8	33.7	14.7	10.4	1.3	5.9	17.7	307
2034	53.6	48.2	42.7	36.9	17.6	30.1	20.3	41.1	18.6	1.5	3.8	19.7	334.2
2035	23.1	59.6	61.2	44.6	38.1	8	41.7	32.4	43.5	10.5	7.6	21.6	392
2036	27.2	71	19.2	28.7	13.8	27	33.2	23.8	9.4	7	20.6	15	295.9
2037	32.9	57.6	41.8	24.7	29.4	14.9	34.8	37	8.9	21.1	12.9	16.9	332.8
2038	49	34.2	41.9	26	28.1	20.8	31.8	29.4	29	18.6	26.7	32.4	367.8
2039	81.4	33.3	28.5	46.5	37.5	16.4	34.2	23.1	7	7.6	35.8	17.1	368.4
2040	58.6	45	56.2	55.7	27.9	37.6	24	29.3	9	9.3	16.8	36.3	405.7
2041	40	85.3	30.3	24.9	24.2	8.2	16.6	25.3	12.2	13.9	4.9	12.5	298.4
2042	40.6	76.3	30.1	14.6	19.6	20.9	58.3	29.4	5.3	5.3	7.6	26.7	334.6
2043	50.8	41.6	27.6	9	11.2	11.8	14.4	7.5	5.2	2.9	44.2	31.1	257.3
2044	41.5	19.4	30.9	37.7	4.5	26.9	92	64.3	16	1.1	16.7	23.8	374.7
2045	29.4	24.4	30.6	11	10	3.9	18	22.7	5.3	11	33.6	36.4	236.4
2046	76.6	34	51.8	37.4	13.2	24.1	56.9	77.1	27.9	6.3	25.7	20.6	451.8
2047	82.5	48.4	28.3	32.9	28.3	1.2	41.7	33.5	29.9	6.7	27.9	13.8	375.2
2048	34.8	35.7	43.4	36	13.2	3	29.8	41.4	4.7	16.3	29	28.3	315.7
2049	66.3	82.7	45.2	17.1	18.6	8.4	86.9	76.3	9.4	3.7	9.5	20.1	444.1
2050	18	15.1	21	10.3	10.1	44.4	46.4	19	4	5.2	6.1	56.4	256
2051	81.9	39.9	21.7	7.3	11.1	12.3	27.4	34.8	16.1	10.4	16.4	32.8	312.1
2052	49.7	55.5	34.2	35.4	38.9	17.8	19.7	46.2	25	5.2	20.1	27.6	375.4

Continued on next page

Year	Jan	Feb	Mar	Apr	May	Jun	Jul	Aug	Sep	Oct	Nov	Dec	Total
2053	26.9	22.5	76.5	17.7	7.1	19.8	37.6	24.6	5.7	16.4	7.2	16.6	278.6
2054	32.4	50	56.7	65.8	13.7	17.3	23.7	11.4	6.1	3.6	7.2	23.1	311.1
2055	37.8	84.4	20.3	27.7	17.6	13.1	25	26.5	31	4	9.8	10.6	307.7
2056	36	69.3	26.4	28.8	12.1	13.4	45.4	40.5	11.8	19.7	16.8	17	337.4
2057	29.8	45.2	47.2	32.4	5.3	21	24.8	27.9	8	7.9	9.5	14.3	273.2
2058	49.8	27.1	29.6	38.4	11.4	32.6	22.4	37.7	7.5	13.9	20	53.6	343.9
2059	60.7	22.5	38.2	40.1	4.8	48.6	15	41.4	3.8	4.6	25.7	33.3	338.6
2060	42.7	21.7	38.3	51.8	17	8.7	17	18.9	18.7	15.2	7.6	32.7	290.2
2061	29.2	19.9	22.4	30.1	27.7	22.8	21.1	31.2	9.6	5.2	23	20.3	262.5
2062	27.4	9.2	27.8	35.3	8.1	47.9	32.1	20.6	14.6	25.2	21.4	26	295.6
2063	90.8	62.8	77.7	35.5	8.4	16.7	33.3	25.2	14.9	5.3	11.6	27.6	409.7
2064	58	52.2	50.9	28.2	11.9	45.4	17.6	39.8	17.3	30.2	5.8	12	369.3
2065	35.5	47.9	49.8	17.2	19.2	14.1	27.5	19.8	15.8	4.1	5.9	20.2	277
2066	133	38.5	44.3	27.3	7.1	27.6	41.3	46.5	6.3	47.8	16.9	22.3	459
2067	36.6	34.5	39.3	19.7	12.6	30.9	13.1	43.5	8.1	3.5	14.9	16.5	273.1
2068	19.7	24.5	32.8	17.7	8.4	35.7	44.1	52.5	13.6	6.5	42.4	22.8	320.6
2069	61.5	24.3	39.1	29.6	9.7	18.2	36.1	62.8	16.2	14.4	21	22.8	355.7
2070	34.8	44.7	18.9	14.2	9.9	5.6	79.6	40.1	21.8	11.9	13.3	30.4	325.1
2071	69.8	78.3	66.7	22.2	19.4	11.5	35.5	28.5	2.4	12.1	12.6	11.4	370.5
2072	43.9	48.5	30.5	19	5.5	21.8	8.9	30.9	22.9	15.9	14.9	21.9	284.7
2073	78.4	25.9	34	25	29.9	34.6	57.1	38.8	22.2	7.2	4.4	17.8	375.3
2074	32.6	35.5	25.7	20.9	11.2	10.4	25.2	54	21.2	4.2	3.7	28.6	273.1
2075	20.5	55.7	40	48.8	14.8	5.7	30.2	15.8	7.3	1.9	10.1	10.4	261.3
2076	51.2	44.4	29.6	16.1	16.3	19.9	19.7	17.4	65.3	29.5	12.1	21.3	342.8
2077	41.4	49.6	31.5	30.7	35.5	39	71.7	71	19.1	6.5	19.3	17.6	432.8
2078	19.8	34.3	32.7	35.4	45.4	17.3	24.6	41.2	13.4	16.1	4.2	29.1	313.4
2079	15.8	76.9	25.8	75.4	23.2	4.6	44.3	71	24.9	40.3	2.3	14.7	419.1
2080	29	19	17.5	34.1	8.7	15.1	34.4	57.7	12.7	15.9	39.1	19.2	302.3
2081	64.4	30.7	23.9	33.2	11.5	14.3	20	28.2	54.8	10.6	15.5	17.9	325
2082	19.9	52.5	34.7	22.9	8.2	57.5	59.8	92.7	8.6	15.4	19.1	5.5	396.8
2083	33.6	37	22.2	21.2	18.8	7.9	70.7	39.5	40.8	17.8	9.4	5.9	325
2084	41.4	57.2	40.9	24.7	20	23.1	41.6	33.9	19.7	13.7	9.7	23.7	349.6
2085	39.7	37.2	39.8	33.7	27.4	35	17	43	10.3	14.4	20.9	26.8	345.4
2086	32.2	53	36.9	19.3	21.6	32.5	44.8	15.7	4.3	14.1	22.1	45.3	342
2087	45.8	82.9	48.4	28.5	33.6	13	14.5	40.7	11.1	4	22.2	34.3	379
2088	34.6	46.2	66.8	36.3	14.6	11.7	36.1	54.4	12.6	8.7	17.3	17.8	357.1
2089	28.9	71	25.9	24.1	26.6	13.1	33.5	50.9	16.8	15.8	11.6	22.2	340.4

Continued on next page

Year	Jan	Feb	Mar	Apr	May	Jun	Jul	Aug	Sep	Oct	Nov	Dec	Total
2090	24.2	36.8	38.1	25	17.4	36.7	26.2	34.1	27	9.5	15.5	14.6	305.2
2091	31.5	21.4	20.1	13.9	5	17.3	41.2	54.6	24.8	21.7	4.4	31.3	287.3
2092	26.1	26.7	41.8	24.6	9	38.6	53.9	50	8.7	15.3	20.9	18.5	334
2093	54.4	23.7	25.7	37.6	16.4	14	47	41.2	3.8	3.9	7.9	31.2	306.8
2094	26.2	18.1	14.9	25.8	6.1	35.5	28.5	10.8	13.4	8.7	7.9	13.4	209.3
2095	69	53.4	42	16.4	19	19.6	20.1	56.9	9.4	3.4	5.2	36.8	351.2
2096	41.5	34.8	47	11	9.6	31.3	40.4	25	10.7	13.7	15.2	16	296.2
2097	26.4	39	14.7	27	16.1	12.7	33	19.6	26.5	8.5	14.3	4.4	242
2098	47.6	15.1	16.2	12.4	26.6	24.7	19.2	50.1	45.4	32.3	7.2	24.6	321.5
2099	67.8	61	33.9	38.5	39.3	88	71.6	40.9	15.3	5.6	11.3	17.1	490.2
2100	51.8	27.3	38.4	29.1	9	66.8	78.6	78.4	35.9	3.1	24.2	39.4	482.2
Average	**43.8**	**42.8**	**36.9**	**30.6**	**18.2**	**22.3**	**34.8**	**38.8**	**15.6**	**11.2**	**15.7**	**24.5**	**335.4**

The precipitation projections for the SSP5-8.5 scenario, based on five GCMs, reveal significant variability in annual and seasonal rainfall patterns. The total annual precipitation fluctuates considerably, with values ranging from a minimum of 246.9 mm to a maximum of 578.4 mm, indicating a high degree of interannual variability. The average annual precipitation is estimated at 395.8 mm, suggesting a potential increase in rainfall intensity compared to historical trends.

Seasonal distribution highlights that the monsoon months, particularly July and August, contribute the highest rainfall, averaging 41.1 mm and 45.8 mm, respectively. The winter months, such as January and February, also receive substantial precipitation, with average values of 51.7 mm and 50.6 mm, primarily influenced by westerly weather systems. In contrast, pre-monsoon months like May and June show relatively lower rainfall, with averages of 21.5 mm and 26.4 mm, respectively.

The data indicate that future precipitation patterns under SSP 5-8.5 are expected to be more intense and irregular, increasing the likelihood of extreme rainfall events. This variability underscores the need for robust flood management strategies, considering potential risks associated with higher precipitation levels. The findings are crucial for hydrological modeling in HEC-HMS, where these projections help simulate flood hydrographs and peak discharges, forming the foundation for subsequent dam breach analysis using HEC-RAS.

TABLE 3.3: Mean Monthly Precipitation of 5GCMS (mm) of SSP 5-8.5

Year	Jan	Feb	Mar	Apr	May	Jun	Jul	Aug	Sep	Oct	Nov	Dec	Total
2017	25.4	69.6	61.3	33.5	20.1	13.2	54.8	57.3	6.3	1.9	16.8	70.9	431.1
2018	30.4	20.5	41.4	99.4	32.3	22.5	33.2	25.2	11.7	13.6	22.1	88.9	441.1
2019	41	27.4	63.1	26.8	9.5	25.7	39.8	79.5	24.9	1.5	20.1	16.6	375.9
2020	44.3	30.7	33	36.7	22.8	17	22.3	73.1	3.7	2	12.8	47.9	346.4
2021	64.9	54.1	43	76	29.8	23.7	30.7	46.8	5	46.5	35.1	49.5	505
2022	33.4	48	37.5	35.6	10.8	23.6	17.5	11.5	22.8	21.9	44.5	24.7	331.7
2023	41.3	54.7	32.2	14.2	39.6	27.6	37.7	48	27.6	8.3	33.4	44.5	409
2024	19	49.1	73.4	30.9	27.4	27.4	28.7	26	7.2	5.5	16.4	14.6	325.7
2025	91.2	83.3	24.2	21	20.9	51.1	45.1	48.9	19.5	2	9.5	10.5	427.1
2026	21.2	23.8	60.2	31.3	20.2	7.8	25.7	67.1	19.2	3	23.2	39.6	342.3
2027	40	58.4	93.9	62.9	8.9	73.6	26.7	50.6	22.4	5.2	10.1	42.4	495.3
2028	88.4	69.4	23.4	69.1	8.6	7.8	32.1	40.5	2.9	3.6	8.1	11.9	365.7
2029	40	54.1	44.8	48.8	22.7	5.1	14.5	49	5.4	13.6	7.7	20.2	325.9
2030	42.9	53.6	37	34.1	51.6	15.6	32	22.7	13.2	12.4	10.7	31.7	357.5
2031	81.1	86.7	37.9	27.3	25	14.3	62.9	102.2	9.3	17.1	4.2	39.1	507
2032	41	16	32	29.8	52.4	9.9	35.5	24.7	4.4	18.2	36.2	23.4	323.6
2033	69.8	23.9	53.1	77.6	19.2	19.8	39.8	17.4	12.3	1.6	6.9	20.9	362.2
2034	63.3	56.8	50.4	43.6	20.8	35.5	24	48.5	21.9	1.8	4.4	23.3	394.3
2035	27.3	70.4	72.2	52.6	45	9.5	49.2	38.2	51.3	12.4	9	25.5	462.5
2036	32.1	83.8	22.7	33.9	16.3	31.8	39.2	28.1	11.1	8.3	24.3	17.7	349.1
2037	38.9	68	49.3	29.1	34.6	17.5	41.1	43.7	10.5	24.8	15.2	20	392.8
2038	57.8	40.3	49.4	30.7	33.2	24.5	37.5	34.7	34.3	21.9	31.5	38.2	434
2039	96	39.3	33.6	54.8	44.2	19.3	40.3	27.3	8.3	9	42.3	20.2	434.7
2040	69.2	53.1	66.3	65.7	33	44.4	28.3	34.6	10.6	11	19.8	42.8	478.7
2041	47.2	100.7	35.8	29.4	28.6	9.7	19.6	29.9	14.4	16.3	5.8	14.8	352.2
2042	47.9	90.1	35.5	17.2	23.2	24.7	68.8	34.7	6.2	6.3	9	31.6	394.9
2043	59.9	49.1	32.6	10.6	13.2	13.9	17	8.9	6.2	3.4	52.2	36.7	303.7
2044	48.9	22.9	36.5	44.4	5.4	31.7	108.6	75.9	18.9	1.2	19.7	28	442.2
2045	34.7	28.8	36.2	13	11.8	4.6	21.3	26.8	6.2	13	39.7	43	279
2046	90.4	40.1	61.2	44.2	15.6	28.4	67.2	90.9	32.9	7.5	30.3	24.3	533.1
2047	97.4	57.1	33.4	38.9	33.4	1.5	49.1	39.6	35.3	7.9	33	16.3	442.7
2048	41.1	42.2	51.2	42.5	15.6	3.5	35.1	48.9	5.6	19.2	34.2	33.4	372.5
2049	78.2	97.5	53.4	20.2	22	9.9	102.5	90	11.1	4.3	11.2	23.7	524
2050	21.2	17.8	24.7	12.2	12	52.3	54.7	22.4	4.7	6.1	7.3	66.5	302
2051	96.7	47.1	25.6	8.7	13.1	14.5	32.4	41	19	12.2	19.3	38.7	368.3
2052	58.7	65.4	40.4	41.7	46	21	23.3	54.5	29.5	6.2	23.7	32.6	442.9
2053	31.8	26.5	90.3	20.9	8.4	23.4	44.3	29	6.7	19.3	8.5	19.6	328.7

Continued on next page

Year	Jan	Feb	Mar	Apr	May	Jun	Jul	Aug	Sep	Oct	Nov	Dec	Total
2054	38.3	59	66.9	77.6	16.1	20.5	27.9	13.4	7.2	4.3	8.6	27.3	367.1
2055	44.6	99.6	23.9	32.7	20.7	15.4	29.5	31.2	36.5	4.7	11.6	12.5	363
2056	42.5	81.8	31.2	34	14.3	15.8	53.5	47.8	13.9	23.3	19.9	20	398.1
2057	35.1	53.3	55.7	38.2	6.2	24.8	29.2	32.9	9.5	9.3	11.2	16.9	322.3
2058	58.7	32	34.9	45.3	13.4	38.5	26.4	44.5	8.8	16.4	23.6	63.2	405.8
2059	71.6	26.5	45	47.4	5.7	57.4	17.7	48.9	4.4	5.4	30.3	39.3	399.6
2060	50.4	25.6	45.2	61.1	20.1	10.3	20.1	22.3	22.1	17.9	8.9	38.6	342.4
2061	34.4	23.5	26.4	35.5	32.7	26.9	25	36.8	11.3	6.1	27.1	23.9	309.7
2062	32.3	10.8	32.8	41.7	9.6	56.5	37.9	24.3	17.2	29.8	25.2	30.7	348.8
2063	107.2	74.1	91.6	41.8	9.9	19.7	39.3	29.7	17.5	6.2	13.7	32.6	483.4
2064	68.4	61.6	60.1	33.2	14	53.5	20.7	47	20.5	35.6	6.8	14.2	435.7
2065	41.8	56.5	58.8	20.2	22.7	16.6	32.4	23.4	18.7	4.8	7	23.9	326.8
2066	156.9	45.4	52.3	32.2	8.4	32.5	48.7	54.9	7.5	56.4	20	26.3	541.6
2067	43.2	40.7	46.4	23.3	14.9	36.4	15.4	51.3	9.6	4.1	17.6	19.4	322.3
2068	23.2	28.9	38.6	20.9	9.9	42.2	52	61.9	16.1	7.7	50	26.9	378.4
2069	72.5	28.7	46.1	34.9	11.5	21.5	42.6	74.1	19.1	17	24.8	26.9	419.7
2070	41.1	52.7	22.3	16.7	11.6	6.6	93.9	47.4	25.7	14	15.7	35.9	383.6
2071	82.4	92.3	78.7	26.2	22.9	13.6	41.9	33.6	2.8	14.3	14.9	13.5	437.2
2072	51.8	57.2	36	22.5	6.5	25.7	10.5	36.4	27	18.8	17.6	25.9	336
2073	92.6	30.5	40.1	29.4	35.2	40.8	67.4	45.8	26.2	8.5	5.2	21	442.9
2074	38.5	41.9	30.4	24.7	13.2	12.2	29.7	63.7	25	5	4.3	33.7	322.3
2075	24.2	65.8	47.2	57.6	17.4	6.8	35.6	18.7	8.6	2.3	12	12.3	308.4
2076	60.5	52.4	34.9	19	19.3	23.5	23.2	20.5	77.1	34.8	14.3	25.1	404.5
2077	48.9	58.5	37.2	36.2	41.8	46	84.6	83.8	22.5	7.6	22.7	20.8	510.7
2078	23.3	40.4	38.5	41.8	53.6	20.4	29.1	48.6	15.8	19	5	34.3	369.9
2079	18.7	90.8	30.4	88.9	27.4	5.4	52.3	83.8	29.3	47.6	2.7	17.3	494.6
2080	34.2	22.4	20.6	40.3	10.2	17.8	40.6	68	15	18.7	46.1	22.7	356.7
2081	76	36.3	28.1	39.2	13.5	16.9	23.6	33.3	64.7	12.5	18.3	21.1	383.6
2082	23.4	62	40.9	27	9.7	67.8	70.6	109.4	10.1	18.2	22.6	6.5	468.3
2083	39.7	43.7	26.2	25	22.2	9.3	83.4	46.6	48.2	21	11.1	7	383.5
2084	48.9	67.5	48.2	29.2	23.6	27.3	49	40	23.2	16.2	11.4	28	412.5
2085	46.8	43.9	47	39.8	32.4	41.3	20.1	50.8	12.2	17	24.7	31.7	407.6
2086	38	62.6	43.6	22.8	25.5	38.4	52.8	18.6	5.1	16.7	26.1	53.5	403.6
2087	54.1	97.8	57.1	33.7	39.7	15.4	17.1	48.1	13.1	4.7	26.2	40.4	447.2
2088	40.8	54.5	78.8	42.9	17.2	13.8	42.6	64.1	14.9	10.3	20.4	21	421.3
2089	34	83.8	30.6	28.5	31.4	15.4	39.6	60.1	19.8	18.6	13.6	26.2	401.7
2090	28.5	43.4	45	29.6	20.5	43.3	31	40.3	31.8	11.2	18.3	17.3	360.1

Continued on next page

Year	Jan	Feb	Mar	Apr	May	Jun	Jul	Aug	Sep	Oct	Nov	Dec	Total
2091	37.2	25.3	23.8	16.5	5.9	20.5	48.6	64.4	29.2	25.6	5.2	37	339.1
2092	30.8	31.5	49.3	29.1	10.7	45.5	63.6	59	10.3	18	24.6	21.8	394.1
2093	64.2	28	30.3	44.4	19.3	16.5	55.5	48.6	4.5	4.6	9.3	36.9	362
2094	31	21.4	17.6	30.4	7.2	41.9	33.6	12.7	15.8	10.2	9.4	15.8	246.9
2095	81.5	63	49.6	19.4	22.4	23.2	23.7	67.1	11.1	4.1	6.1	43.4	414.4
2096	49	41.1	55.4	13	11.3	36.9	47.7	29.5	12.7	16.2	17.9	18.9	349.6
2097	31.1	46	17.4	31.8	19	14.9	38.9	23.1	31.3	10	16.8	5.2	285.5
2098	56.2	17.8	19.2	14.7	31.4	29.1	22.6	59.1	53.6	38.2	8.5	29	379.3
2099	80	71.9	40	45.4	46.3	103.9	84.5	48.3	18	6.6	13.3	20.1	578.4
2100	61.1	32.3	45.3	34.3	10.6	78.9	92.8	92.5	42.3	3.6	28.6	46.5	568.9
Average	**41.4**	**40.5**	**34.9**	**28.9**	**17.2**	**21.1**	**32.9**	**36.7**	**14.8**	**10.6**	**14.9**	**23.1**	**316.9**

3.4.2 Temperature

The mean monthly temperature data for Muslim Bagh Climate Station for the period 1990-2014 demonstrates distinct seasonal variations in both maximum and minimum temperatures throughout the year. The hottest months are June, July, and August, with July recording the highest mean maximum temperature at 29.2°C, followed by August at 28.5°C. During these months, the minimum temperatures also remain relatively high, with values such as 14.1°C in July and 11.9°C in August. On the other hand, the coldest months are December and January, with December showing the lowest mean minimum temperature of -5.9°C and January at -5.7°C. Maximum temperatures during the winter months, such as January and December, remain mild, averaging 7.4°C and 11.1°C, respectively.

The transition months, including April and October, exhibit moderate maximum temperatures of around 18.9°C and 25.2°C, with minimum temperatures closer to freezing or slightly above. These variations reflect the semi-arid climate of the region, characterized by hot summers and cold winters, with significant daily and seasonal temperature fluctuations. The temperature data over the 35-year period highlights the extreme temperature range experienced in Muslim Bagh, which has implications for agriculture, water resource management, and overall

living conditions in the region. Understanding these long-term trends is crucial for effective climate adaptation strategies and resource planning in this climate-sensitive area.

TABLE 3.4: Temperature (°C) of the project area.

Month	Jan	Feb	Mar	Apr	May	Jun	Jul	Aug	Sep	Oct	Nov	Dec	Mean
Max Temp	7.4	8.4	13.4	18.9	23.5	25	29.2	28.5	25.2	18.5	14.3	11.1	**18.6**
Min Temp	*-5.7*	-4	-1.2	3	6.6	11.2	14.1	11.9	7.7	0.8	-3.3	-5.9	**2.9**

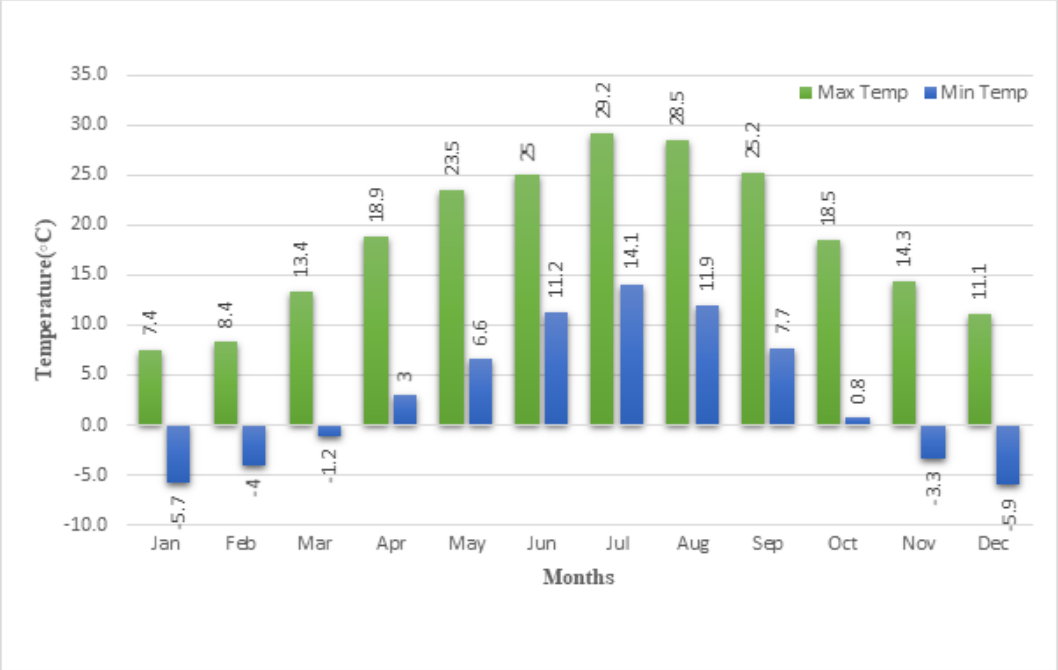

FIGURE 3.4: Mean monthly temperature of Muslim Bagh Climate Station

3.5 Data Analysis

This Research study conducts a detailed analysis of Muslim Bagh data, analyzing precipitation data from 1990 to 2014, Similarly, Temperature data of same period was adopted such as (1990-2014). It aims to discern long-term climatic trends and explore the implications of climate change. The research utilizes an extensive dataset derived from meteorological records, employing sophisticated statistical techniques and data visualization tools for in-depth examination. The analysis of temperature and precipitation patterns, variations, and changes provides essential insights into the dynamics of the local climate.

3.5.1 General-Circulation-Models (GCMs)

3.5.1.1 Climate Change Assessment

A comprehensive methodology was applied for selecting climate change models and performing bias correction, as illustrated in Figure 3-5 and detailed in the following sub-sections.

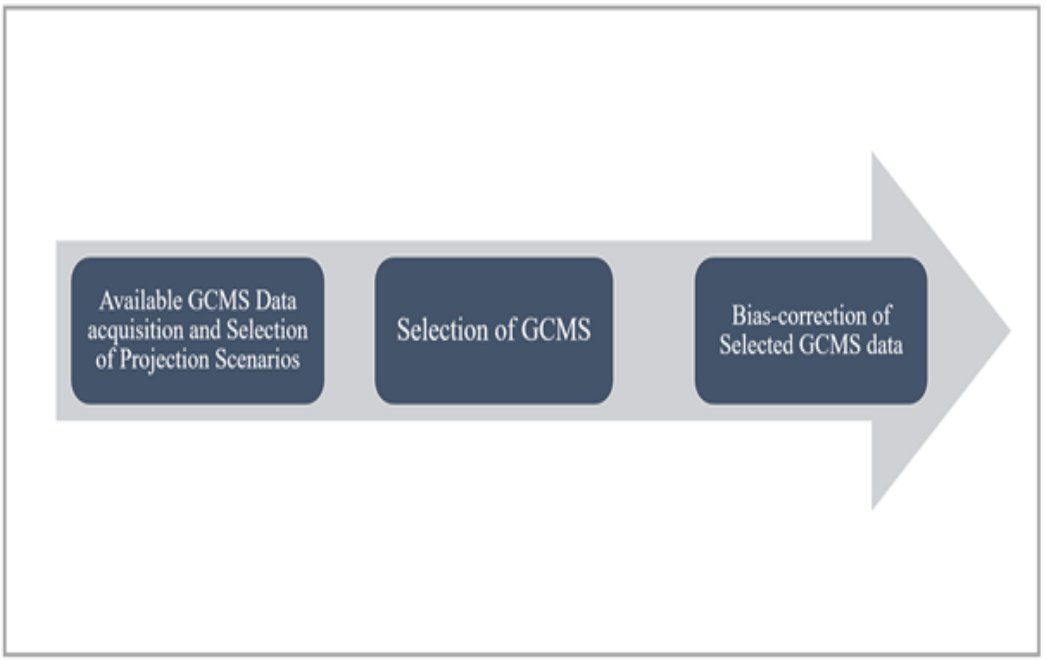

FIGURE 3.5: Schematic Diagram for climate change models selection and bias-correction

3.5.1.2 Available GCMS Data

To evaluate potential future climate scenarios at Malgagi Dam, data from various global climate models (GCMs) provided by the Coupled Model Intercomparison Project Phase 6 (CMIP-6) of the World Climate Research Programme (WCRP) were examined. Unlike CMIP-5, which allowed for the selection of any Representative Concentration Pathway (RCP) and Shared Socioeconomic Pathway (SSP), the latest CMIP-6 data is primarily available for specific combinations such as SSP1-2.6, SSP2-4.5, SSP3-7.0, and SSP5-8.5 scenarios. It should be noted that CMIP-6 has significantly expanded from CMIP-5, including more modeling groups, a wider array of future scenarios, and a greater variety of experiments.

However, CMIP-6 data at the daily scale is less available compared to CMIP-5. Furthermore, the climate data underwent quality control, and model selections were refined by focusing on the middle-of-the-road scenario SSP2-4.5 and the business-as-usual (extreme) scenario SSP5-8.5, which are recommended for climate change-inclusive hydrological impact studies.

Consequently, daily data from all CMIP-6 based GCMs for the SSP2-4.5 and SSP5-8.5 scenarios were acquired and downloaded. Approximately 31 GCMs provide daily climate data for the study area, as indicated in Table 3.4. These models were thoroughly evaluated and utilized in the analysis.

TABLE 3.5: List of available GCMs used for the study area

No.	**CMIP6 Global Climate Model**	**Country**	**Resolution (long X, lat Y) in degrees**
1	ACCESS-CM2	Australia	1.3° x 1.9°
2	ACCESS-ESM1-5	Australia	1.3° x 1.9°
3	CanESM5	Canada	2.8° x 2.8°
4	CNRM-CM6-1	France	1.4° x 1.4°
5	CNRM-ESM2-1	France	1.4° x 1.4°
6	EC-Earth3	Europe	0.7° x 0.7°
7	EC-Earth3-Veg	Europe	0.7° x 0.7°
8	GFDL-ESM4	USA	1.3° x 1.0°
9	INM-CM4-8	Russia	1.5° x 2.0°
10	INM-CM5-0	Russia	1.5° x 2.0°
11	IPSL-CM6A-LR	France	1.3° x 2.5°
12	MIROC6	Japan	1.4° x 1.4°
13	MPI-ESM1-2-HR	Germany	0.9° x 0.9°
14	MPI-ESM1-2-LR	Germany	1.9° x 1.9°
15	NorESM2-LM	Norway	1.9° x 2.5°
16	MRI-ESM2-0	Japan	1.1° x 1.1°
17	BCC-CSM2-MR	China	1.1° x 1.1°
18	CESM2	USA	0.9° x 1.3°
19	CESM2-WACCM	USA	0.9° x 1.3°
20	UKESM1-0-LL	UK	1.3° x 1.9°
21	CNRM-CM6-1-HR	France	0.5° x 0.5°
22	FGOALS-g3	China	2.3° x 2.0°
23	FIO-ESM-2-0	China	1.3° x 0.9°
24	KACE-1-0-G	South Korea	1.3° x 1.9°
25	MIROC-ES2L	Japan	2.8° x 2.8°
26	NESM3	China	1.88 x 1.88
27	NorESM2-MM	Norway	0.9° x 1.3°
28	CAMS-CSM1-0	China	1.1° x 1.1°
29	CIESM	China	0.9° x 1.3°
30	FGOALS-f3-L	China	1.0° x 1.3°
31	AWI-CM-1-1-MR	Germany	0.9° x 0.9°

3.5.1.3 Selection of Climate Scenarios

In this research, we utilized two climate scenarios, SSP 2-4.5 and SSP 5-8.5, as outlined in the IPCCs Sixth Assessment Report. The SSP 2-4.5 scenario, often referred to as a "middle-of-the-road" approach, envisions a future where greenhouse gas emissions remain substantial but begin to decline gradually after mid-century, with projected global warming of approximately 2.7°C by 2100. Conversely, SSP 5-8.5 depicts a more drastic scenario characterized by robust economic growth fueled predominantly by fossil fuels, resulting in an estimated global temperature rise of about 4.4C by the centurys end. These scenarios were selected to examine the range from moderate to severe impacts of climate change on flood frequency, thereby enhancing our understanding of future flood risks and informing effective management strategies.

3.5.1.4 Selection of GCMs

To understand the effects of future climate change in Balochistan, data from Global Climate Models (GCMs) of the CMIP-6 project was analyzed. CMIP-6 focuses on specific scenarios like SSP 2-4.5 (moderate change) and SSP 5-8.5 (extreme change). A total of 31 GCMs providing daily temperature and precipitation data were reviewed (Table 3.5).

From these, five GCMs (Table 3.6) were selected based on their resolution and ability to represent the study area accurately. These included models like AWI-CM-1-1-MR (Germany) and BCC-CSM2-MR (China). The data was then processed, and any errors or biases were corrected using the delta method to match observed historical data.

The corrected data was used to analyze how climate change under SSP 2-4.5 and SSP 5-8.5 scenarios could impact Balochistans rainfall and temperature patterns, helping predict future water challenges and risks. This information provides a solid foundation for planning and managing the regions water resources and flood risks.

TABLE 3.6: List of final selected GCMs

S. No	GCMs	Country	Horizontal grid spacing (in degrees)
1	AWI-CM-1-1-MR	Germany	0.9°x0.9°
2	BCC-CSM2-MR	China	1.1°x1.1°
3	MPI-ESM1-2-HR	Germany	0.9°x0.9°
4	MPI-ESM1-2-LR	Germany	1.9°x1.9°
5	NorESM2-MM	Norway	0.9°x1.3°

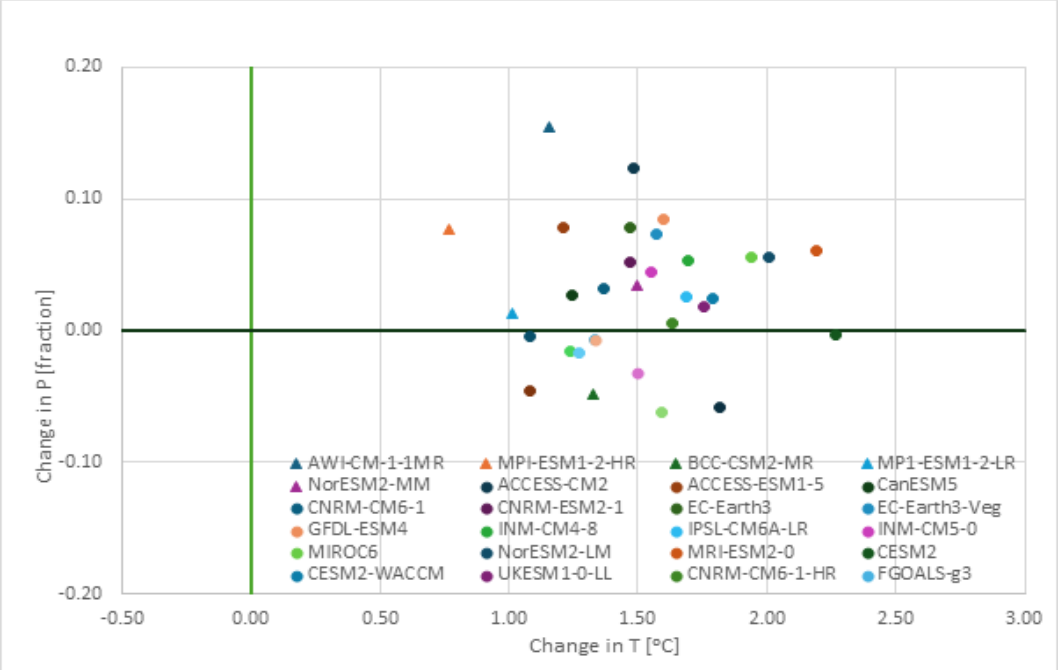

FIGURE 3.6: CMIPG GCMs Climate Change 2020-2050 Vs 1989-2014 (SSP2-4.5)

3.5.2 Statistical Downscaling of Selected GCMs Data

The statistical downscaling of selected General Circulation Models (GCMs) data was conducted using Climate Data Operators (CDO). The nearest neighbor method was applied to refine the GCM data to a 5x5 km grid resolution, ensuring localized focus for the study area. A custom grid file defined the target resolution, and the CDO remapnn operator was used for interpolation. This method efficiently assigned the value of the nearest GCM grid point to the target grid, preserving the original data characteristics.

The processed data, covering SSP 2-4.5 and SSP 5-8.5 scenarios, were downscaled and stored in NetCDF format for further analysis. The nearest neighbor method

was particularly effective for this study as it maintained data integrity while enabling high-resolution datasets essential for flood risk assessments in Balochistan.

The Nearest Neighbour method is particularly advantageous due to its simplicity, transparency, and its ability to preserve temporal variability and extremes inherent in historical observations. It does not rely on assumptions about the statistical distribution of variables, making it flexible across diverse climatic regimes. However, its accuracy is highly dependent on the availability of high-quality, long-term observational datasets and appropriate selection of predictors. The method has been effectively applied in hydrological and climate impact assessments, especially in data-scarce or topographically complex regions such as mountainous basins. Recent studies have demonstrated that the NN approach, when combined with bias correction techniques such as quantile mapping and Delta Method, can significantly improve the reliability of future climate projections at the local scale.

3.5.3 Trend Analysis and Correctness of Precipitation and Temperature

The trend analysis of precipitation and temperature for the study area was conducted using historical climate data from 1981 to 2016 and bias-corrected future projections under SSP 2-4.5 and SSP 5-8.5 scenarios for the periods 2026-2050, 2051-2075, and 2076-2100. The analysis revealed an increasing trend in precipitation intensities and temperature anomalies under future climate conditions, indicating a higher likelihood of extreme events. To ensure the correctness of the projections, the Delta Method was applied for bias correction, adjusting model outputs relative to observed historical data. This approach minimizes systematic errors present in raw GCM data, enhancing the accuracy of future estimates. Additionally, the use of five different GCMs provided a robust ensemble range, reducing uncertainty and capturing variability across wetter, drier, and hotter scenarios. The methodology ensures that precipitation and temperature trends used for hydrological modeling and dam breach analysis are reliable, realistic, and appropriately reflect the potential impacts of climate change.

3.5.4 Bias Correction of Selected GCMs Data

Above Selected five GCMs under both SSP 2-4.5 and SSP 5-8.5 scenario have been downscaled and bias-corrected using the climate stations of Muslim Bagh. Delta Change methods for bias-correction of precipitation and temperature data were used. These datasets are used for flood estimation of the Dam. Climate change impact and risk assessment has been done with bias-corrected data.

3.5.4.1 Bias-Correction Methods

The Delta Method is a widely used technique for bias correction in Global Climate Models (GCMs) and Regional Climate Models (RCMs), helping to adjust model outputs to better align with observed climate data. This method effectively corrects systematic biases in simulated climate variables such as temperature and precipitation, ensuring more reliable future projections. While various bias correction techniques exist, the Delta Method is specifically used in this study due to its simplicity and effectiveness.

3.5.4.2 Concept of the Delta Method

The Delta Method operates on the assumption that while climate models may not accurately replicate present climate conditions, they can reasonably capture relative changes or anomalies in climate variables. Instead of relying on raw climate model outputs, adjustments are applied to observed historical data to refine future projections, enhancing the accuracy of climate impact assessments.

3.5.4.3 Methodology for Bias Correction Using the Delta Method

I. Temperature Analysis

A stepwise approach is adopted for temperature analysis, beginning with the calculation of the temperature change factor (δT) using Equation 3.1,

$$\Delta T = T_{\text{model future}} - T_{\text{model historical}} \tag{3.1}$$

$T_{\text{model future}}$: Future simulated temperature from GCM

$T_{\text{model historical}}$: Historical simulated temperature from GCM

To improve the accuracy of future temperature estimates, bias correction is applied. The bias-corrected future temperature is computed using Equation 3.2, following the Delta Method approach

$$T_{\text{corrected future}} = T_{\text{observed historical}} \cdot \Delta T \tag{3.2}$$

$T_{\text{observed historical}}$: Observed historical temperature

Applying Equation 3.2 ensures that future temperature projections are adjusted based on observed historical values, improving their reliability and real-world applicability 3

II. Precipitation Analysis

For precipitation projections, a similar stepwise approach is used. The precipitation change factor (δP) is first determined using Equation 3.3.

$$\Delta P = \frac{P_{\text{model@future}}}{P_{\text{model@historical}}} \tag{3.3}$$

$T_{\text{model future}}$: Future simulated precipitation

$T_{\text{model historical}}$: Historical precipitation

This equation represents the ratio of future to historical precipitation, providing insight into projected changes in rainfall intensity.

To enhance accuracy, bias correction is applied using Equation 3.4, based on the Delta Method approach.

$$P_{\text{corrected future}} = P_{\text{observed historical}} \cdot \Delta P \tag{3.4}$$

$P_{\text{observed historical}}$: Observed historical precipitation

By applying Equation 3.4, future precipitation projections are adjusted based on observed historical data, ensuring that the estimated values more accurately reflect real-world climate conditions.

3.6 Watershed Characteristics

The catchment area of the dam at the proposed site has been delineated using the Shuttle Radar Topography Mission (SRTM) 30m Digital Elevation Model (DEM). The total catchment area is approximately 1242.12 square kilometers (480 square miles) and is situated in the Killa Saifullah District of Balochistan. The map illustrates the hydrological boundaries of the catchment, highlighting the longest stream extending 56 km, which plays a significant role in channeling runoff towards the dam reservoir. The delineation of the catchment is crucial for understanding surface water flow patterns, assessing flood potential, and conducting hydrological modeling for the region. The spatial extent of the catchment enables effective flood forecasting, watershed management, and climate impact assessments for the dam. Catchment area characteristics are shown below in Table 3.7 whereas Catchment area map of the dam site is referred below in Figure 3.7.

TABLE 3.7: Characteristics of catchment

Name	Catchment Area (Sq Km)	Length of Longest Stream (Km)
Malgagai Dam	1242.11	56

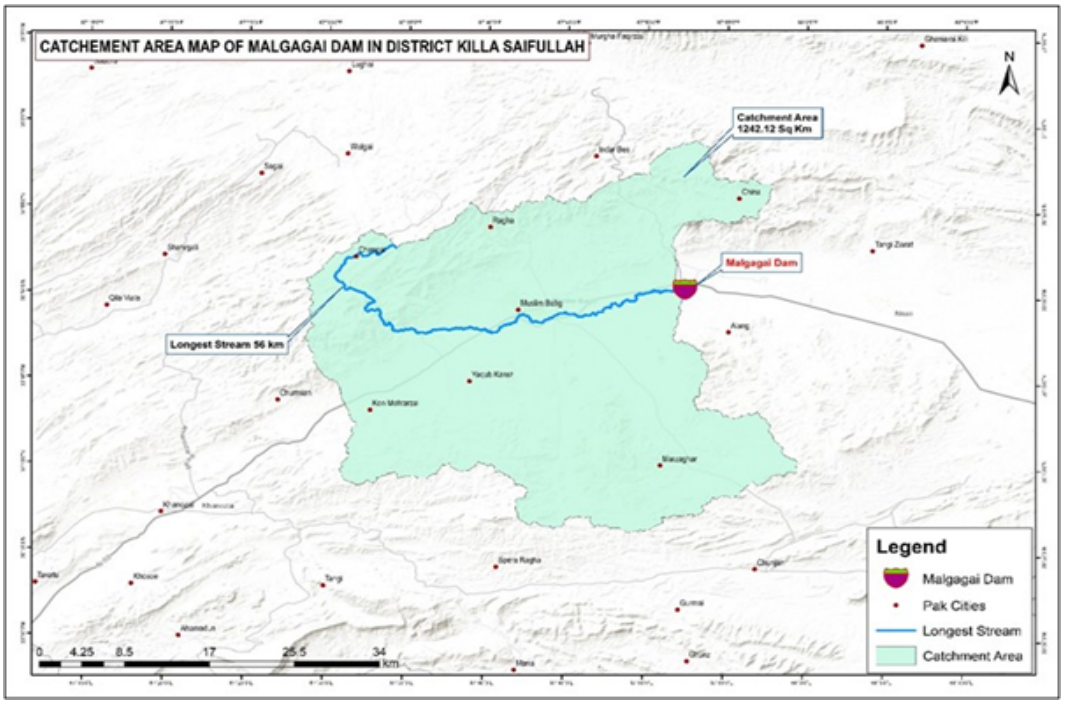

FIGURE 3.7: Catchment area map of the Dam

3.7 Hydrological Modeling Using HEC-HMS

The Hydrologic Engineering Center's Hydrologic Modeling System (HEC-HMS) was utilized in this study to simulate the rainfall-runoff processes within the watershed of dam. The analysis incorporated Geographic Information System (GIS)-derived watershed characteristics, such as land use, soil type, and topography, to calculate runoff using the SCS Curve Number (SCS-CN) method, a widely used approach for estimating direct runoff. The SCS-CN method integrates these factors to provide accurate surface runoff estimates based on rainfall intensity and catchment properties.

For this research, HEC-HMS simulated runoff under both historical climate conditions and future scenarios (SSP 2-4.5 and SSP 5-8.5) using precipitation data for various return periods, including the 100-year and 200-year floods. Precipitation data was processed to account for different return period events associated with the climate scenarios. This approach enabled the model to provide detailed flood hydrographs and peak discharge estimates, which were critical for subsequent dam breach analysis.

By combining watershed characteristics with return-period-specific precipitation data, HEC-HMS generated precise flood estimates that informed flood risk assessment and spillway design for the dam. The results contributed significantly to understanding the hydrological response of the watershed under varying climatic conditions, providing a foundation for effective dam safety and flood management strategies.

3.8 Time Correction

The catchment area was marked on 1:50,000 scale topo sheets. Similarly, 30 m resolution DEM was used to find the catchment limits and stream pattern. The catchment DEM was super imposed on the scanned SOP sheets and the catchment area and other design parameters computed from the two were found to be in close

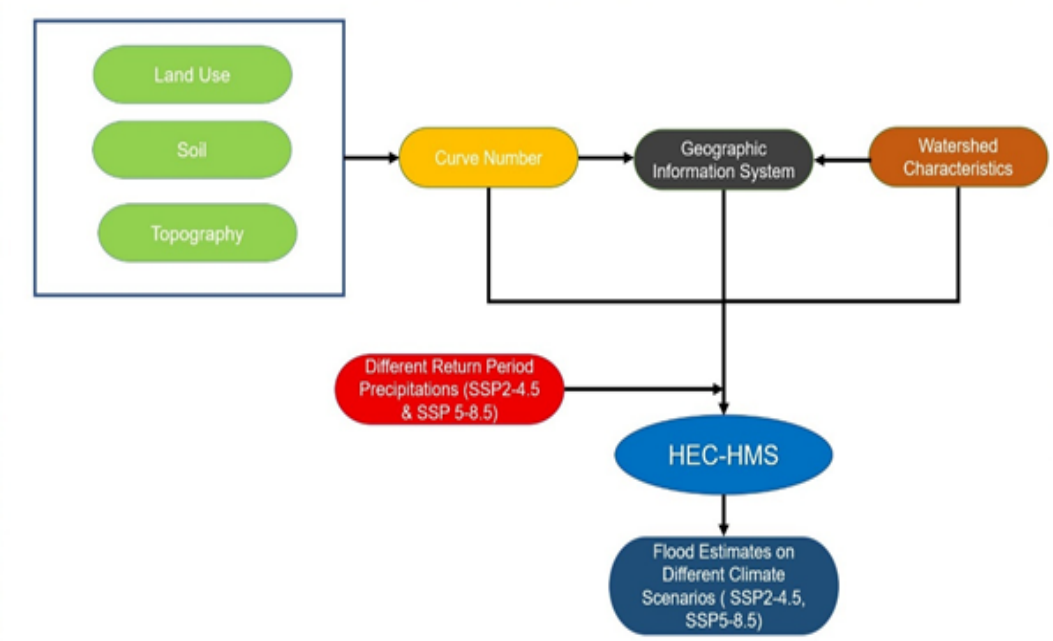

FIGURE 3.8: Methodology for HEC - HMS modelling

conformity. The time of concentration (Tc) has been calculated from Kirpichs formula as given below [164], [165]:

$$T_c = \left[\frac{11.9L^3}{H}\right]^{0.385} \tag{3.5}$$

Where,

L = Length of the longest stream in km / miles and

H = Difference in altitude of the stream at start and point of interest in m / ft.

3.9 Time Distribution of Excess Rainfall

The 24 hours time distribution of rainfall recommended by Wirasatullah Khan for Balochistan has been used. The relationship is as follows.

$$P_t = \left(\frac{t}{24}\right)^{0.2} \cdot P_{T_{(a-24)}} \tag{3.6}$$

Where,

t = time in hours;

$P_{T_{(a-24)}}$ = total 24-Hour design rainfall

3.10 Breach Parameters

In the context of this research, which focuses on dam breach analysis for an earthen dam, the use of observed breach parameters from the actual failure of the Dam forms the basis for simulating breach development and downstream impacts. This approach enables a more realistic representation of breach behavior, as it incorporates site-specific data such as the actual breach width, side slopes, and formation time observed during the 2022 overtopping event. Using these measured parameters in HEC-RAS simulations, the study captures the dynamics of the dam failure more accurately, including flood wave propagation, water surface profiles, and inundation extents.

The MacDonald-Langridge method [166], which emphasizes breach volume, offers an alternative approach to calculate breach dimensions. However, it does not explicitly estimate formation time, which is a critical parameter for understanding the rate of flood wave propagation. Similarly, the National Weather Service (NWS) method is valuable for peak discharge estimation, but it lacks explicit formulas for formation time, making it less suitable for applications requiring detailed breach evolution analysis. The Von Thun and Gillette method, which correlates breach parameters with dam height, is useful for deriving breach dimensions for simpler scenarios. Lastly, the USBR method provides a material-based approach, relying on observed dam failure data, making it a supplementary tool for validating breach parameters.

For Earthen embankment structure, the Froehlich method aligns well with the dam's characteristics, offering precise calculations of breach width, side slopes, and formation time. As highlighted in the study, for earth fill and rockfill dams, breach widths can range from 0.5 to 5.0, with side slopes varying from 0 to 1.0 (horizontal to vertical). Failure times typically range from 0.1 to 4.0 hours, depending on dam material and failure conditions, as per guidelines from agencies like USACE (1980, 2007), [167] FERC, and NWS.

This methodology allows for a regionally adapted assessment of dam safety, flood risks, and emergency response planning. By relying on actual breach data rather than generalized empirical equations, the study provides practical insights for future breach modeling, especially in data-scarce but flood-prone regions like Balochistan.

TABLE 3.8: Comparison of different methods

Method	**Breach Width**	**Formation Time**	**Peak Discharge**
Froehlich	Based onVw and Hd	Based onVw and Hd	
MacDonald-Langridge	Uses breach volume	Not directly estimated	Empirical relationship
NWS	Empirical equation	Not explicitly estimated	Based onVw and Hd
Von Thun and Gillette	Based on dam height (Hd)	Linear relationship with (Hd)	Derived indirectly
USBR	Material-dependent	Not explicitly provided	Based on observed failures

TABLE 3.9: Breach Parameters for Earthen/Rockfill dams proposed by different agencies

Dam Type	**Average Breach Width (Bav)**	**Horizontal Components of Breach side Slope (H) (H: V)**	**Failure Time, tf (Hours)**	**Agency**
Earthen/ Rockfill	(0.5 to 3.0) *HD	0 to 1.0	0.5 to 4.0	USACE 1980
	(1.0 to 5.0) * HD	0 to 1.0	0.1 to 1.0	FERC
	(2.0 to 5.0) * HD	0 to 1.0 (slightly Larger)	0.1 to 1.0	NWS
	(0.5 to 5.0) * HD	0 to 1.0	0.1 to 4.0*	USACE 2007

3.11 Method of Dam Break

Various empirical and analytical methods have been developed to estimate dam breach parameters, such as breach width, side slopes, formation time, and peak discharge. These methods are based on data from historical dam failures and consider factors like dam height, reservoir volume, and material type. Below is an explanation of commonly used methods:

3.11.1 Froehlich Method

The Froehlich method is an empirical approach that estimates breach dimensions and formation time based on dam height and reservoir characteristics. It is widely

used for earth and rockfill dams [168]. The following are the formulas which are used in Froehlich method referred as Eq. 3.1, 3.2 and 3.3.

Formulas:

I. Breach Width (Bm):

$$B_m = 0.180 \cdot V_w^{0.32} \cdot H_d^{0.19} \tag{3.7}$$

Where:

B_m: Average breach width (m) V_w: Volume of water above the breach invert (m^3) H_d: Height of the dam (m)

II. Formation Time (Tf):

$$T_f = 0.00254 \cdot V_w^{0.53} \cdot H_d^{-0.9} \tag{3.8}$$

Where:

- T_f: Breach formation time (hours)

III. Peak Outflow (Qp)

$$Q_p = 0.607 \cdot V_w^{0.295} \cdot H_d^{1.24} \tag{3.9}$$

Where:

- Q_p: Peak outflow (m^3/s)
- V_w: Volume of water above the breach invert (m)
- H_d: Height of the dam (m)

3.11.2 MacDonald and Langridge-Monopolis Method

This method is based on the relationship between dam size and breach characteristics, emphasizing the energy available for breach formation [166]. Following are the formulas which are used

Formulas:

1. Breach Volume (Bv):

$$B_v = 0.01 \cdot V_w \cdot S \tag{3.10}$$

Where:

- B_v: Breach volume (m^3)
- V_w: Reservoir volume (m^3)
- S: Spillway factor (unitless)

2. Peak Discharge (Qp):

$$Q_p = 0.367 \cdot V_w^{0.5} \cdot H_d^{1.25} \tag{3.11}$$

Where:

- Q_p: Peak outflow (m^3/s)
- V_w: Volume of water above the breach invert (m^3)
- H_d: Height of the dam (m)

3.11.3 National Weather Service (NWS) Method

This method focuses on peak discharge estimation and is commonly used for emergency planning [169].

Formulas:

1. Peak Discharge (Qp):

$$Q_p = 3.1 \cdot V_w^{0.41} \cdot H_d^{1.24} \tag{3.12}$$

Where:

- Q_p: Peak outflow (m^3/s)
- V_w: Volume of water above the breach invert (m^3)
- H_d: Height of the dam (m)

2. Breach Width (Bm):

The breach width is estimated from observed dam failures and varies depending on material type.

3.11.4 Von Thun and Gillette Method

This method is specific to earthfill dams and calculates breach parameters based on empirical relationships [168].

Formulas:

1. Breach Formation Time (Tf):

$$T_f = 0.015 \cdot H_d \tag{3.13}$$

Where:

- T_f: Breach formation time (hours)
- H_d: Dam height (m)

2. Breach Width (Bm):

$$B_m = 3.9 \cdot H_d \tag{3.14}$$

Where:

- B_m: Breach width (m)
- H_d: Dam height (m)

3.11.5 (United States Bureau of Reclamation) Method

The USBR method uses historical dam failure data to estimate breach dimensions [170].

Formulas:

1. Breach Width (Bm):

$$B_m = K \cdot H_d \tag{3.15}$$

Where K depends on the dam material:

- Cohesive soils: $K = 1.0$
- Non-cohesive soils: $K = 2.5$

3.12 Methodology for HEC RAS modelling

3.12.1 General

A systematic methodology was applied to assess the overtopping-induced dam failure and its subsequent flood impacts using the Hydrologic Engineering Center's River Analysis System (HEC-RAS). The primary focus of this study was to analyze flood hazards caused by overtopping failure of Malgagai Dam under unsteady flow conditions using a two-dimensional hydraulic model. The dam breach was simulated for historical and future climate scenarios (SSP2-4.5 and SSP5-8.5) for 100-year and 200-year return periods, allowing for a detailed assessment of downstream flood risks and their implications under changing climate conditions.

3.12.2 Data Collection and Model Setup

The first step in the dam breach analysis involved comprehensive data collection, which included:

- **Dam Specifications:** Structural attributes such as height, crest width, spillway capacity, and reservoir storage volume.
- **Breach Parameters:** Defined breach width, depth, and formation time following USACE (2007) guidelines.
- **Hydrological Data:** Inflow hydrographs, precipitation records, and peak discharge estimations.
- **Boundary Conditions:** Upstream inflow hydrographs and downstream normal depth settings.
- **Topographical Data:** High-resolution Digital Elevation Model (DEM) processed in RAS-Mapper to generate a terrain file for hydraulic analysis.

The DEM was projected into the WGS_1984_UTM_Zone 42N spatial reference system, ensuring accurate terrain representation. The study area was divided into a 2D computational mesh with a 30m 30m cell size, capturing flood flow variations effectively. Cross-sectional profiles of the river and floodplain were extracted to build geometric data for the model.

3.12.3 Hydraulic Modeling and Breach Parameters Definition

The breach was modeled as an overtopping failure, meaning that the dam's spillway and embankment were unable to safely handle excess water inflows, leading to erosion and failure. Breach width, depth, and formation time were assigned based on empirical formulas, ensuring realistic failure simulations.

- Mannings roughness coefficients (n-values) were assigned to the computational mesh according to land-use classification, following the Chow method for flow resistance calculations.
- The model incorporated various overtopping scenarios, adjusting breach width and formation time to reflect potential worst-case flood conditions.

3.12.4 Boundary Conditions and Flow Simulation

For **unsteady flow simulation**, boundary conditions were carefully defined:

- **Upstream Boundary Condition:** Represented by the dam breach outflow hydrograph, modeling overtopping flood release.
- **Downstream Boundary Condition:** Modeled using the normal depth method, ensuring accurate flood routing through the river system.

The HEC-RAS model simulated the flood wave propagation from the dam breach, evaluating flow velocity, peak discharge, flood depth, and inundation extent over time.

3.12.5 HEC-RAS Outputs and Flood Risk Assessment

The **HEC-RAS simulation** generated crucial **hydraulic outputs**, including:

- **Water Surface Profiles:** Displaying flood elevations along the river and floodplain.
- **Flood Hydrographs:** Representing discharge variations over time at critical downstream locations.
- **Stage Hydrographs:** Illustrating water level changes throughout the flood event.

These outputs provided valuable insights into peak discharge, flood depth variations, and the extent of flooding across different return periods, enabling a comprehensive risk assessment for downstream areas.

3.12.6 Flood Inundation Mapping and Risk Mitigation

The final step involved generating flood inundation maps using HEC-RAS outputs. These maps illustrated the spatial distribution and severity of flooding for different overtopping failure scenarios.

3.12.7 Conclusion

By integrating hydrological, hydraulic, and topographical data, this study offers a robust dam breach analysis framework for evaluating flood risks and mitigation strategies. The overtopping-induced failure of Malgagai Dam under various climate scenarios illustrates the growing threat posed by extreme precipitation and climate change impacts. The study emphasizes the importance of climate adaptation strategies in dam safety planning, ensuring that future flood risks are effectively managed to protect downstream communities and infrastructure.

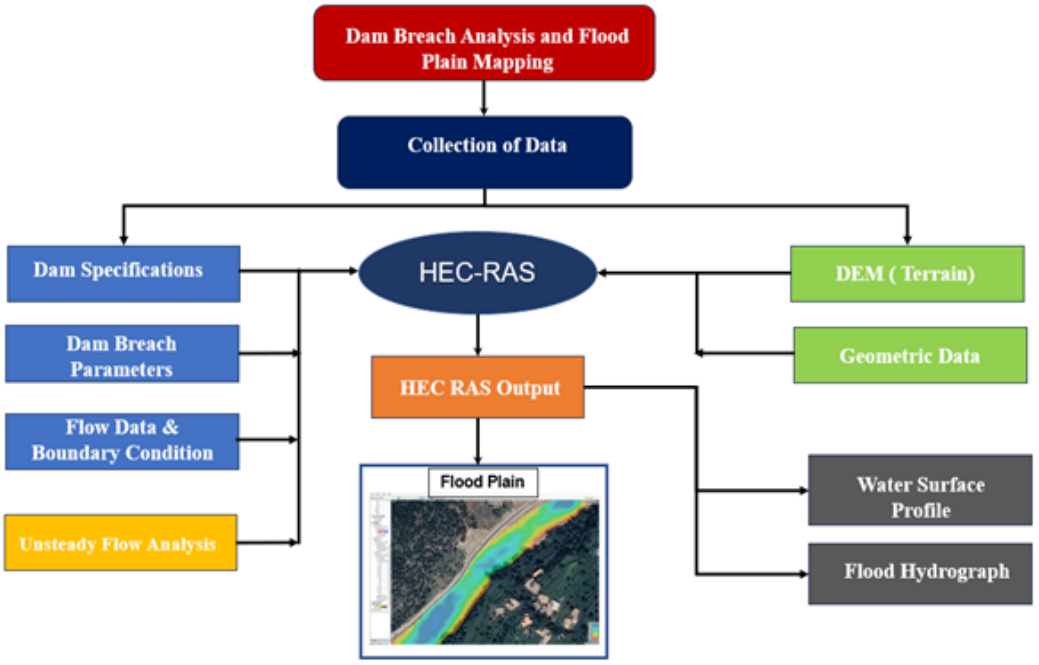

FIGURE 3.9: Methodology for HEC Ras modeling

Chapter 4

Results and Analysis

4.1 General

The results of this study provide a detailed assessment of flood risks for Malgagai Dam, considering historical conditions and future climate scenarios (SSP2-4.5 and SSP5-8.5). Findings show increasing precipitation trends for higher return periods, leading to higher inflows, peak discharges, and prolonged flood durations under future climate projections.

HEC-HMS simulations confirm that future floods will be more intense, stressing the dam's capacity. HEC-RAS breach analysis reveals wider breaches, higher velocities, and greater outflows in extreme scenarios, significantly increasing downstream flood risks. The inundation assessment shows that more villages will be affected under SSP2-4.5 and SSP5-8.5, with deeper flood levels compared to historical conditions. The Froehlich method, which considers a reduced breach width (28m vs. 151m actual), results in lower discharges but still poses substantial flood hazards. Overall, the results emphasize the growing impact of climate change on dam safety. Future extreme rainfall and flood events could exceed the dams designed capacity, highlighting the urgent need for enhanced flood management, spillway improvements, early warning systems, and mitigation strategies to protect downstream communities.

For flood frequency analysis, the Gumbel Extreme Value Distribution has been applied to precipitation data obtained from the Muslim Bagh Climate Station and

five Global Climate Models (GCMs) under the SSP 2-4.5 and SSP 5-8.5 climate scenarios. This statistical approach is widely used for predicting extreme hydrological events, such as heavy rainfall and floods, by estimating return period values for different levels of precipitation intensity. The analysis provides insights into the recurrence intervals of extreme rainfall events, which are essential for assessing flood risks and designing resilient infrastructure.

After performing the frequency analysis, the Delta Method is used to calculate the Delta Factor, which represents the relative change in climate variables between historical and future projections. This correction factor is applied to observed precipitation data to estimate future precipitation levels under the SSP 2-4.5 and SSP 5-8.5 scenarios. The adjusted values help in refining projections and reducing biases in climate model outputs.

The future projections are analyzed for different time slices, namely:

- 2026-2050
- 2051-2075
- 2076-2100

By incorporating bias-corrected climate projections, this approach ensures a more reliable assessment of future precipitation patterns. The findings highlight potential increases in extreme rainfall events, which can significantly impact flood frequency, reservoir inflows, and dam safety. These projections are crucial for hydrological modeling, flood risk assessment, and dam breach analysis, ultimately aiding in the development of adaptation strategies and mitigation measures to enhance climate resilience.

4.2 Frequency Analysis on Climate Station and Un-biased GCMs data

To evaluate potential future changes in extreme precipitation events due to climate change, a frequency analysis was conducted using both observed station data and bias-corrected outputs from Global Climate Models (GCMs). The baseline data

Table 4.1: Peak annual precipitation of base period and future for climate change scenario of SSP 2-4.5.

Base Period		**Un-Biased Future Projected Data (SSP 2-4.5)**					
Annual Prcp Peaks (1990-2014)		**Annual Prcp Peak (2026-2050)**		**Annual Prcp Peak (2051-2075)**		**Annual Prcp Peak (2076-2100)**	
Year	**Precipitation (mm)**	**Year**	**Precipitation (mm)**	**Year**	**Precipitation (mm)**	**Year**	**Precipitation (mm)**
1990	31.072	2026	27.56	2051	36.7	2076	33.24
1991	31.64	2027	44.75	2052	38.12	2077	41.87
1992	24.16	2028	34.26	2053	29.38	2078	26.82
1993	28.86	2029	29.59	2054	29.17	2079	48.05
1994	25.14	2030	31.36	2055	39.27	2080	29.12
1995	21.74	2031	38.11	2056	30.81	2081	38.55
1996	24.91	2032	37.71	2057	28.06	2082	32.08
1997	32.11	2033	24.26	2058	31.83	2083	32.99
1998	21.40	2034	31.18	2059	46.41	2084	27.64
1999	29.94	2035	32.03	2060	29.11	2085	28.22
2000	30.20	2036	27.13	2061	33.90	2086	42.76
2001	31.06	2037	26.35	2062	42.99	2087	39.00
2002	25.40	2038	26.84	2063	48.40	2088	35.39
2003	38.31	2039	37.71	2064	38.27	2089	37.93
2004	34.87	2040	34.55	2065	27.61	2090	26.19
2005	27.68	2041	44.14	2066	36.03	2091	30.90
2006	30.23	2042	36.97	2067	32.21	2092	41.56
2007	29.38	2043	36.13	2068	33.74	2093	36.83
2008	31.45	2044	30.10	2069	39.21	2094	20.89
2009	26.75	2045	28.94	2070	44.73	2095	31.78
2010	29.21	2046	37.93	2071	39.83	2096	30.26
2011	26.67	2047	31.86	2072	30.55	2097	37.53
2012	30.33	2048	30.95	2073	41.07	2098	35.85
2013	17.59	2049	48.97	2074	28.48	2099	45.47
2014	27.82	2050	30.63	2075	31.68	2100	42.11

TABLE 4.2: Peak annual precipitation of base period and future for climate change scenario of SSP 5-8.5.

Base Period		**Un-Biased Future Projected Data (SSP 5-8.5)**					
Annual Prcp Peaks (1990-2014)		**Annual Prcp Peak (2026-2050)**		**Annual Prcp Peak (2051-2075)**		**Annual Prcp Peak (2076-2100)**	
Year	**Precipitation (mm)**	**Year**	**Precipitation (mm)**	**Year**	**Precipitation (mm)**	**Year**	**Precipitation (mm)**
1990	32.44	2026	45.1	2051	41.41	2076	26.27
1991	24.03	2027	31	2052	33.84	2077	40.63
1992	28.57	2028	42.02	2053	29.19	2078	30.39
1993	39.06	2029	33.73	2054	48.2	2079	41.54
1994	21.5	2030	24.19	2055	69.49	2080	30.21
1995	24.15	2031	43.44	2056	34.98	2081	29.2
1996	30.52	2032	34.87	2057	25.78	2082	35.65
1997	20.86	2033	41.62	2058	26.04	2083	42.38
1998	30.39	2034	50.91	2059	31.05	2084	36.57
1999	30.8	2035	19.66	2060	32.39	2085	37.97
2000	32.47	2036	65.96	2061	29.23	2086	34.42
2001	26.19	2037	36.66	2062	23.85	2087	40.48
2002	33.81	2038	36.31	2063	47.48	2088	47.1
2003	34.6	2039	36.43	2064	57.52	2089	36.83
2004	29.86	2040	53.7	2065	69.39	2090	34.51
2005	32.15	2041	35.54	2066	38.55	2091	43.31
2006	46.2	2042	36.05	2067	47.39	2092	66.31
2007	33.86	2043	63.28	2068	27.23	2093	51.94
2008	35.86	2044	35.71	2069	21.85	2094	53.76
2009	29.06	2045	36.91	2070	28.22	2095	35.54
2010	27.25	2046	36.11	2071	51.85	2096	44.37
2011	41.95	2047	41.6	2072	48.32	2097	45.88
2012	19.39	2048	35	2073	45	2098	41.36
2013	29.66	2049	43.05	2074	39.45	2099	24.73
2014	29.55	2050	24.33	2075	31.94	2100	32.89

covered the period from 1990 to 2014, while future projections were analyzed for three distinct time slices: 2026-2050, 2051-2075, and 2076-2100. These future datasets were corrected for bias and correspond to two representative concentration pathways: SSP2-4.5 and SSP5-8.5.

The Gumbel Extreme Value Distribution, a widely accepted method for modeling extreme hydrological events, was applied to both the observed precipitation at the climate station and the annual maximum precipitation values from the unbiased GCM projections. This analysis enabled the estimation of peak precipitation values for various return periods (5, 10, 25, 50, 100, 200, 500, and 1000 years), helping to quantify the potential future changes in flood-inducing rainfall.

Tables 4.1 and 4.2 present the annual peak precipitation values for each year under SSP2-4.5 and SSP5-8.5 scenarios, respectively.

Tables 4.3 and 4.4 provide the results of the frequency analysis for different return period. The results indicate a consistent increase in projected peak precipitation values across all future time slices, with higher intensities observed under the SSP 5-8.5 scenario. For instance, under SSP 5-8.5, the 1000-year return period precipitation increases from 4.39 inches in the historical record to 4.12 inches in 2076-2100 (with some GCMs projecting even higher peaks up to 4.39 inches), suggesting a growing risk of extreme flood events.

TABLE 4.3: Results of frequency analysis on different return periods of climate station and un biased corrected GCMs of SSP 2-4.5 for base period and future.

Return Period (YR)	**Climate Stn Historical Muslim Bagh**	**GCM Ens 1985-2014**	**Unbiased Corrected SSP 2-4.5**		
			GCM 2026-2050 (inches)	**GCM 2051-2075 (inches)**	**GCM 2076-2100 (inches)**
5	1.72	1.24	1.50	1.57	1.56
10	2.09	1.34	1.64	1.71	1.72
25	2.56	1.47	1.82	1.89	1.91
50	2.90	1.57	1.95	2.02	2.06
100	3.25	1.66	2.08	2.15	2.20
200	3.59	1.76	2.21	2.28	2.34
500	4.05	1.89	2.39	2.46	2.53
1000	4.39	1.98	2.52	2.59	2.67

TABLE 4.4: Results of frequency analysis on different return periods of climate station and un biased corrected GCMs of SSP 5-8.5 for base period and future.

Return Period (YR)	Climate Stn Historical Muslim Bagh	GCM Ens 1985-2014	Unbiased Corrected SSP 2-4.5		
			GCM 2026-2050 (inches)	GCM 2051-2075 (inches)	GCM 2076-2100 (inches)
5	1.72	1.38	1.85	1.92	1.81
10	2.09	1.53	2.1	2.22	2.02
25	2.56	1.71	2.41	2.61	2.29
50	2.9	1.84	2.64	2.9	2.49
100	3.25	1.98	2.87	3.18	2.69
200	3.59	2.11	3.1	3.47	2.89
500	4.05	2.29	3.41	3.84	3.15
1000	4.39	2.42	3.63	4.12	3.34

4.3 Bias Correction and Variation in Precipitation

For Precipitation bias correction, the output from frequency analysis as shown in table 4.5 and table 4.6 were further used for bias correction. A delta factor is calculated between climate station and GCMs for based period of 1990 to 2014. The delta factor was then applied to future unbiased corrected GCMs for three time periods: 2026 - 2050, 2051 - 2075, 2076 - 2100 to obtain future biased corrected precipitation under two climate scenarios SSP 2-4.5 and SSP 5-8.5. The results of Bias correction on both climate scenarios of SSP 2-4.5 and SSP 5-8.5 are shown in table 4.5 and table 4.6.

The results presented in Tables 4.5 and 4.6 provide bias-corrected precipitation estimates obtained using the delta method under two climate scenarios such as SSP 2-4.5 and SSP 5-8.5. Table 4.5 (SSP 2-4.5) shows a consistent upward trend in precipitation with increasing return periods across future time slices. For instance, precipitation for the 5-year return period rises from 2.08 inches (2026-2050) to 2.17 inches (2076-2100), while the 1000-year return period increases from 5.58 inches to 5.93 inches. In contrast, Table 4.6 (SSP5-8.5) shows a more pronounced increase in extreme precipitation, particularly for longer return periods. The 100-year return period increases from 4.72 inches (2026-2050) to 5.23 inches (2051-2075), followed by a slight decline to 4.42 inches (2076-2100)-yet still significantly higher than the historical baseline. The 1000-year return period reaches a peak of 6.05 inches by the end of 2100.

Table 4.5: Results of Bias Correction on Climate Scenario of SSP 2-4.5

Return Period (YR)	Climate Stn Historical Muslim Bagh	GCM Ens 1985-2014	Delta Factor Δ	Un Biased Corrected 2-4.5			Biased Corrected 2-4.5		
				GCM 2026-2050 (inches)	GCM 2051-2075 (inches)	GCM 2076-2100 (inches)	GCM 2026-2050 (inches)	GCM 2051-2075 (inches)	GCM 2076-2100 (inches)
5	1.72	1.24	1.39	1.50	1.57	1.56	2.08	2.18	2.17
10	2.09	1.34	1.56	1.64	1.71	1.72	2.55	2.67	2.68
25	2.56	1.47	1.74	1.82	1.89	1.91	3.16	3.29	3.33
50	2.90	1.57	1.85	1.95	2.02	2.06	3.62	3.75	3.81
100	3.25	1.66	1.95	2.08	2.15	2.20	4.07	4.21	4.30
200	3.59	1.76	2.04	2.21	2.28	2.34	4.52	4.66	4.79
500	4.05	1.89	2.15	2.39	2.46	2.53	5.13	5.27	5.43
1000	4.39	1.98	2.22	2.52	2.59	2.67	5.58	5.73	5.93

Table 4.6: Results of Bias Correction on Climate Scenario of SSP 5-8.5

Return Period (YR)	Climate Stn Historical Muslim Bagh	GCM Ens 1985-2014	Delta Factor Δ	Un Biased Corrected 2-4.5			Biased Corrected 2-4.5		
				GCM 2026-2050 (inches)	GCM 2051-2075 (inches)	GCM 2076-2100 (inches)	GCM 2026-2050 (inches)	GCM 2051-2075 (inches)	GCM 2076-2100 (inches)
5	1.72	1.38	1.24	1.85	1.92	1.81	2.3	2.39	2.25
10	2.09	1.53	1.37	2.1	2.22	2.02	2.87	3.04	2.77
25	2.56	1.71	1.5	2.41	2.61	2.29	3.61	3.91	3.43
50	2.9	1.84	1.57	2.64	2.9	2.49	4.16	4.56	3.92
100	3.25	1.98	1.64	2.87	3.18	2.69	4.72	5.23	4.42
200	3.59	2.11	1.7	3.1	3.47	2.89	5.28	5.89	4.91
500	4.05	2.29	1.77	3.41	3.84	3.15	6.02	6.79	5.56
1000	4.39	2.42	1.81	3.63	4.12	3.34	6.58	7.47	6.05

These trends are further illustrated in Figures 4.1 and 4.2, which plot the frequency curves of precipitation under both scenarios. Figure 4.1 (SSP2-4.5) shows a steady increase in precipitation across all future periods, with the 100-year return period rising from 50.3 mm (1990-2014) to 67.9 mm (2076-2100). Figure 4.2 (SSP5-8.5) displays an even steeper increase, particularly during the mid-century period (2051-2075), where the 100-year return period reaches 92.3 mm, compared to 61.6 mm in the historical period. Although a slight reduction is seen in the late-century (2076-2100), precipitation values still remain significantly elevated, indicating persistent hydrological risks. Under the SSP 2-4.5 climate scenario, future

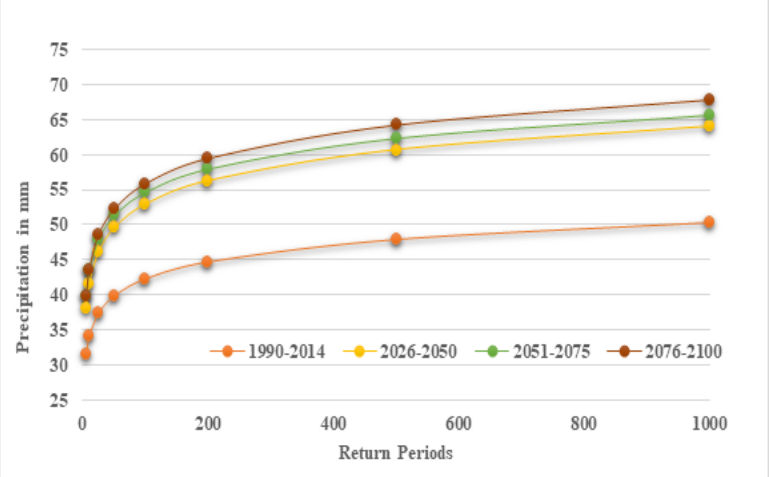

FIGURE 4.1: Results of Frequency plot of Historic, SSP 2-4.5 (2026-2050,2051-2075,2076-2100)

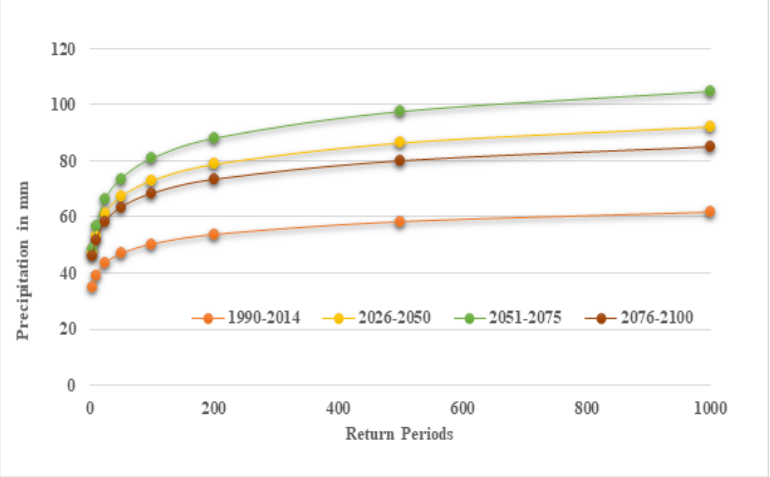

FIGURE 4.2: Results of Frequency plot of Historic, SSP 5-8.5 (2026-2050,2051-2075,2076-2100)

precipitation levels are projected to increase significantly across all return periods

when compared to the historical baseline (1990-2014). The table 4.7 presents precipitation values (in inches) for various return periods (5-year to 1000-year) across three future time slices: 2026-2050, 2051-2075, and 2076-2100. This trend is fur-

TABLE 4.7: Results of Annual Peak Precipitation for Historic and GCMs of for different return period

Precipitation in inches (SSP 2-4.5)								
Time Period	**5**	**10**	**25**	**50**	**100**	**200**	**500**	**1000**
Historical (1990-2014)	1.72	2.09	2.56	2.9	3.25	3.59	4.05	4.39
SSP 2-4.5 (2026-2050)	2.08	2.55	3.16	3.62	4.07	4.52	5.13	5.58
SSP 2-4.5 (2051-2075)	2.18	2.67	3.29	3.75	4.21	4.66	5.27	5.73
SSP 2-4.5 (2076-2100)	2.17	2.68	3.33	3.81	4.3	4.79	5.43	5.93

ther emphasized in table 4.8, which highlight significant changes in precipitation. Under the SSP 2-4.5 scenario, projected increases in precipitation are 17%-21% for the years 2026 to 2050. For the period 2051 to 2075, precipitation is expected to rise by 21% to 23%, and from 2076 to 2100, the increase is estimated to be between 21% and 26%.

These findings indicate a clear intensification of extreme precipitation events under the SSP2-4.5 scenario, highlighting the growing risk of flood hazards in the coming decades.

TABLE 4.8: Results of increase and decrease between Historic and GCMs of for different return period

Percentage Increase / Decrease								
Time Period	**5**	**10**	**25**	**50**	**100**	**200**	**500**	**1000**
SSP 2-4.5 (2026-2050)	17%	18%	19%	20%	20%	21%	21%	21%
SSP 2-4.5 (2051-2075)	21%	22%	22%	22%	23%	23%	23%	23%
SSP 2-4.5 (2076-2100)	21%	22%	23%	24%	24%	25%	26%	26%

Similarly, for SSP 5-8.5 scenario, future precipitation levels are projected to increase even more substantially than under SSP 2-4.5, particularly for higher return periods and mid-century projections. The table 4.9 presents precipitation values (in inches) for various return periods (5-year to 1000-year) over three future time slices: 2026-2050, 2051-2075, and 2076-2100. For instance, the 100-year precipitation is expected to rise from 3.25 inches in the historical baseline (1990-2014)

to 4.72 inches (2026-2050), 5.23 inches (2051-2075), and slightly decrease to 4.91 inches in the 2076-2100 period, though still significantly above historical levels. The 4.10 table shows projected increases under the SSP 5-8.5 scenario in pre-

TABLE 4.9: Results of Annual Peak Precipitation for Historic and GCMs of for different return period

Precipitation in inches (SSP 5-8.5)								
Time Period	**5**	**10**	**25**	**50**	**100**	**200**	**500**	**1000**
Historical (1990-2014)	1.72	2.09	2.56	2.9	3.25	3.59	4.05	4.39
SSP 5-8.5 (2026-2050)	2.3	2.87	3.61	4.16	4.72	5.28	6.02	6.58
SSP 5-8.5 (2051-2075)	2.39	3.04	3.91	4.56	5.23	5.89	6.79	7.47
SSP 5-8.5(2076-2100)	2.25	2.77	3.43	3.92	4.42	4.91	5.56	6.05

cipitation are 25-33% for the years 2026 to 2050. For the period 2051 to 2075, precipitation is expected to rise by 28% to 41%, and from 2076 to 2100, the increase is estimated to be between 24% and 28%.

These findings indicate a strong likelihood of more intense and frequent extreme precipitation events under the SSP5-8.5 scenario. The sharp increases, particularly for rare and severe events (e.g., 200- to 1000-year return periods), underscore the heightened flood risk associated with continued high emissions. This scenario emphasizes the urgent need for proactive adaptation strategies, robust hydrological infrastructure, and integrated water resource planning to mitigate the compounding effects of climate change. These findings collectively empha-

TABLE 4.10: Results of increase and decrease between Historic and GCMs of for different return period

Percentage Increase / Decrease								
Time Period	**5**	**10**	**25**	**50**	**100**	**200**	**500**	**1000**
SSP 5-8.5 (2026-2050)	25%	27%	29%	30%	31%	32%	33%	33%
SSP 5-8.5 (2051-2075)	28%	31%	35%	36%	38%	39%	40%	41%
SSP 5-8.5 (2076-2100)	24%	25%	25%	26%	26%	27%	27%	28%

size the intensification of extreme rainfall under future climate conditions - more

severely under SSP5-8.5and highlight the growing need for climate-resilient flood management. The upward trajectory in precipitation with return periods necessitates integrating climate projections into dam safety evaluations and flood risk assessments. Enhanced design strategies such as increasing spillway capacity, reassessing reservoir storage, and establishing effective emergency response plans are vital. Furthermore, the bias-corrected precipitation values serve as critical inputs for hydrological simulations in HEC-HMS, which are used to generate flood hydrographs and estimate peak discharges. These outputs, in turn, inform dam breach analysis in HEC-RAS, enabling comprehensive hazard assessment and the development of robust mitigation and adaptation measures.

4.4 Bias Correction and Variation in Temperature

For temperature analysis, data from the Muslim Bagh climate station (1990-2014) and five GCMs for the same period were initially used for bias correction. Daily temperature data from both sources were converted to mean monthly values. The same methodology was applied to the unbias-corrected temperature data of the GCMs for the future period (2014-2100). A delta factor (δ) was calculated as the difference between the historical observed temperature (Muslim Bagh) and the corresponding GCM values. This delta factor was then added to the future unbias-corrected GCM temperatures to obtain the future bias-corrected temperature values.

The table 4.7 below summarizes the monthly temperature data and the bias correction process under the SSP2-4.5 scenario.

Similarly, for SSP 5-8.5 scenario, the same bias correction method was applied. In this case, some historical GCM temperatures were found to be higher than the observed temperatures, resulting in negative delta values for certain months. These negative deltas indicate that the GCM over-estimated temperatures during the historical baseline period.

Table 4.11: Results of Bias correction under Climate change Scenario of SSP 2-4.5

Year	Historic		Delta	Unbiased Corrected Future Temperature GCM 2-4.5	Biased Corrected Future Temperature GCM 2-4.5
	Muslim Bagh (1985-2014)	GCM (1985-2014)		2014-2100	2014-2100
Jan	0.9	-0.7	1.6	1.45	3.02
Feb	2.2	0.7	1.5	3.41	4.91
Mar	6.1	4.5	1.6	7.04	8.66
Apr	11	9	2	11.58	13.57
May	15.1	13	2.1	15.44	17.49
Jun	18.1	16.1	2	18.78	20.77
Jul	21.7	19.9	1.7	21.15	22.88
Aug	20.2	18.3	1.9	19.03	20.88
Sep	16.5	14.3	2.2	14.63	16.82
Oct	9.7	7.3	2.3	8.45	10.79
Nov	5.5	3.5	2	4.77	6.74
Dec	2.6	0.8	1.8	2.4	4.19

Table 4.12: Results of Bias correction under Climate change Scenario of SSP 5-8.5

Year	Historic		Delta	Unbiased Corrected Future Temperature GCM 2-4.5	Biased Corrected Future Temperature GCM 2-4.5
	Muslim Bagh (1985-2014)	GCM (1985-2014)		2014-2100	2014-2100
Jan	0.9	-1	1.8	2	3.78
Feb	2.2	0.9	1.3	4.6	5.85
Mar	6.1	6	0.1	9.5	9.55
Apr	11	12.1	-1.2	15.6	14.48
May	15.1	17.5	-2.5	20.8	18.35
Jun	18.1	21.8	-3.7	25.4	21.7
Jul	21.7	26.9	-5.2	28.6	23.32
Aug	20.2	24.8	-4.6	25.7	21.12
Sep	16.5	19.2	-2.8	19.7	16.95
Oct	9.7	9.9	-0.2	11.4	11.18
Nov	5.5	4.8	0.7	6.4	7.17
Dec	2.6	1.1	1.5	3.2	4.75

Figure 4.3 illustrates the variation in mean monthly temperatures between the historical period (1985-2014) at the Muslim Bagh climate station and the future bias-corrected temperature projections (2014-2100) under the SSP 2-4.5 scenario. The blue curve represents historical observations, while the orange curve shows future projections after bias correction using the delta method.

The graph clearly demonstrates a consistent rise in temperatures throughout the year under the SSP 2-4.5 scenario. The increase is most prominent during the summer months. For instance, the mean monthly temperature in July rises from 21.65C (historic) to 22.9°C (future), and in June from 18.1°C to 20.8°C. Even in cooler months, such as January and February, the future temperatures increase noticeably from 0.85°C to 3.0°C and from 2.2°C to 4.9°C respectively.

This upward shift in temperature across all months highlights the warming trend associated with the SSP 2-4.5 pathway, which represents a stabilization scenario with moderate mitigation efforts. The minimum temperature varies in the month of September i.e. 0.40°C and maximum temperature variation of 2.7°C was expected in the month of February. The increased temperature levels may significantly affect evapotranspiration rates, snowmelt timing, and overall hydrological responses in the region. Such changes reinforce the need to consider temperature-driven impacts in water resource planning and climate resilience strategies. Similarly, Figure 4.4 displays the variation in mean monthly temperatures between the historical period (1985-2014) recorded at the Muslim Bagh climate station and future bias-corrected temperature projections (2014-2100) under the high-emission SSP 5-8.5 scenario. The blue line represents historical observations, while the orange line depicts future bias-corrected values from GCM data.

Compared to the historical record, there is a substantial and more pronounced increase in temperatures throughout the year under SSP 5-8.5. The minimum temperature varies in the month of September i.e. 0.50°C and a maximum temperature variation of 3.7°C was expected in the month of February. The difference is particularly noticeable during the spring and summer months. For instance, the mean temperature in April increases from 10.95°C to 14.48°C, and in July from 21.65°C to 23.32°C. Similarly, even during the cooler months, January and

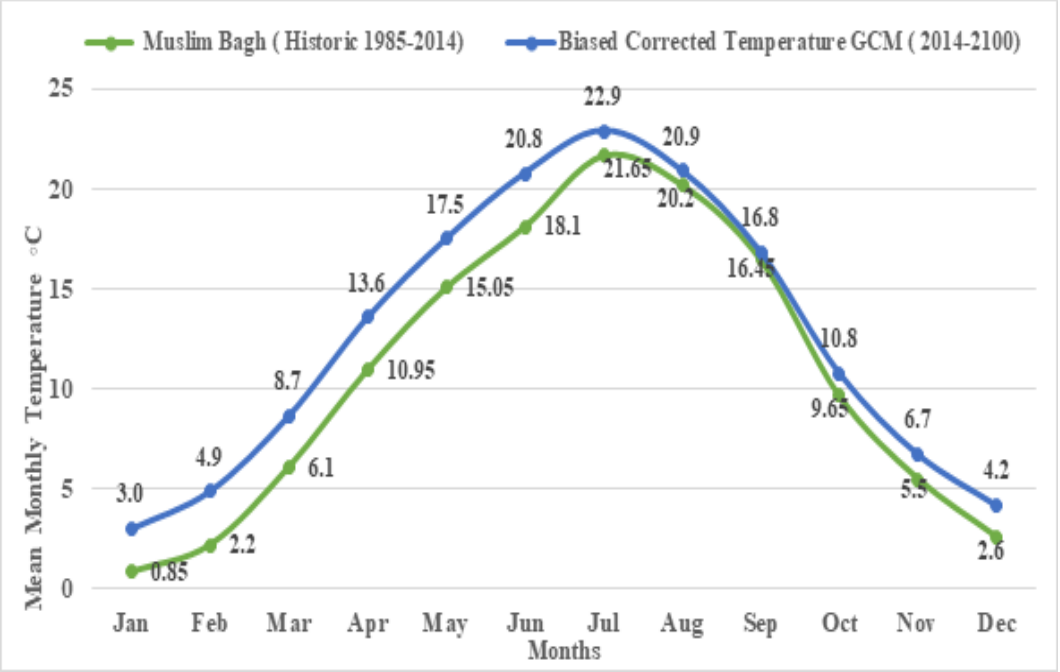

FIGURE 4.3: Results of temperature variation between Historic and Future bias corrected temperature SSP 2-4.5

February exhibit significant warming, increasing from 0.85°C to 3.78°C and from 2.2°C to 5.85°C, respectively.

This pattern suggests a more intense warming trend under the SSP 5-8.5 pathway when compared to SSP 2-4.5. The elevated future temperatures could have wide-ranging implications on snowmelt, water availability, agriculture, and ecosystem health. The projected rise in temperature, especially during peak summer, indicates an increased likelihood of heatwaves and altered seasonal hydrology, further emphasizing the need for climate adaptation and mitigation measures in the region. In conclusion, the application of bias correction using the delta method ensures that future temperature projections from GCMs are more accurately aligned with observed historical data from the Muslim Bagh climate station. This process enhances the reliability of climate model outputs by correcting systematic deviations inherent in raw GCM simulations. The results clearly show that under both SSP 2-4.5 and SSP 5-8.5 scenarios, future temperatures are projected to increase across all months, with higher warming observed under the high-emission SSP 5-8.5 pathway. These corrected temperature datasets provide a critical input for further hydrological modeling and climate impact assessments, ultimately supporting more informed planning and adaptation strategies in the region.

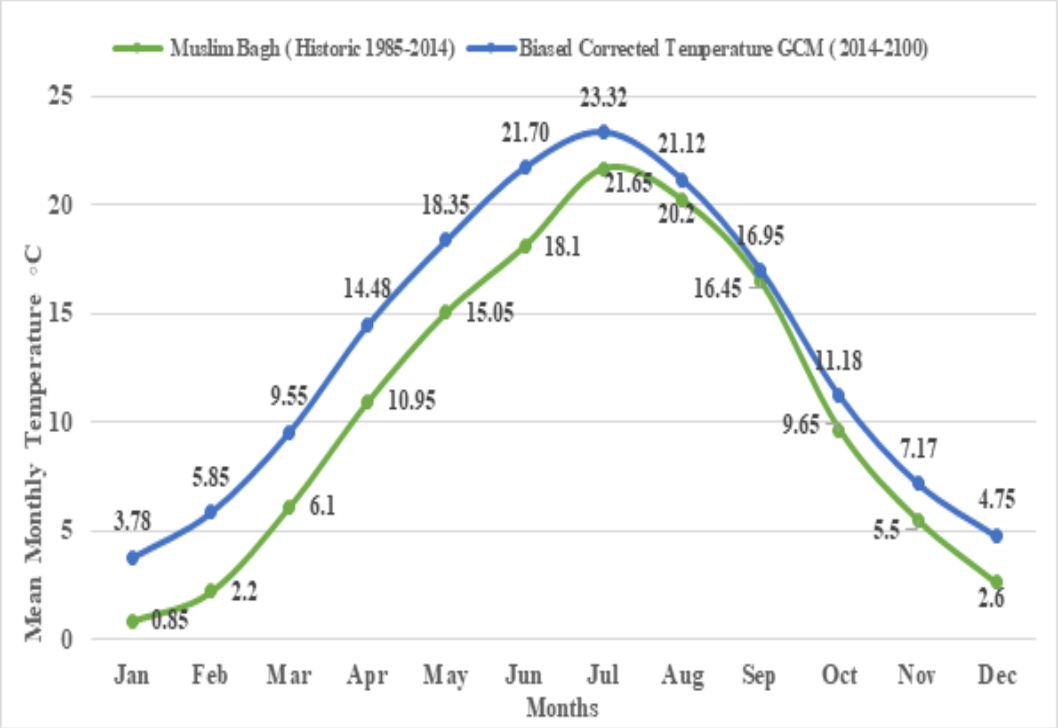

FIGURE 4.4: Results of temperature variation between Historic and Future bias corrected temperature SSP 5-8.5

4.5 Flood Estimation

The Hydrologic Engineering Centers Hydrologic Modeling System (HEC-HMS) was used to simulate for the estimation of flood discharge on different return period. The Soil Conservation Service Curve Number (SCS-CN) method was selected for runoff estimation due to its wide applicability and suitability for ungauged basins. The SCS-CN method computes direct runoff based on rainfall depth, land use, hydrologic soil group, and antecedent moisture condition. Land use and soil data were extracted from Sentinel-2 satellite imagery (2021) and soil maps, respectively, to calculate a weighted curve number for the catchment.

Precipitation inputs obtained from table 4.5 and 4.6, including bias-corrected rainfall for different return periods under climate scenarios (SSP2-4.5 and SSP5-8.5), were used to simulate excess precipitation. The SCS Unit Hydrograph method was used for transformation of excess rainfall into direct runoff hydrographs. Muskingum routing method was applied for channel flood routing to model the attenuation and translation of flood waves through the reservoir and downstream channel system.

Model parameters such as time of concentration and lag time were estimated using empirical formulas, including Kirpichs equation, which considers basin length and slope.

The peak outflow from the Dam, corresponding to a 100-year return period, is estimated at 47,464.6 cusecs under the SSP 2-4.5 climate scenario, and 56,130.0 cusecs under the SSP 5-8.5 scenario. The inflow and outflow values for the historical period, SSP 2-4.5, and SSP 5-8.5 across various return periods are presented in Tables 4.11, 4.12, and 4.13, respectively. Flood Hydrographs are shown below from Figure no. 4.5 to Figure no. 4.10.

The flood hydrograph results for the 100-year and 200-year return periods under historical and future climate scenarios show that flood levels are expected to increase over time. The historical flood hydrographs indicate lower peak discharges compared to future projections, meaning that as climate change progresses, extreme rainfall events will generate higher inflows into the reservoir.

For SSP 2-4.5, the peak discharges for both 100-year and 200-year floods are greater than the historical values, suggesting an increase in flood intensity. Under SSP5-8.5, the highest peak discharges are observed, indicating that more extreme climate conditions will result in significantly larger flood volumes.

These findings indicate that future floods will be more intense and last longer, increasing the risk of dam overtopping or failure if proper mitigation measures are not taken. The simulated outflow hydrographs from HEC-HMS served as input boundary conditions for subsequent dam breach and inundation modeling in HEC-RAS, providing a comprehensive assessment of flood behavior under both historical and future climate conditions which helps in evaluating potential flood risks in downstream areas and developing inundation maps for emergency planning.

Table 4.13: Output of Flood discharges from HEC-HMS Model (Conventional Scenario)

Flood Analysis (Climate Station Based)		
Return Period	**Inflow Flood (Cusecs)**	**Outflow Flood (Cusecs)**
100	31292.1	30008
200	37893.2	36573.4

TABLE 4.14: Output of Flood discharges from HEC-HMS Model (Climate Change Scenario SSP 2-4.5)

Flood Analysis (SSP 2 -4.5)		
Return Period	**Inflow Flood (Cusecs)**	**Outflow Flood (Cusecs)**
100	48177.6	47464.6
200	57766.4	57039

TABLE 4.15: Output of Flood discharges from HEC-HMS Model (Climate Change Scenario SSP 5-8.5)

Flood Analysis (SSP 5 -8.5)		
Return Period	**Inflow Flood (Cusecs)**	**Outflow Flood (Cusecs)**
100	57118.3	56130
200	68009.6	66998.9

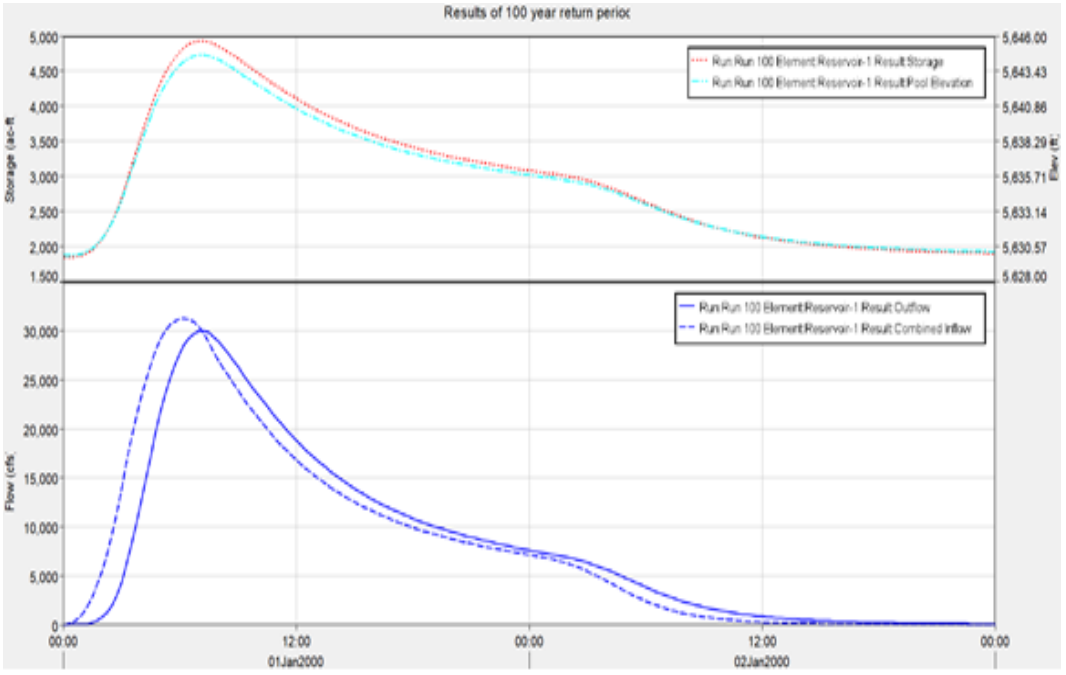

FIGURE 4.5: Flood Hydrograph of Historic (Muslim Bagh) of 100 Year Return Period

4.6 DAM Breach Modeling

4.6.1 General

The Hydrologic Engineering Centers River Analysis System (HEC-RAS) was used to simulate dam breach scenarios and model the downstream flood propagation from the Dam. The outflow hydrographs generated by HEC-HMS served as the

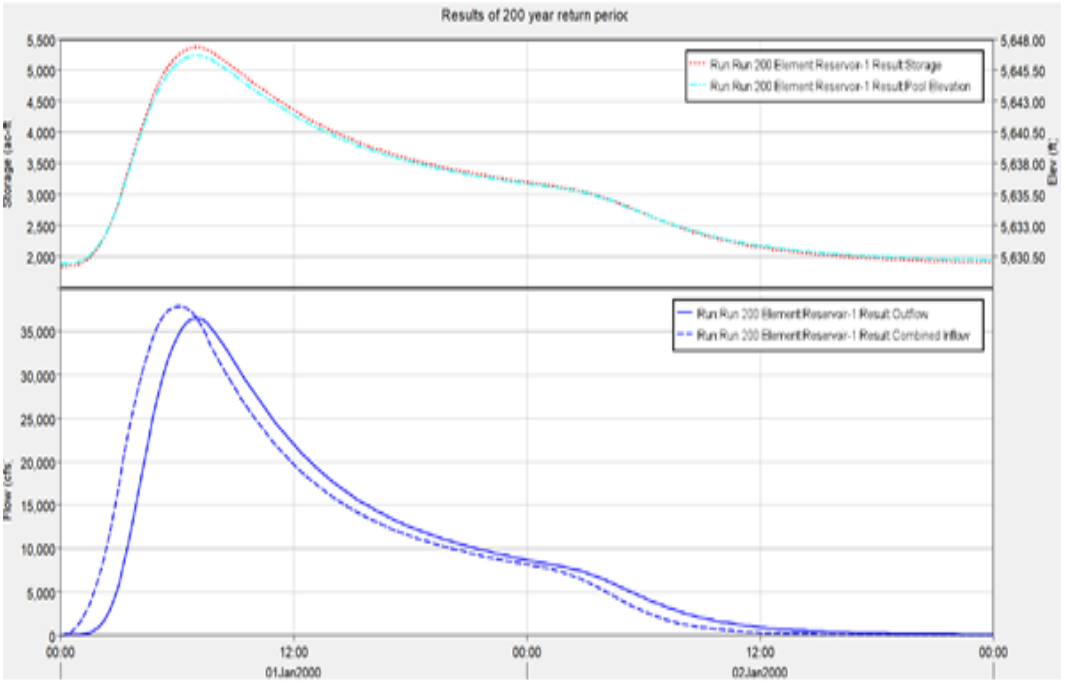

FIGURE 4.6: Flood Hydrograph of Historic (Muslim Bagh) of 200 Year Return Period

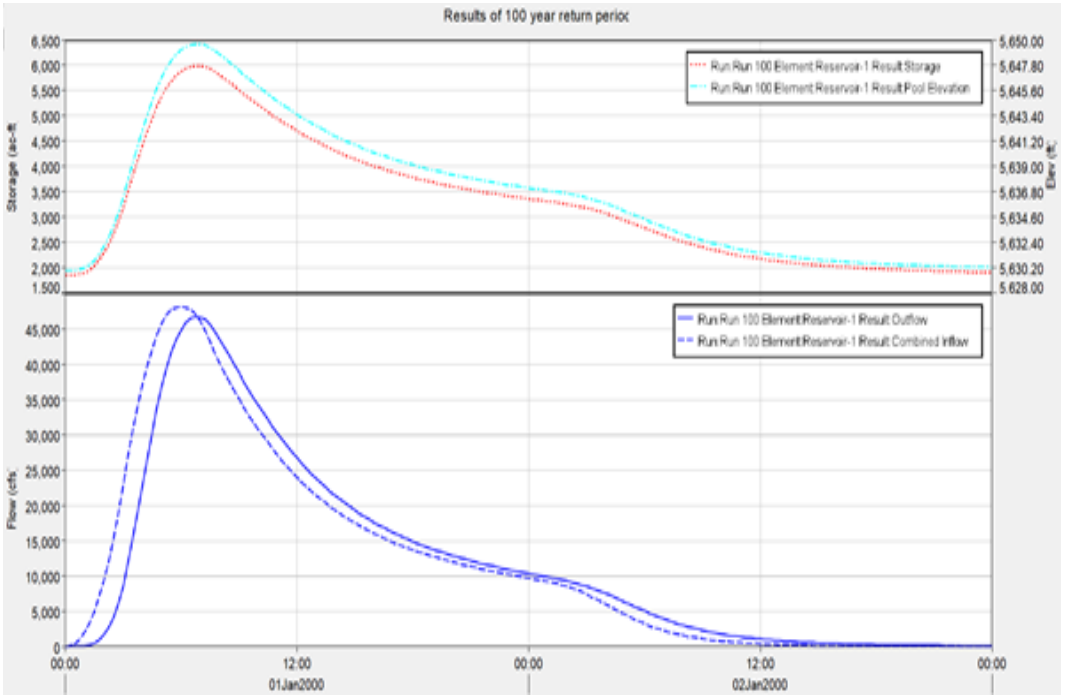

FIGURE 4.7: Flood Hydrograph of SSP 2-4.5 of 100 Year Return Period

primary input for unsteady flow simulations. These hydrographs, developed using the SCS Curve Number method, represent flood discharges for different return periods and climate scenarios (historical, SSP 2-4.5, and SSP 5-8.5), and were used as upstream boundary conditions in the HEC-RAS model.

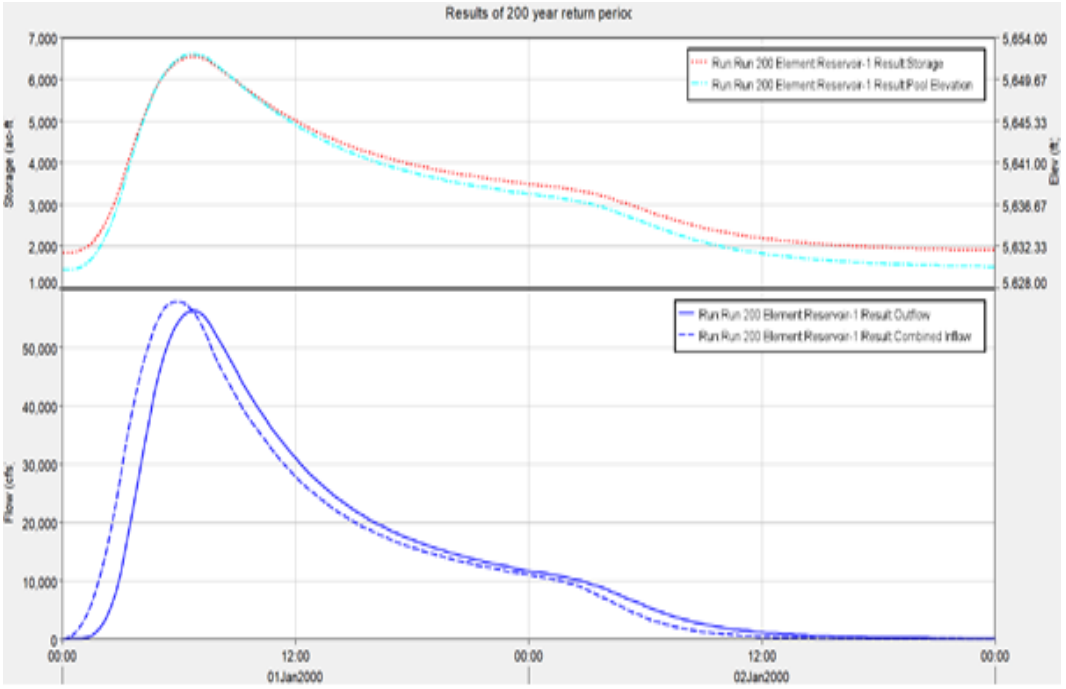

FIGURE 4.8: Flood Hydrograph of SSP 2-4.5 of 200 Year Return Period

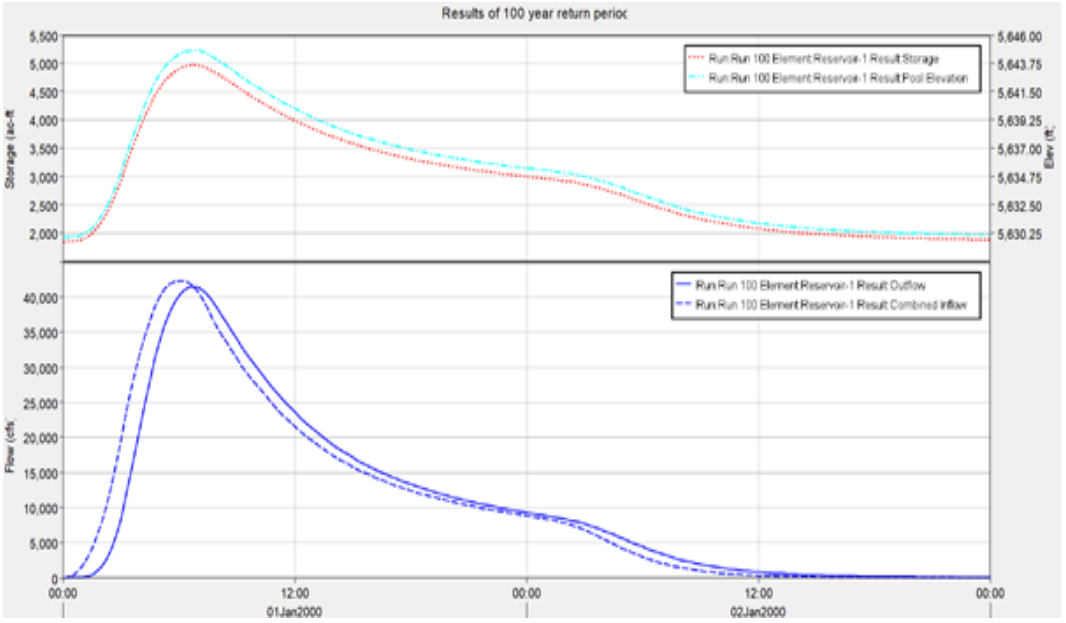

FIGURE 4.9: Flood Hydrograph of SSP 5-8.5 of 100 Year Return Period

The dam breach simulation was carried out in the 2D unsteady flow module of HEC-RAS. The dam breach parameters including breach width, side slopes, and failure time were based on empirical relationships and physical characteristics of the earthen dam. The computational domain was constructed using high-resolution SRTM DEM (1 arc-second) and processed through RAS Mapper to delineate terrain features, assign hydraulic boundaries, and generate the 2D flow

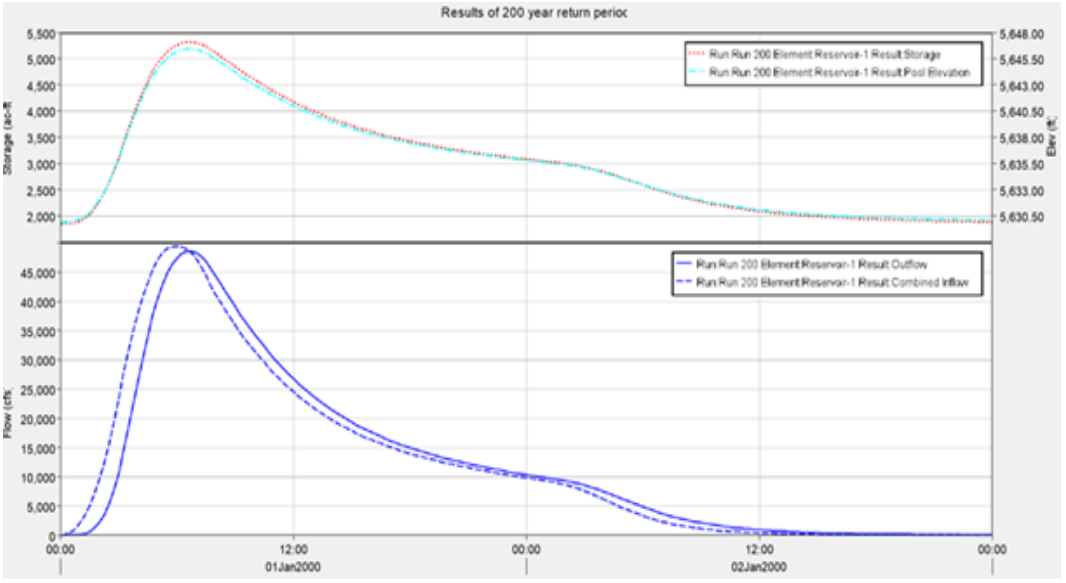

FIGURE 4.10: Flood Hydrograph of SSP 5-8.5 of 200 Year Return Period

area. Figure 4.11 shows the defined storage area behind the dam and the downstream computational grid used for hydraulic routing. The dam breach geometry,

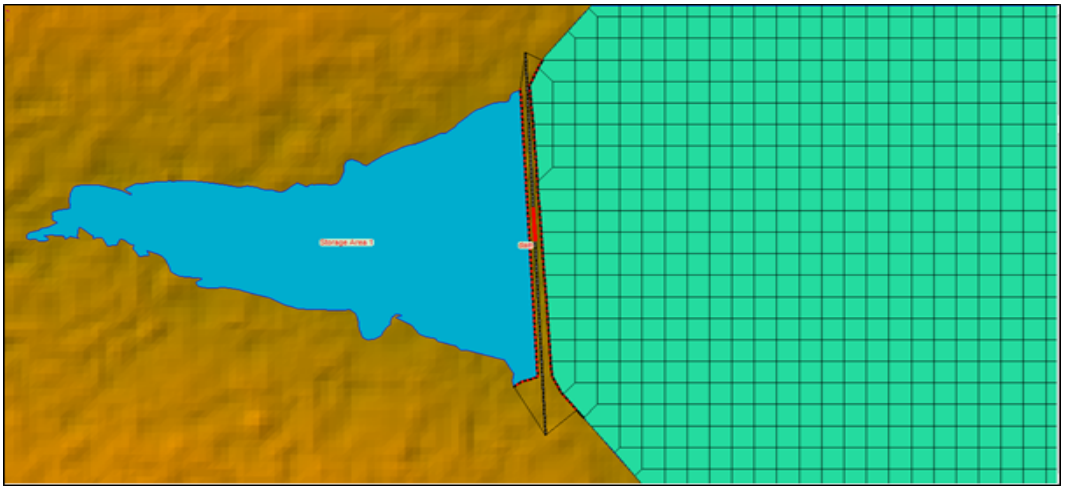

FIGURE 4.11: Dam Storge Area, Dam Connection and Downstream 2D area

including the final breach shape and elevation profile, is illustrated in Figure 4.12, where the centerline terrain, spillway, and breach cross-section are shown. This profile forms the basis for calculating breach outflow hydrographs and the resulting flood wave. The model was executed for 100 and 200-year return periods, with outputs including peak flow, water surface elevation and flood extent which are explained in the below sections. These outputs were used to generate flood inundation maps for historical and future climate scenarios, enabling a robust evaluation of dam safety, downstream risk, and emergency planning.

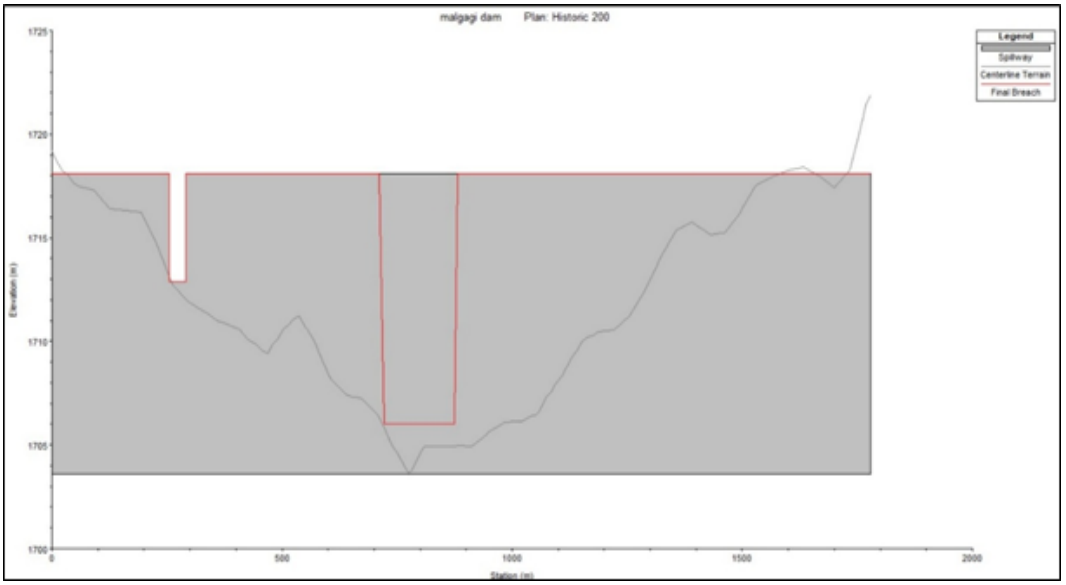

FIGURE 4.12: Dam profile along with spillway and Breach width

4.6.2 Breach Width Development under Different Scenarios

The breach width analysis offers valuable understanding of the failure behavior of Dam under both historical and projected climate scenarios. The actual breach event resulted in a final breach width of 151 meters, with a right abutment side slope of 0.65:1 and a left abutment slope of 1:1. Across all simulation cases, the breach width initially remains at 0 meters, reflecting the dam's structural stability. However, once the failure is triggered, a rapid and sharp increase in breach width is observed, reaching the maximum width of approximately 151 meters in all scenarios. This abrupt expansion indicates a high-energy erosion process, typical of dam breaches occurring under intense hydrological conditions.

4.6.2.1 Historic Scenarios

In the Historic 100-Year Return Period scenario (Figure 4.13), breach formation is observed during the early morning hours of December 6. The breach width increases rapidly, reaching approximately 75 meters during the initial stage and then expanding to the maximum width of 151 meters. In comparison, the Historic 200-Year Return Period (Figure 4.14) shows an earlier breach initiation, with the width initially rising to 105.11 meters before reaching and maintaining the same

maximum width of 151 meters. The faster breach development in the 200-year event reflects the influence of higher inflow intensity, resulting in a more rapid structural failure.

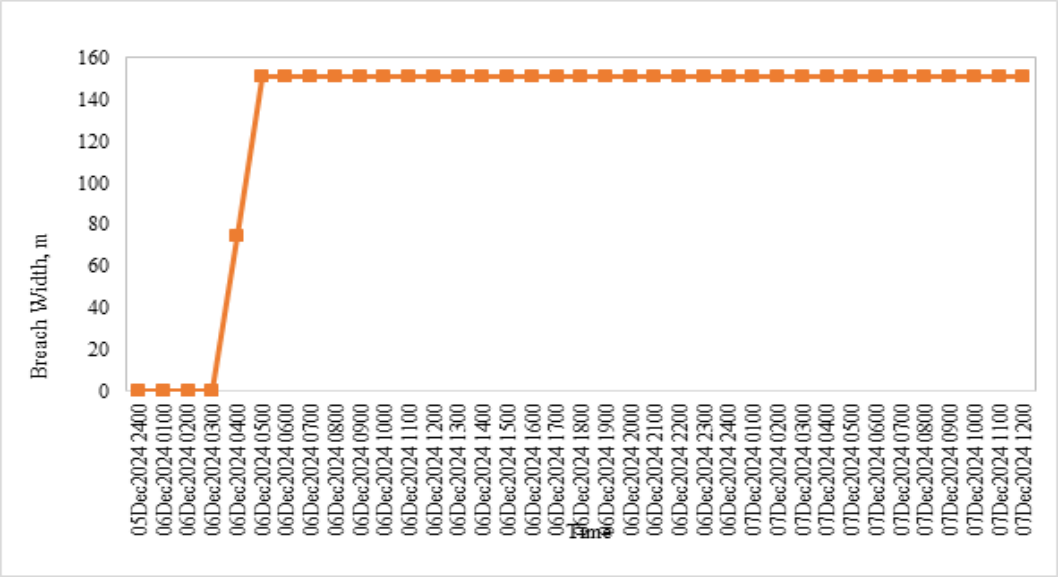

FIGURE 4.13: Breach Width on Historic 100 Year Return Period

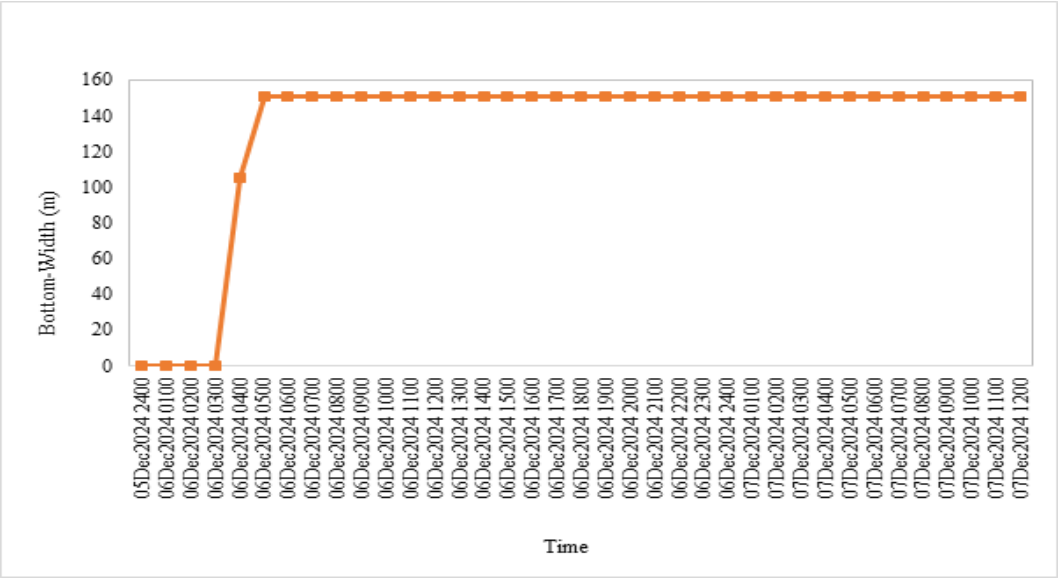

FIGURE 4.14: Breach Width on Historic 200 Year Return Period

4.6.2.2 Future Scenarios - SSP 2-4.5

Under the SSP 2-4.5 (moderate emission) scenario, the breach exhibits a similarly rapid development pattern. In the 100-Year Return Period event (Figure 4.15),

breach initiation occurs during the early hours of December 6, with the width rapidly increasing to approximately 94.56 meters, and reaching the maximum breach width of 151 meters within a span of two hours. For the 200-Year Return Period (Figure 4.16), breach development begins shortly afterward, expanding to 136.64 meters in the initial phase and stabilizing at 151 meters within the next hour. These results indicate heightened structural vulnerability of the dam even under moderate climate change conditions, as increased inflow rates accelerate breach formation and peak expansion.

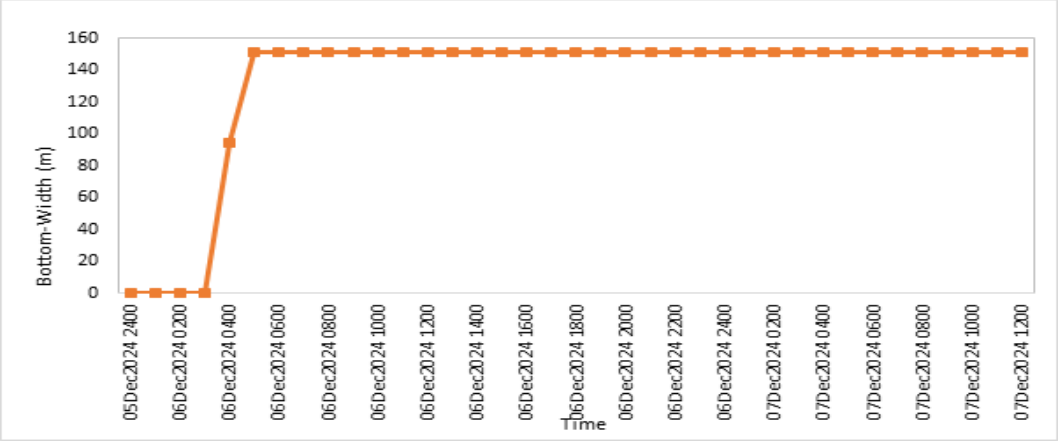

FIGURE 4.15: Breach Width on SSP 2-4.5 of 100 Year Return Period

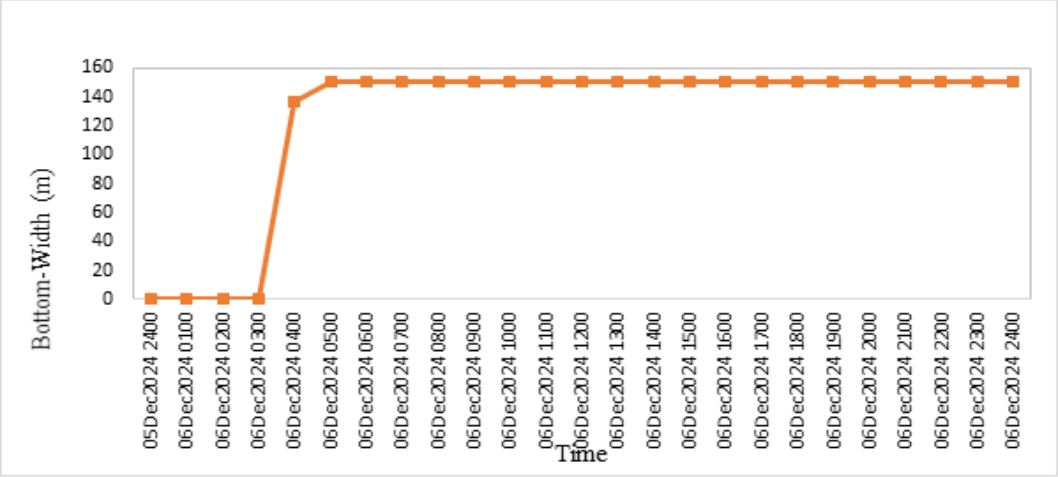

FIGURE 4.16: Breach Width on SSP 2-4.5 of 200 Year Return Period

4.6.2.3 Future Scenarios - SSP 5-8.5

Under the SSP 5-8.5 climate scenario, breach development occurs earlier and more rapidly, driven by intensified hydrological inputs. In the 100-Year Return Period

event (Figure 4.17), breach initiation takes place during the early hours, with the width quickly expanding to approximately 104.64 meters and reaching the maximum breach width of 151 meters shortly thereafter. A similar trend is observed in the 200-Year Return Period (Figure 4.18), where the breach rapidly widens to 146.17 meters before stabilizing at 151 meters within a short time frame. These results highlight the accelerated failure progression associated with more extreme inflow conditions under high-emission scenarios.

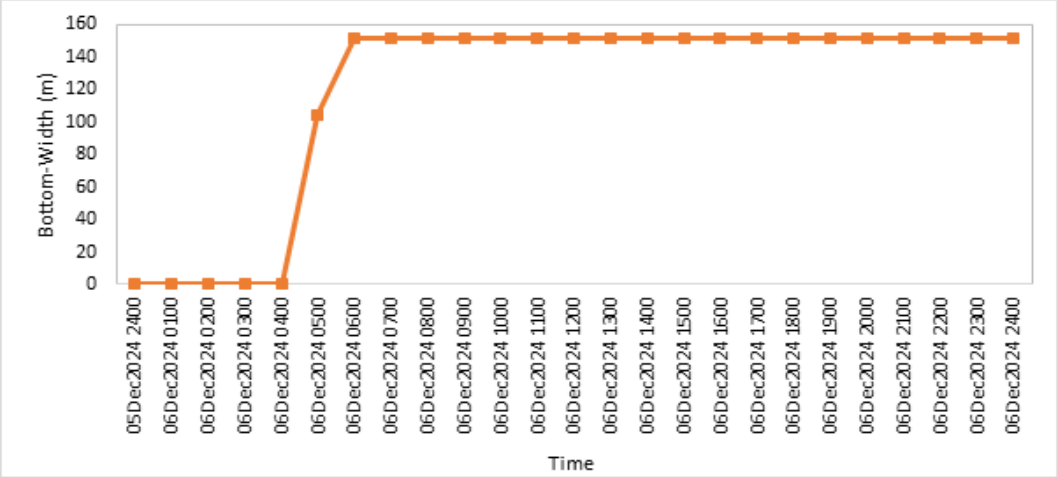

FIGURE 4.17: Breach Width on SSP 5-8.5 100 Year Return Period

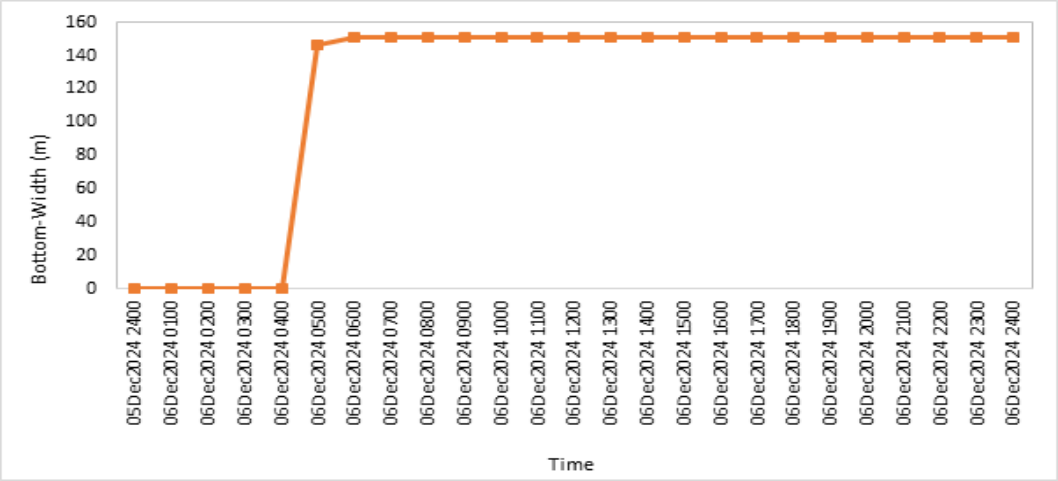

FIGURE 4.18: Breach Width on SSP 5-8.5 200 Year Return Period

4.6.3 Breach Velocity Analysis Under Different Scenarios

The breach velocity analysis offers critical insight into the hydraulic behavior of water flow through the failed section of dam across various climate scenarios and

return periods. Initially, velocities remain at zero, indicating no outflow prior to breach initiation. As the breach forms, however, there is a sharp rise in velocity across all scenarios, reflecting the sudden release of reservoir water and the generation of a high-energy flood wave moving downstream.

4.6.3.1 Historic Scenario

Under historic conditions, the breach velocity peaks at 2.24 m/s (Figure 4.19) for the 100-year return period and 2.41 m/s (Figure 4.20) for the 200-year return period. This indicates a moderately intense but relatively controlled outflow typical of historical flood events.

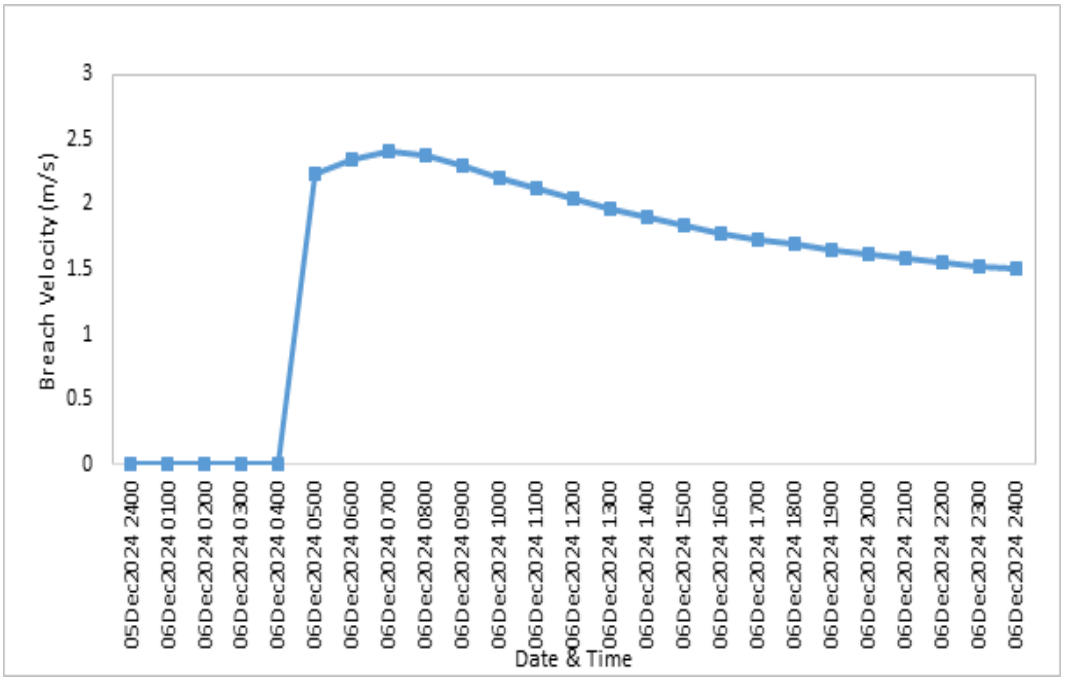

FIGURE 4.19: Breach Velocity Historic (100-year return period)

4.6.3.2 Future Scenarios - SSP 2-4.5

In comparison, the SSP 2-4.5 scenario shows more dynamic flow behavior, with peak velocities reaching 2.47 m/s (Figure 4.21) on 100-year and a significantly higher 2.75 m/s (Figure 4.22) on 200-year. These increased velocities suggest that climate-induced changes may result in faster and more forceful breaches, thereby elevating the risk of downstream flooding and erosion.

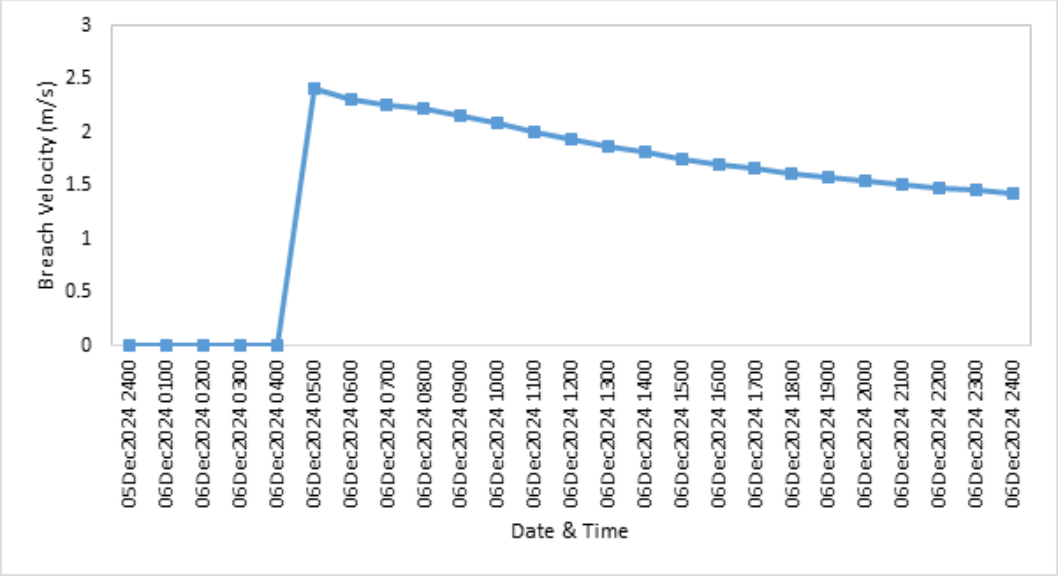

FIGURE 4.20: Breach Velocity Historic (200-year return period)

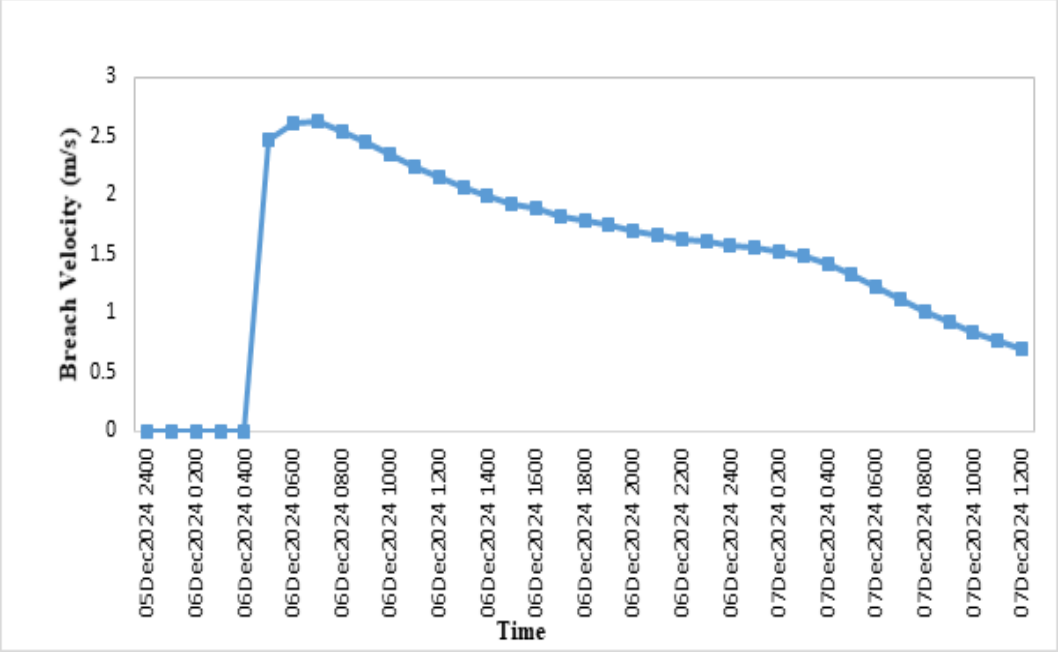

FIGURE 4.21: Breach Velocity on SSP 2-4.5 Scenario (100-year return period)

4.6.3.3 Future Scenario - SSP 5-8.5

The SSP 5-8.5 scenario, representing a high-emission future, displays even higher breach velocities i.e. 3.22 m/s (Figure 4.23) for the 100-year return period and 3.81 m/s (Figure-4.24) for the 200-year return period. While these velocities are higher than historical values, the breach appears to stabilize faster than in SSP 2-4.5, possibly due to differences in hydrological response or storm patterns under this scenario.

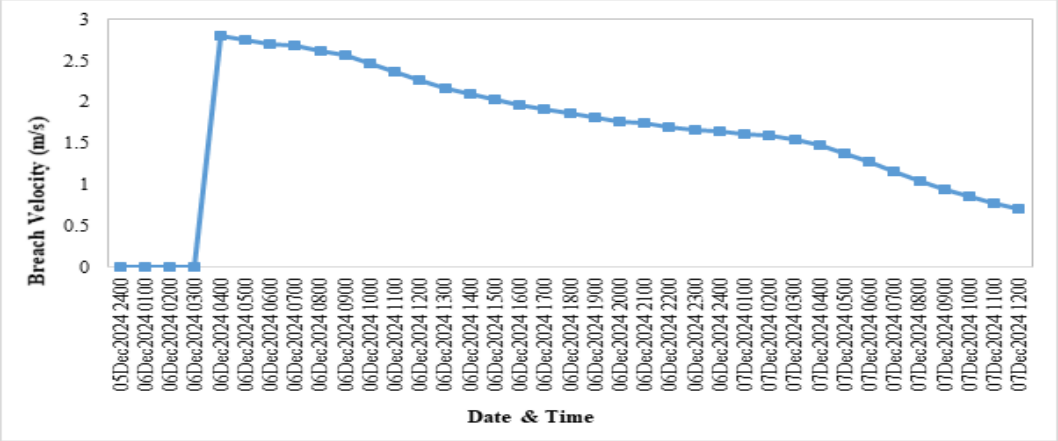

FIGURE 4.22: Breach Velocity on SSP 2-4.5 Scenario (200-year return period)

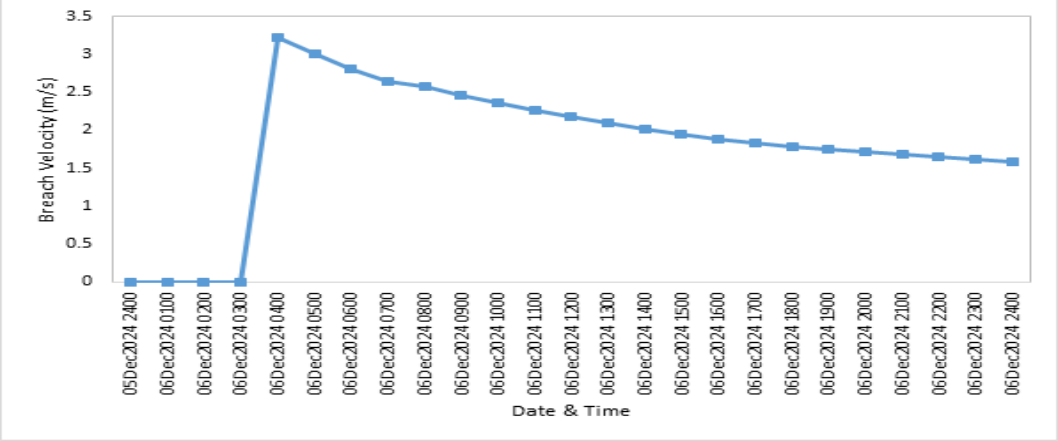

FIGURE 4.23: Breach Velocity on SSP 5-8.5 Scenario (100-year return period)

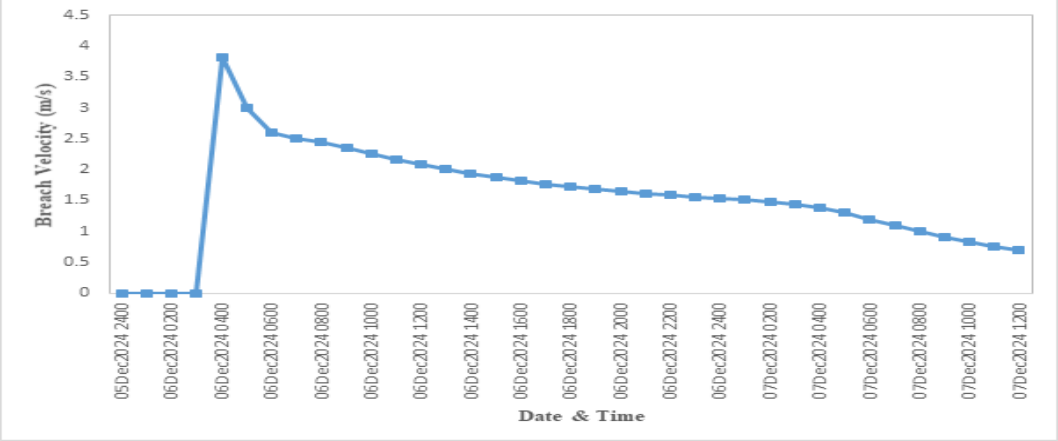

FIGURE 4.24: Breach Velocity on SSP 5-8.5 Scenario (200-year return period)

Following the peak, all scenarios show a gradual decline in breach velocity, falling below 1.0 m/s by the end of the simulation. This downward trend corresponds to the depletion of reservoir storage, resulting in reduced energy flow and diminished downstream flood intensity. The timing of peak velocity is critical, as the

highest impact occurs shortly after breach initiation. Understanding breach velocity is vital for evaluating erosion potential, channel instability, and structural vulnerability downstream. Higher velocities are directly associated with greater scouring and can cause severe damage to riverbanks and infrastructure. These velocity outputs are integral to HEC-RAS dam breach simulations, helping to model flood wave propagation, define inundation zones, and generate hazard maps that support comprehensive risk assessment and mitigation strategies.

4.6.4 Breach Flow Analysis Under Different Scenarios

The breach flow hydrograph of Dam shows how water discharge changes over time after the dam starts to fail. In the beginning, the flow is zero, meaning there is no water escaping. However, once the breach forms, the flow rises very quickly, releasing a large amount of water downstream. The highest flow rate (peak breach flow) is different for each scenario, showing how climate change can affect flood severity.

After reaching its highest point, the water flow gradually decreases as the reservoir drains. This means that most of the floodwater is released very quickly after the breach forms, creating a strong initial flood wave, followed by a slower decline. This pattern is important for understanding how severe the flooding will be and how long the floodwater will last.

This analysis helps in predicting how much flooding will occur if the dam fails. The results are used in HEC-RAS simulations to model flood movement, inundation areas, and risk assessment for downstream communities. These findings highlight the impact of climate change on dam safety, showing that future floods could be much worse than past ones. This study also stresses the importance of early warning systems, better dam safety measures, and flood management strategies to protect communities from possible dam failures.

4.6.4.1 Historic Scenario

Figures 4.25 and 4.26 illustrate a comparison of breach flow hydrographs for the Historic 100-Year and 200-Year Return Period events. In the 100-year scenario

(Figure 4.26), breach outflow increases rapidly during the early hours of December 6, reaching a peak discharge of approximately 848.22 m^3/s, followed by a gradual recession. The flow continues to decline steadily, falling below 100 m^3/s by the end of the simulation period on December 7.

In contrast, the 200-year event (Figure 4.27) exhibits an earlier onset of breach flow, with a sharper rise and a higher peak discharge of approximately 1,035 m^3/s occurring shortly after the breach begins. Additionally, elevated flow rates are sustained over a longer duration compared to the 100-year scenario. The 200-year event demonstrates a more intense hydraulic response, characterized by earlier breach initiation, higher peak flow, and extended flood duration. These distinctions are significant for downstream flood risk assessments and underscore the importance of incorporating higher-return-period scenarios into dam safety evaluations and emergency preparedness planning.

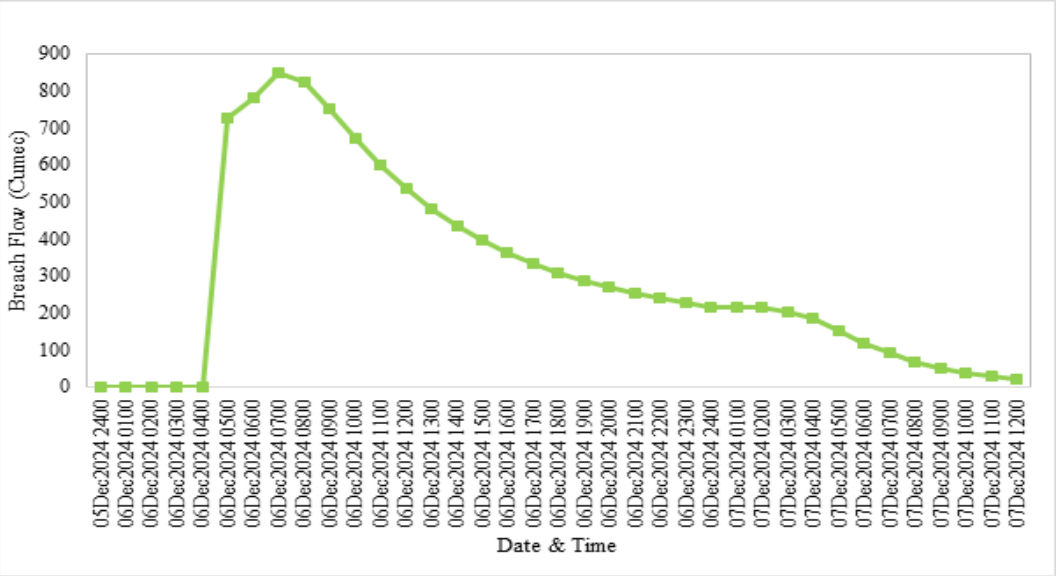

FIGURE 4.25: Breach Flow of Historic (100 Year Return Period)

4.6.4.2 Future Scenario - SSP 2-4.5

Figures 4.27 and 4.28 illustrate the breach outflow hydrographs under the SSP2-4.5 climate scenario for the 100-year and 200-year return periods, respectively. In Figure 4.28 (100-year return period), the breach outflow increases sharply during the early hours of December 6, 2024, reaching a primary peak discharge of approximately 1,301.78 m/s. This peak is followed by a slight decline and then a

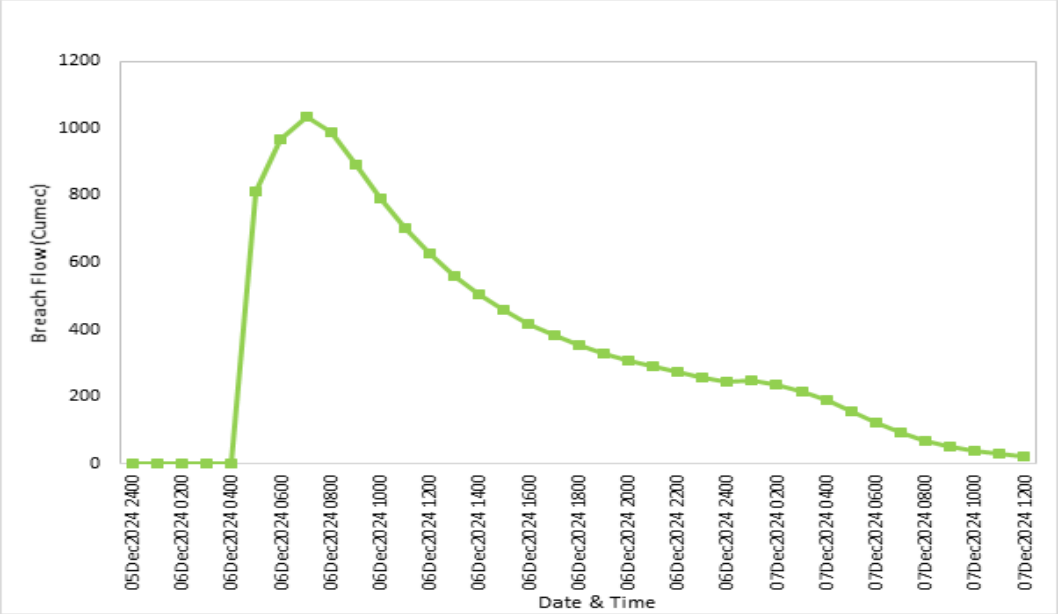

FIGURE 4.26: Breach Flow of Historic (200 Year Return Period)

secondary peak of about 1,171.44 m/s, after which the flow gradually decreases as the reservoir volume diminishes.

In Figure 4.28 (200-year return period), a similar hydrograph pattern is observed, but with greater intensity. The breach initiates at a comparable time, yet the peak discharge increases to 1,368.32 m/s, reflecting a more severe hydrologic event. A brief reduction in flow follows the peak before stabilizing at a secondary crest, after which the hydrograph transitions into a recession limb. The observed double-peak behavior in both events suggests complex breach hydraulics, potentially driven by factors such as temporary reservoir re-filling, spillway interactions, or the staged evolution of breach geometry. These findings demonstrate that under the SSP2-4.5 scenario, higher return periods produce significantly larger and more prolonged breach discharges, thereby increasing downstream flood risk. The results reinforce the need to incorporate detailed breach hydrograph behavior into HEC-RAS simulations to enhance the accuracy of flood extent mapping and risk mitigation planning.

4.6.4.3 Future Scenario - SSP 5-8.5

Figures 4.29 and 4.30 illustrate the breach flow hydrographs for the SSP5-8.5 high-emission scenario under the 100-year and 200-year return periods, respectively.

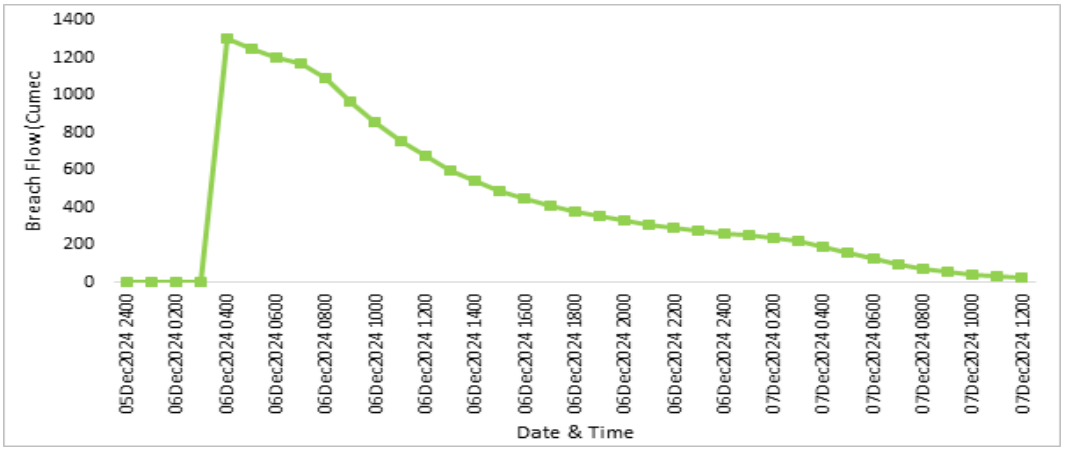

FIGURE 4.27: Breach Flow of SSP 2-4.5 (100 Year Return Period)

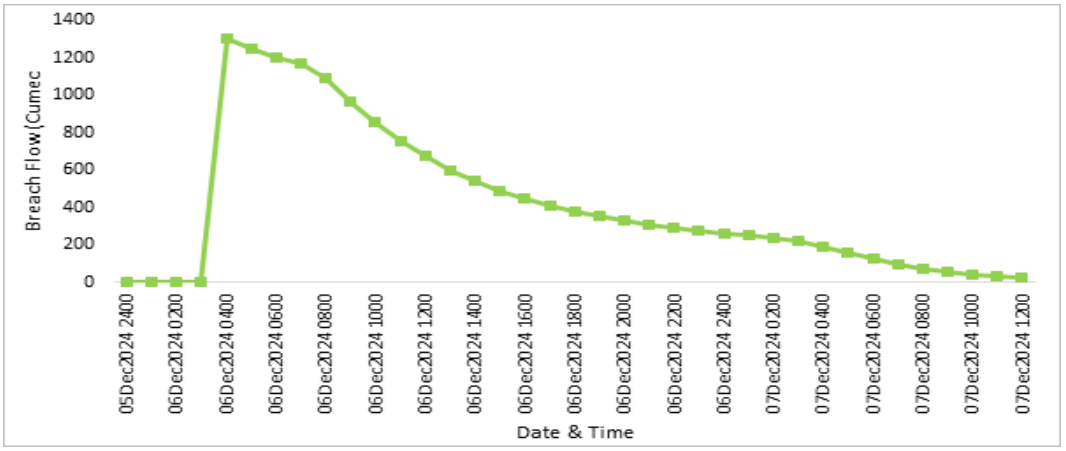

FIGURE 4.28: Breach Flow of SSP 2-4.5 (200 Year Return Period)

In Figure 4.29 (100-year return period), the breach flow exhibits a sharp rise during the early hours of December 6, 2024, initially peaking at approximately 1,144.93 m^3/s, followed by a brief decline and a secondary, more pronounced peak reaching 1,335.82 m^3/s. Thereafter, the outflow gradually decreases throughout the day and continues to recede into December 7, corresponding with the depletion of reservoir storage.

In Figure 4.30 (200-year return period), a similar but more intense pattern is observed. The breach initiates earlier and accelerates more rapidly, with the peak discharge reaching approximately 1,597.86 m^3/s. The hydrograph follows a classical flood wave shape, yet maintains elevated discharge levels for a longer duration compared to the 100-year event, indicating greater downstream impact.

This comparison highlights that, under the SSP5-8.5 scenario, the 200-year return period results in a faster onset, higher peak discharge, and more prolonged flood

wave, signifying a more severe breach scenario. These findings underscore the influence of intensified climatic conditions on dam breach behavior and reinforce the need to integrate future climate projections into flood risk assessments, dam safety evaluations, and emergency preparedness strategies.

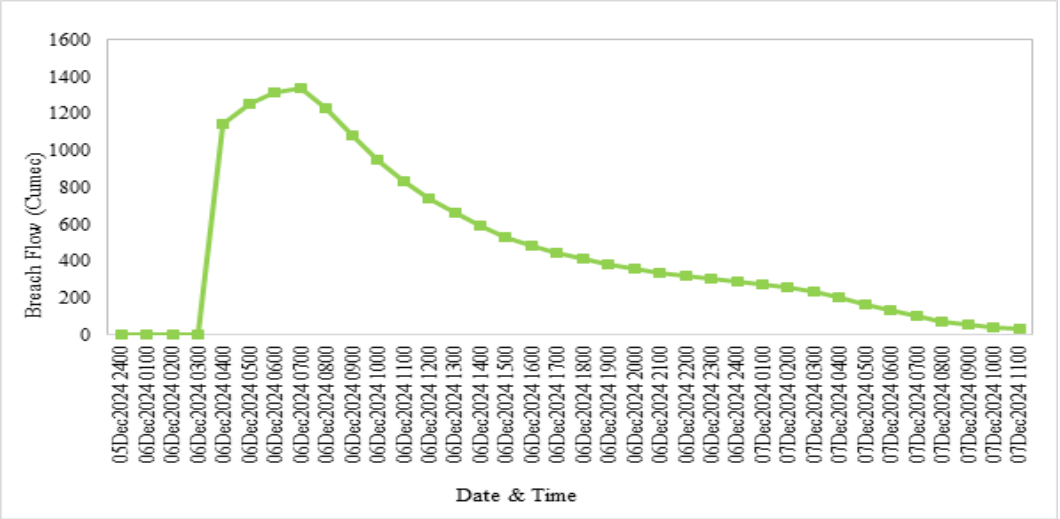

FIGURE 4.29: Breach Flow of SSP 5-8.5 (100 Year Return Period)

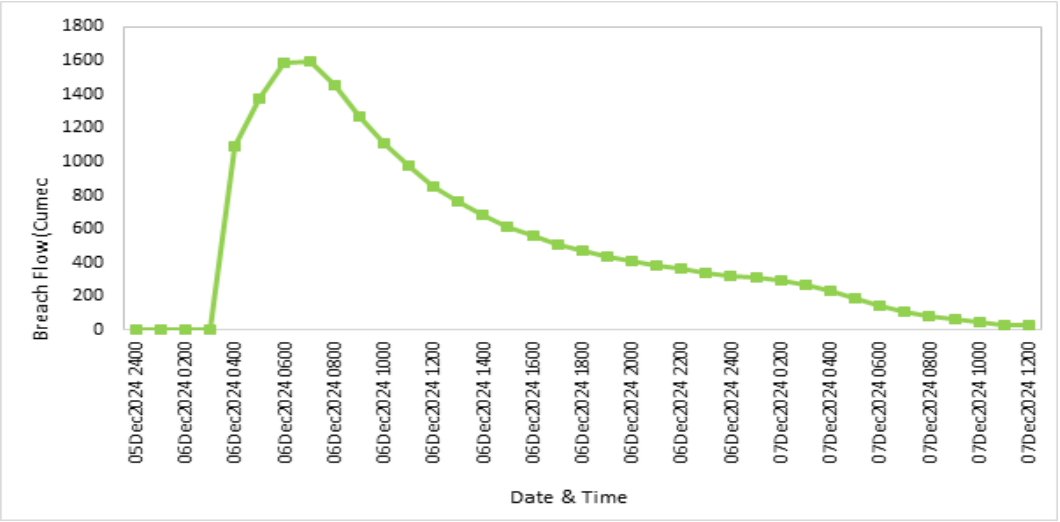

FIGURE 4.30: Breach Flow of SSP 5-8.5 (200 Year Return Period)

4.6.5 Water Surface Elevation Analysis Under Different Scenario

The water surface elevation analysis helps understand how water levels change upstream (headwater stage - HW) and downstream (tailwater stage - TW) during

the dam breach. Initially, both the HW and TW stages remain stable, indicating normal reservoir and river conditions. However, as the breach occurs, the HW stage rises sharply before peaking and then gradually declines, while the TW stage also rises significantly due to the sudden release of water.

These results show that higher return periods and climate change scenarios lead to increased water surface elevations, particularly in the headwater stage. The differences in HW and TW elevations across scenarios highlight the potential impacts of climate change on flood magnitude and reservoir response. The findings emphasize the need for improved dam management strategies, including enhanced spillway capacity and early warning systems to handle extreme weather events effectively.

This analysis is crucial in understanding how water levels respond to a dam failure event, as it provides insights into reservoir drawdown rates and downstream flood wave behavior. The results from this simulation are further utilized in HEC-RAS flood modeling to assess flood inundation, potential damage zones, and emergency preparedness measures for Dam and surrounding areas.

4.6.5.1 Historic Scenario

Figures 4.31 and 4.32 show the head water (HW) and tail water (TW) stage variations for the historic 100-year and 200-year return periods. In both cases, HW and TW stages rise sharply following breach initiation on December 6. For the 100-year event (Figure 4.29), HW peaks at approximately 1711.7 m, while TW reaches around 1705.27 m, after which both gradually decline as the reservoir drains.

In the 200-year event (Figure 4.32), the HW stage rises slightly higher to 1713.03 m, and TW peaks at 1705.61 m, reflecting the increased inflow and flood intensity. Overall, the 200-year scenario results in higher and earlier stage elevations, indicating a more severe breach event and emphasizing the need for enhanced flood preparedness for extreme return periods.

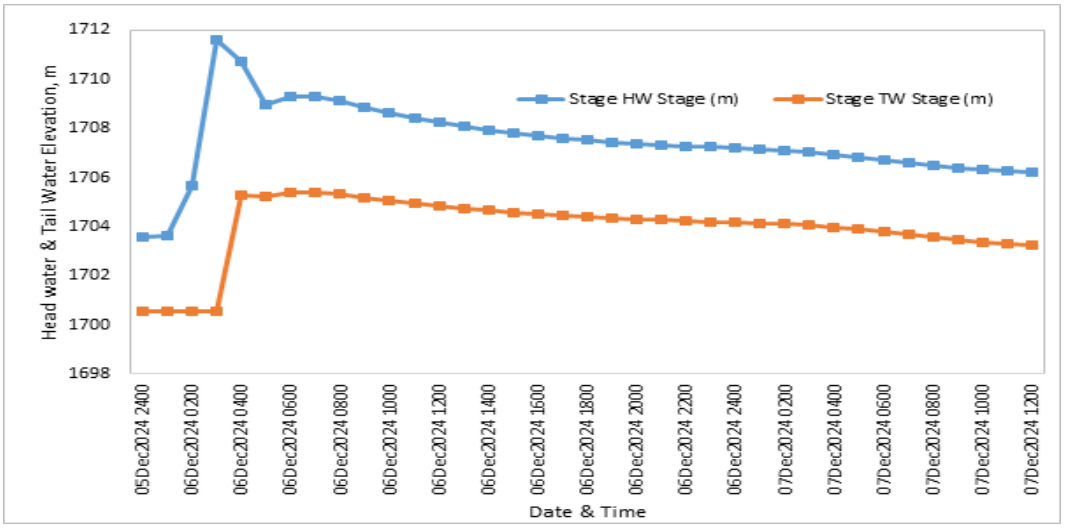

FIGURE 4.31: Stage HW & TW on Historic (100-year return period)

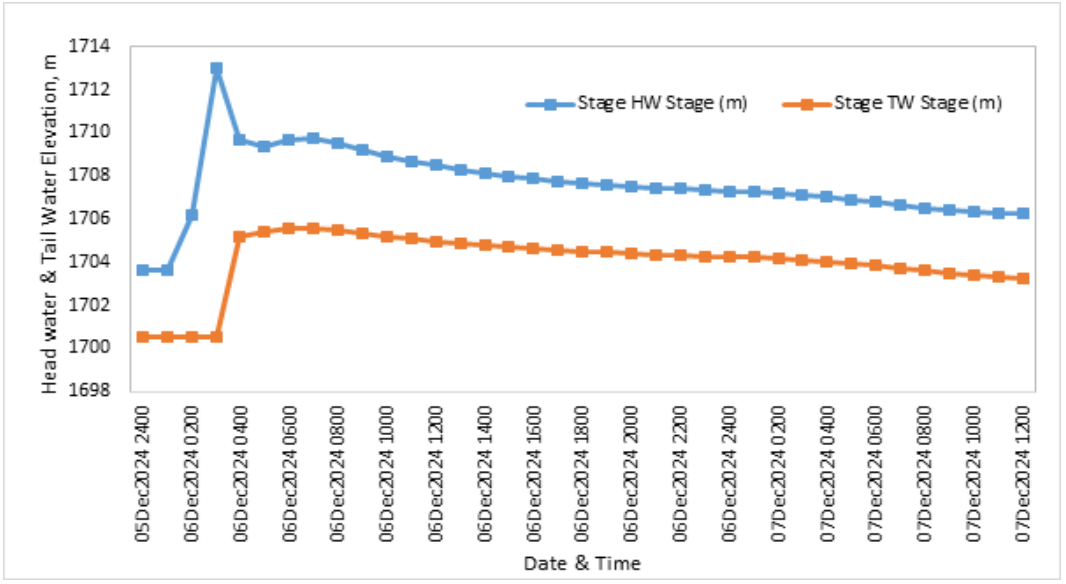

FIGURE 4.32: : Stage HW & TW on Historic (200-year return period)

4.6.5.2 Future Scenario - SSP 2-4.5

Figures 4.33 and 4.34 illustrate the Head Water (HW) and Tail Water (TW) stage elevations under the SSP2-4.5 climate scenario for the 100-year and 200-year return periods, respectively.

In the 100-year return period case (Figure 4.33), the HW elevation exhibits a rapid rise from approximately 1710.3 m, reaching a peak of 1713.39 m during the initial breach phase, indicating a swift reservoir response to sudden outflow. Correspondingly, the TW stage also increases, peaking at around 1705.48 m, before both stages gradually decline as the reservoir outflow stabilizes over time.

For the 200-year return period (Figure 4.34), the HW stage reaches a slightly lower peak of approximately 1711.31 m, while the TW stage peaks at 1705.32 m. Both scenarios follow a similar patterna rapid initial increase in water levels due to breach development, followed by a gradual recession as the reservoir volume decreases and flow stabilizes downstream.

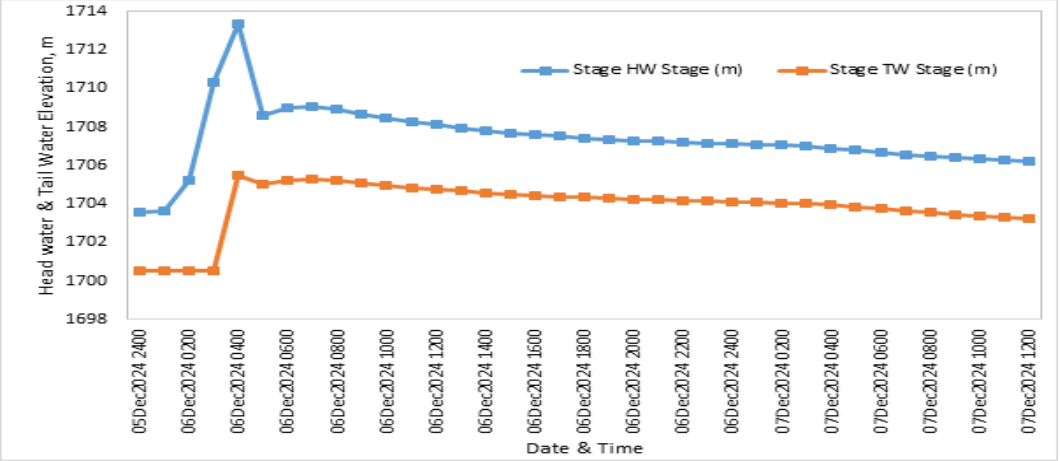

FIGURE 4.33: Stage HW & TW on SSP 2-4.5 (100-year return period)

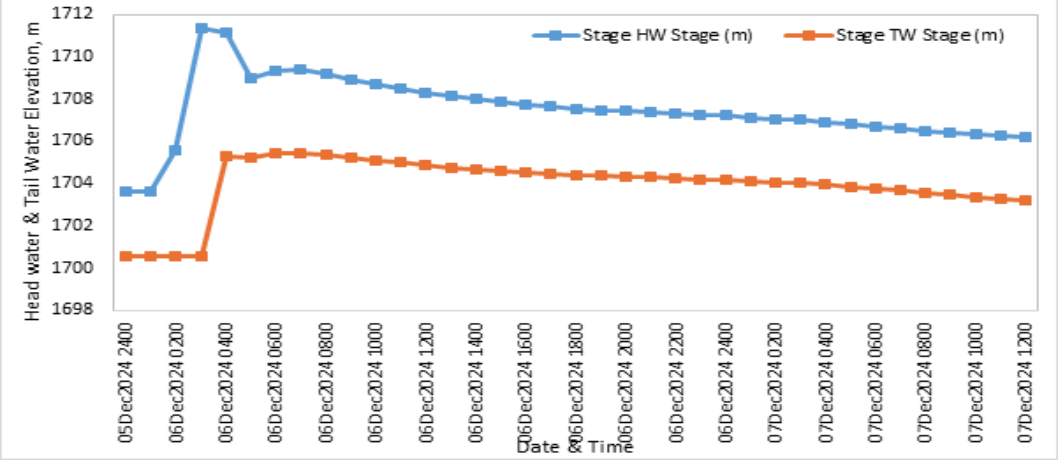

FIGURE 4.34: Stage HW & TW on SSP 2-4.5 (200-year return period)

4.6.5.3 Future Scenario - SSP 5-8.5

The headwater (HW) and tailwater (TW) stage profiles under the SSP5-8.5 climate scenario illustrate the dams hydraulic response to high-magnitude flood events associated with extreme emission conditions. As inflow to the reservoir intensifies during breach events, pronounced fluctuations in water surface elevations are observed both upstream and downstream of the dam.

For the 100-year return period (Figure 4.35), the HW stage exhibits a rapid rise from approximately 1703.5 m, peaking at 1713.7 m during the early morning of December 6, 2024, indicating swift reservoir filling prior to overtopping and breach initiation. The corresponding TW stage (Figure 4.35) peaks at around 1704.82 m, reflecting the immediate impact of the released flood wave on downstream flow conditions. Post-breach, both HW and TW stages gradually recede as the reservoir volume is discharged.

In the case of the 200-year return period, the dam demonstrates an even more severe hydraulic response. The HW stage peaks at 1714.87 m (Figure 4.36), while the TW stage reaches 1704.96 m, suggesting a higher flood volume and more intense downstream impact compared to the 100-year scenario.

Overall, the 200-year event results in both higher and more sustained stage elevations than the 100-year event. This outcome underscores the heightened flood risk associated with more extreme climate projections and emphasizes the critical need to incorporate such scenarios into dam breach evaluations and downstream flood mitigation strategies.

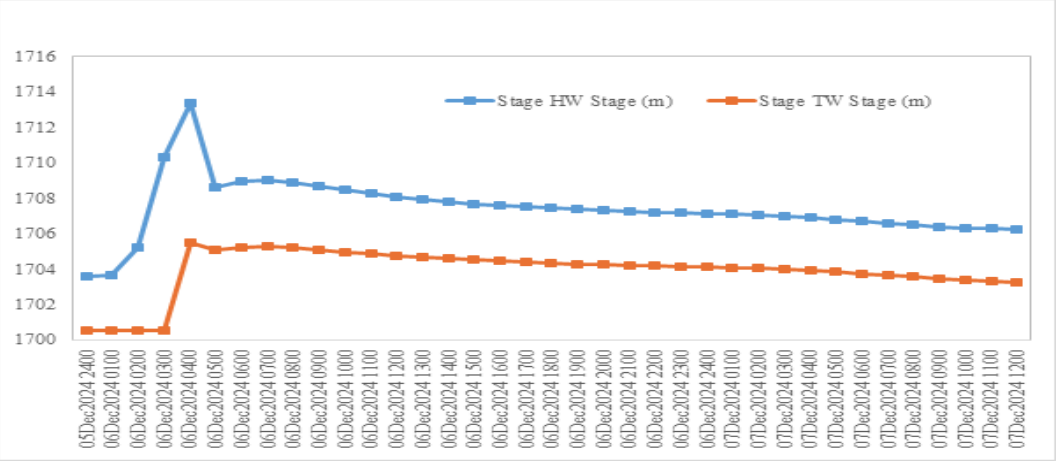

FIGURE 4.35: Stage HW & TW on SSP 5-8.5 (100-year return period)

4.6.6 Total Flow Analysis Under Different Scenarios

The total flow hydrograph provides crucial insights into the variation of discharge during the dam breach event under different climate scenarios and return periods. Initially, the flow remains at zero, indicating stable reservoir conditions with no

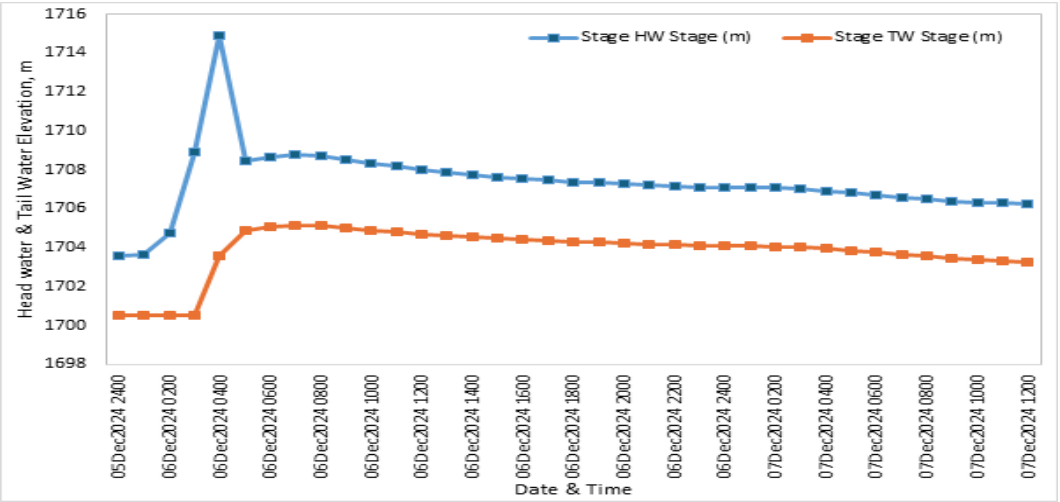

FIGURE 4.36: Stage HW & TW on SSP 5-8.5 (200-year return period)

outflow. However, as the dam breach initiates, there is a rapid escalation in discharge, signifying the sudden and uncontrolled release of stored water from the reservoir. This sudden surge results in the formation of a high-energy flood wave propagating downstream, posing significant flood risks to nearby settlements and infrastructure.

4.6.6.1 Historic Scenario

Figures 4.37 and 4.38 illustrate the total outflow hydrographs of the dam under historical conditions for the 100-year and 200-year return period flood events, respectively. In Figure 4.38, representing the 100-year return period, the outflow remains negligible during the initial hours of December 6, 2024, before rising sharply and reaching a peak discharge of approximately 848 m/s during the early morning. Following the peak, the flow gradually decreases over the course of the day and continues to decline into December 7, eventually dropping below 100 m/s by the end of the simulation period.

In comparison, Figure 4.38, corresponding to the 200-year return period, depicts a more intense flood event. The outflow begins to rise earlier and increases more rapidly, peaking at approximately 1,034.93 m/s, which is not only higher but also sustained for a longer duration than the 100-year event. This behavior indicates a significantly greater volume of water being released as a result of the more extreme hydrologic conditions.

The increase in peak flow - approximately 22% higher from the 100-year to the 200-year return periodhighlights the substantial difference in flood magnitude between the two scenarios. This variation underscores the heightened risk associated with rarer, high-return period events. Such hydrograph data is essential for downstream flood routing using HEC-RAS, and plays a vital role in reservoir safety assessment, breach analysis, and the design of flood protection and mitigation infrastructure.

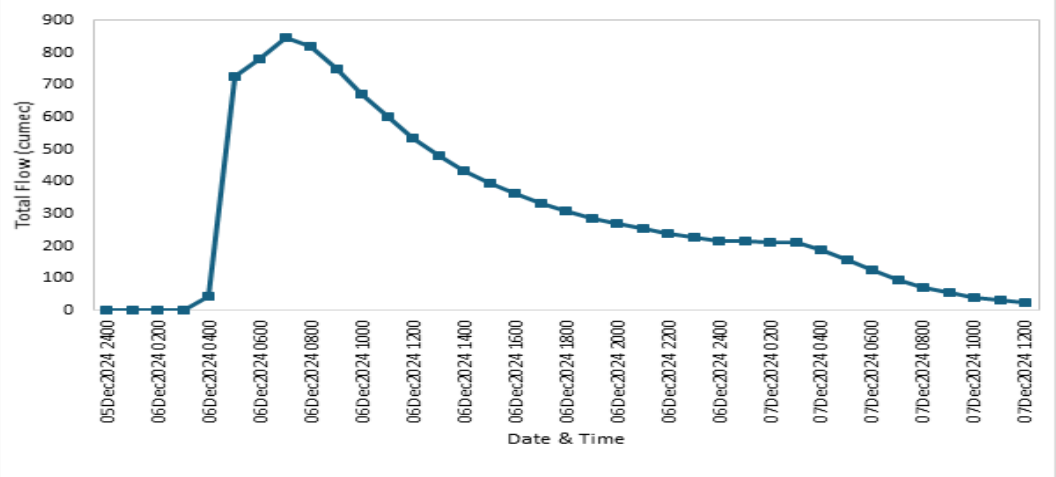

FIGURE 4.37: Total Flow of Dam on Historic (100 Year Return Period)

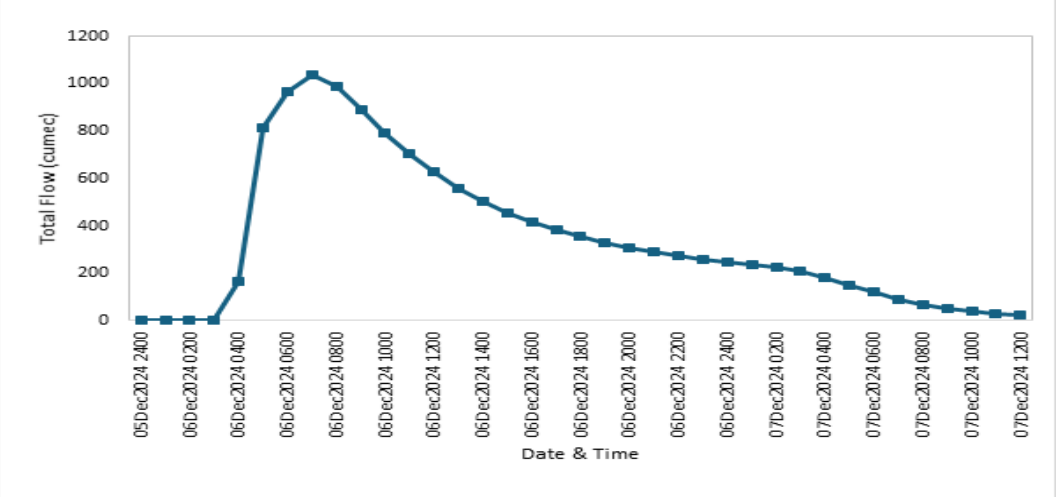

FIGURE 4.38: Total Flow of Dam on Historic (200 Year Return Period)

4.6.6.2 Future Scenario - SSP 2-4.5

Figures 4.39 and 4.40 illustrate the total outflow hydrographs of the dam under the SSP2-4.5 climate scenario for the 100-year and 200-year return periods, respectively.

In Figure 4.39 (100-year return period), the outflow begins to rise sharply during the early hours of December 6, 2024, rapidly reaching a peak discharge of approximately 1,325.49 m/s. This rapid peak is attributed to the swift breach formation combined with intense upstream inflows. Following the peak, the hydrograph exhibits a gradual decline, with outflows dropping below 200 m/s by the evening of December 7, as the reservoir volume is progressively depleted.

Figure 4.40 (200-year return period) represents a more severe flood event, with the total outflow peaking at approximately 1,368.32 m/s in the early morning, reflecting the larger inflow volume associated with the higher return period. Although the recession limb follows a similar pattern to the 100-year scenario, the flow remains elevated for a longer duration, indicating a prolonged and more intense downstream impact.

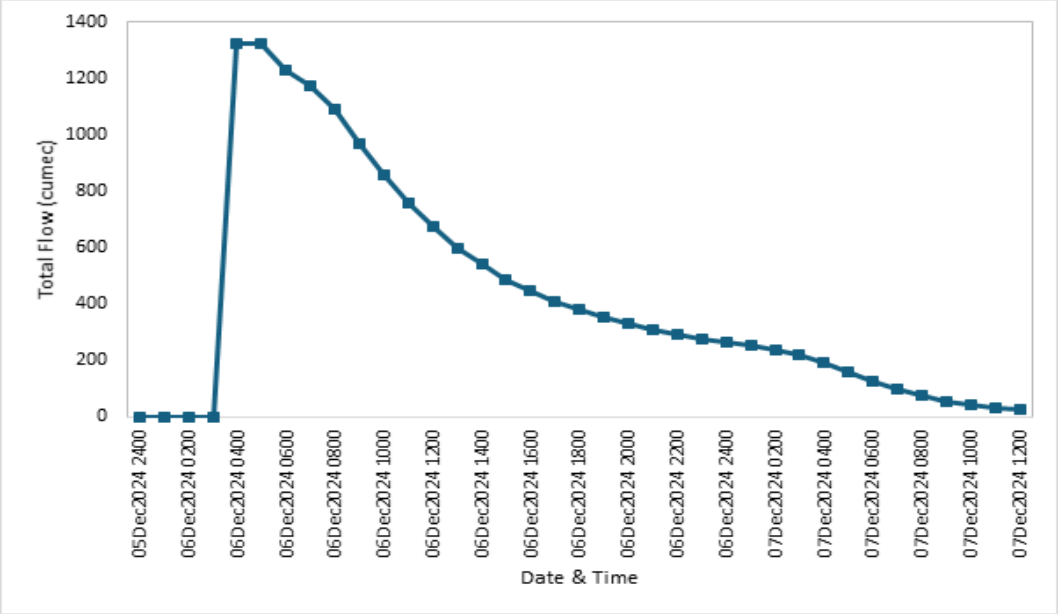

FIGURE 4.39: Total Flow of Dam on SSP 2-4.5 (100 Year Return Period)

The 200-year peak flow is approximately 43 cumec (∼3.2%) higher than the 100-year event. While the percentage increase is modest, the additional volume and duration of high discharge can significantly elevate downstream flood risk. These findings emphasize the importance of including climate-adjusted return periods in dam break analysis to improve flood forecasting, risk mapping, and emergency response planning.

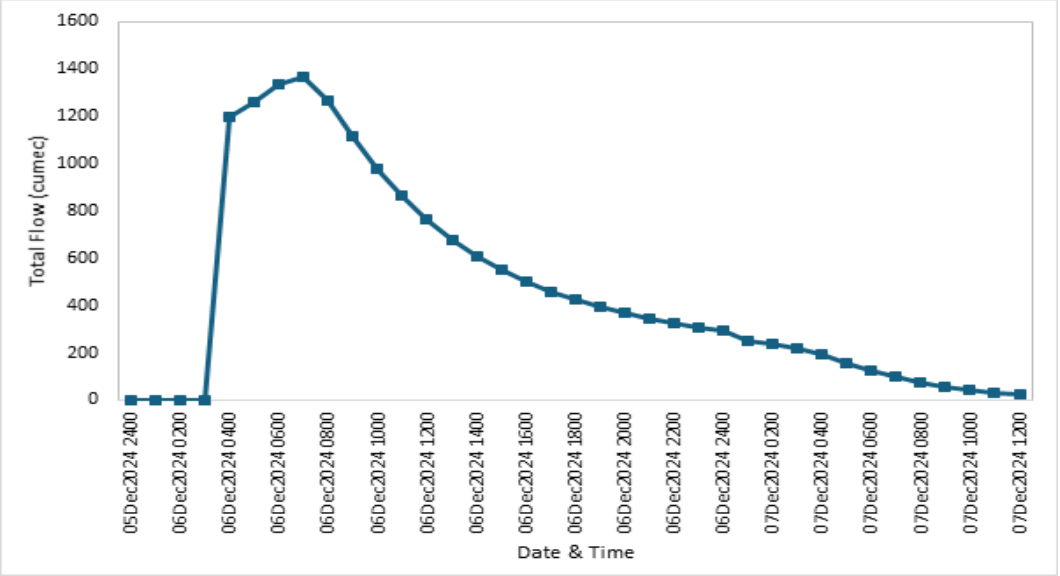

FIGURE 4.40: Total Flow of Dam on SSP 2-4.5 (200 Year Return Period)

4.6.6.3 Future Scenario - SSP 5-8.5

Figures 4.41 and 4.42 present the total outflow hydrographs of the dam under the SSP5-8.5 high-emission scenario, comparing the hydrologic response for the 100-year and 200-year return periods.

In the 100-year event (Figure 4.41), the outflow rises sharply during the early morning hours of December 6, 2024, culminating in a peak discharge of 1335.82 m^3/s. This is followed by a gradual recession phase as the reservoir releases diminish steadily over the subsequent hours.

In the 200-year return period (Figure 4.42), the dam undergoes a more severe hydrologic event, with peak outflow reaching 1589.09 m^3/san increase of approximately 253.27 m^3/s ($\sim$19%) compared to the 100-year scenario. The hydrograph also indicates a longer duration of elevated discharge, suggesting a significantly larger volume of water released during the breach and prolonged downstream inundation.

This analysis is vital for flood risk assessment, as peak discharges directly influence inundation extents, flood depths, and the severity of downstream impacts. Higher discharge values indicate greater flooding potential, leading to widespread inundation, infrastructure damage, and increased risks to human settlements. The results of this total flow analysis are incorporated into HEC-RAS dam breach modeling

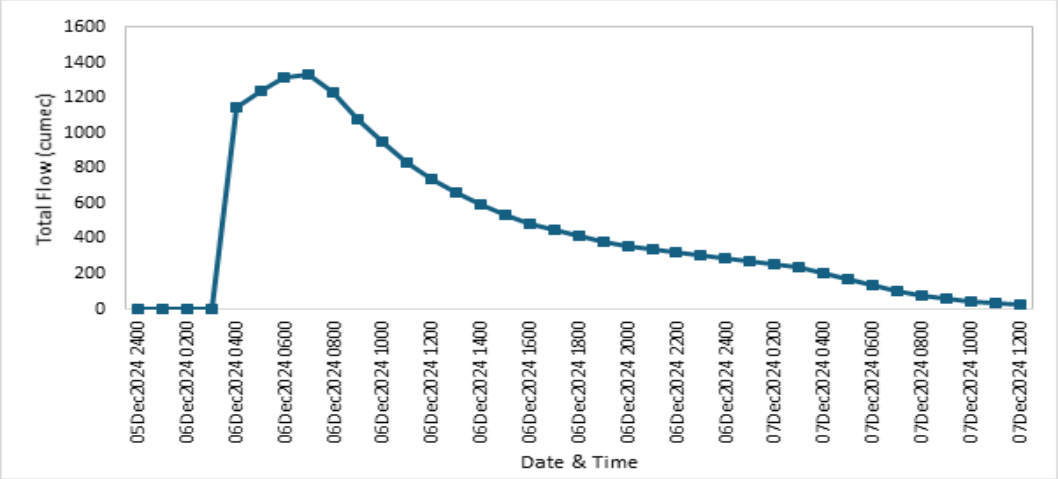

FIGURE 4.41: Total Flow of Dam on SSP 5-8.5 (100 Year Return Period)

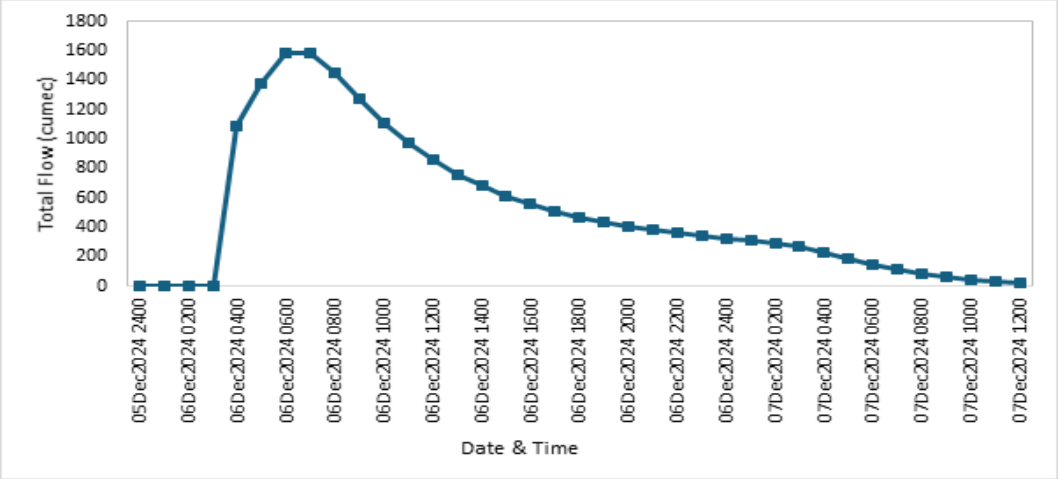

FIGURE 4.42: Total Flow of Dam on SSP 5-8.5 (200 Year Return Period)

to simulate flood wave propagation, develop flood inundation maps, and assess the effectiveness of emergency response measures.

Understanding the differences in peak flow values across different climate scenarios highlights the growing risks associated with future climate change. The substantial rise in peak discharges under SSP 2-4.5 and SSP 5-8.5 scenarios compared to historic conditions suggest that climate change is significantly impacting flood hazards. This emphasizes the urgent need for robust flood mitigation strategies, enhanced reservoir management, reinforced embankments, and early warning systems to mitigate the increasing risks of dam failures. The findings from this study play a critical role in guiding future flood management policies, dam safety improvements, and disaster preparedness initiatives for vulnerable downstream communities.

4.6.7 Downstream Flood Risk Assessment of 100-year Return Period for Different Scenarios

The downstream flood risk assessment for Dam highlights the increasing vulnerability of 31 villages situated immediate downstream of the reservoir, with varying degrees of inundation under different climate scenarios. The analysis considers three major scenarios: SSP 2-4.5 (100-year return period), SSP 5-8.5 (100-year return period), and the historic 100-year return period. The extent of flooding increases significantly in future climate projections, emphasizing the growing risks posed by climate change. The number of villages and inundation depth are shown in Table 4.16.

Under SSP 2-4.5 (100-year return period), the peak discharge reaches 47,464.6 cusecs, resulting in the inundation of 13 villages. This scenario presents the highest flood risk, with villages such as Muhammad Qadir, Khanzada Abdul Samad Talab, and Halimabad experiencing the most severe flood depths, such as 6.70 meters, 3.46 meters, and 2.99 meters, respectively.

The SSP 5-8.5 (100-year return period) scenario, with a peak discharge of 56,130 cusecs, leads to the inundation of 16 villages, showing massive increment in flood extent posing a major risk to the downstream villages. The highest inundation levels in this scenario are recorded in Muhammad Qadir (6.91 meters), Khanzada Abdul Samad Talab (3.74 meters), and Halimabad (3.22 meters).

Comparatively, the historic 100-year return period, which represents past flood conditions, records a peak discharge of 30,008 cusecs, leading to the flooding of only 8 villages. The inundation depths in this scenario are notably lower, with Muhammad Qadir (6.38 meters), Khanzada Abdul Samad Talab (2.79 meters), and Halimabad (2.69 meters) being the most affected. The findings clearly indicate that future climate projections significantly increase flood risks, as the number of inundated villages and flood depths rises under SSP 2-4.5 and SSP 5-8.5 scenarios compared to historical conditions. This trend underscores the urgent need for enhanced flood risk management, including early warning systems, improved reservoir operations, reinforced embankments, and community preparedness programs. The study highlights that climate change is a key factor in escalating flood

TABLE 4.16: Downstream Flood Inundated Villages under 100-year return period for different scenarios

S.No.	NAME	SSP2-4.5 (100 Years)	SSP5-8.5 (100 Years)	Historic (100 Years)
1	Muhammad Qadir	6.7	6.91	6.38
2	Khanzada Abdul Samad Talab	3.46	3.74	2.79
3	Halimabad	2.99	3.22	2.69
4	Malik Fateh Khan Kili	2.32	2.51	1.65
5	Yahyawali	1.7	1.83	
6	Gafur Talab	1.56	1.68	1.35
7	Haji Abdul Rahim Talab	1.01	1.14	0.78
8	Kili Sohbat Khan	0.99	1.07	
9	Kili Khuda Bakhsh	0.97	1.13	
10	Donara	0.94	1	0.57
11	Kili Nautak	0.41	0.48	
12	Lahere	0.41	0.45	0.21
13	Malik Fateh Khan Kili	0.15	0.32	
14	Khankai		0.26	
15	Kili Nali		0.22	
16	Tiari Kili		0.19	
17	Kili Abdul Ali			
18	Kili Haji Amin			
19	Malgai			
20	Kaza Mirzai			
21	Kotan Kili			
22	Kili Sahib Jan			
23	Kili Haji Sanzar Khan			
24	Khalifa Muhammad Nur			
25	Kalu Kili			
26	Ziarat Manjara			
27	Kili Maulvi Bakhtiar			
28	Zari Khotozai			
29	Kabir			
30	Diwan			
31	Qila Sher Ali Khan			

hazards, and proactive adaptation measures must be integrated into future flood management strategies to protect downstream communities from potential dam breach disasters.

4.6.8 Downstream Flood Risk Assessment of 200-year Return Period for Different Scenarios

The downstream flood risk assessment for Dam highlights the increasing vulnerability of 31 villages situated downstream of the reservoir, with varying degrees of

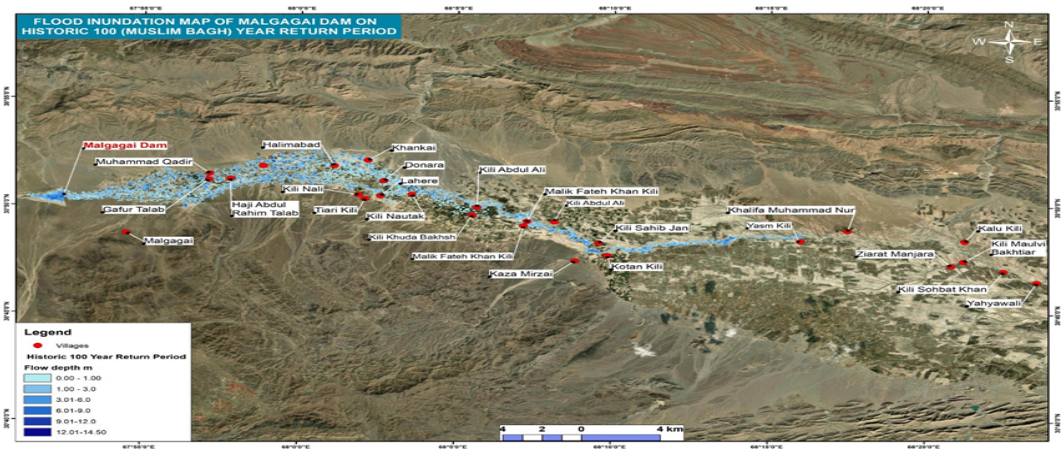

FIGURE 4.43: Flood Inundation Map of Historic 100-year Return period

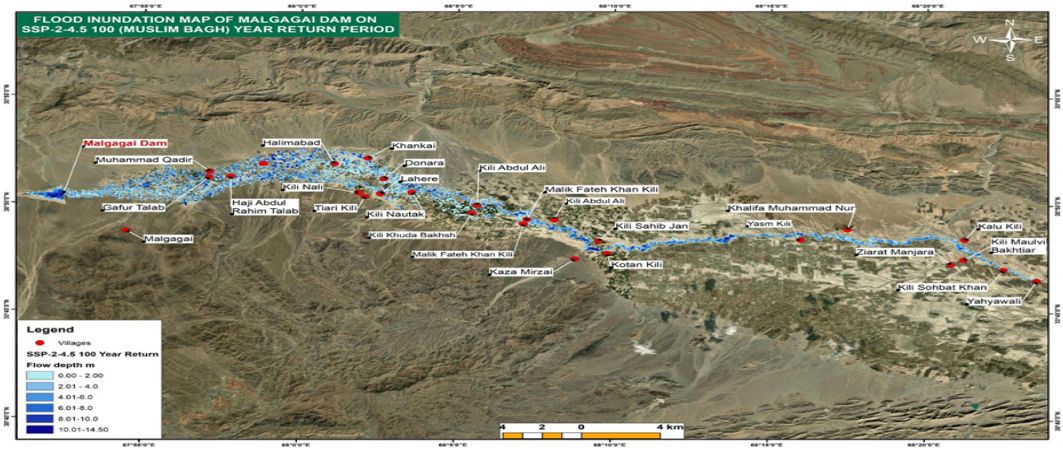

FIGURE 4.44: Flood Inundation Map of SSP 2-4.5 100-year Return period

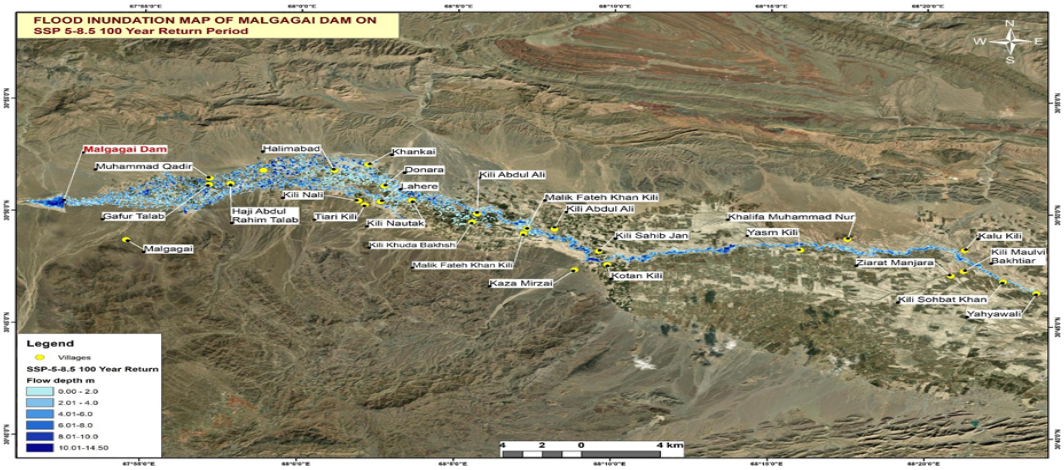

FIGURE 4.45: Flood Inundation Map of SSP 5-8.5 100-year Return period

inundation under different climate scenarios. The analysis considers three major scenarios: SSP 2-4.5, SSP 5-8.5, and the historic 200-year return period. The extent of flooding increases significantly in future climate projections, emphasizing the growing risks posed by climate change.

Under SSP 2-4.5, the peak discharge reaches 57,039 cusecs, resulting in the inundation of 16 villages. The highest flood depths are observed in Muhammad Qadir (6.81 m), Khanzada Abdul Samad Talab (3.62 m), and Halimabad (3.10 m), indicating severe flooding. Other villages such as Malik Fateh Khan Kili (2.61 m), Yahyawali (1.98 m), Gafur Talab (1.65 m), Haji Abdul Rahim Talab (1.20 m) and Kili Sohbat Khan (1.12 m) also experience significant flood levels, demonstrating the widespread impact of extreme flood scenarios.

For SSP 5-8.5, the discharge reaches 66,998.9 cusecs, leading to the inundation of 18 villages. The highest inundation levels in this scenario occur in Muhammad Qadir (7.35 m), Khanzada Abdul Samad Talab (3.90 m), and Halimabad (3.35 m). Additional affected villages include Malik Fateh Khan Kili (2.81 m), Yahyawali (2.14 m), Gafur Talab (1.78 m), Haji Abdul Rahim Talab (1.30 m), and Killi Sohbat Khan (1.29 m) showing extreme inundation depths at downstream that can pose a high risk to the community, whereas a significant number of villages remain at risk.

The historic 200-year return period, with a peak discharge of 36,573.4 cusecs, results in inundation of 12 villages at the downstream side of the dam. The flood depths are recorded as Muhammad Qadir (6.52 m), Khanzada Abdul Samad Talab (3.08 m), and Halimabad (2.81 m). Other villages affected include Malik Fateh Khan Kili (1.93 m), Gafur Talab (1.43 m), and Kili Khuda Bakhsh (0.89 m), indicating a relatively reduced but still substantial flood impact.

The results indicate that future climate scenarios (SSP 2-4.5 and SSP 5-8.5) substantially elevate flood risks, with increased discharges resulting in greater flood depths and broader inundation areas. These outcomes underscore the pressing need for strengthened flood risk management strategies, including advanced early warning systems, optimized reservoir operations, embankment strengthening, and community preparedness initiatives. The study highlights the significant influence of climate change in intensifying flood hazards and reinforces the importance of adopting proactive adaptation measures to safeguard downstream communities against potential dam breach events.

TABLE 4.17: Downstream Flood Inundated Villages under 200-year return period for different scenarios

S.No.	NAME	SSP 2-4.5 (200 Years)	SSP 5-8.5 (200 Years)	Historic(200 Years)
1	Muhammad Qadir	6.81	7.35	6.52
2	Khanzada Abdul Samad Talab	3.62	3.9	3.08
3	Halimabad	3.1	3.35	2.81
4	Malik Fateh Khan Kili	2.61	2.81	1.93
5	Yahyawali	1.98	2.14	-
6	Gafur Talab	1.65	1.78	1.43
7	Haji Abdul Rahim Talab	1.2	1.3	0.86
8	Kili Sohbat Khan	1.12	1.29	
9	Kili Khuda Bakhsh	1.38	1.59	0.89
10	Donara	1.13	1.3	0.72
11	Kili Nautak	0.64	1.02	0.13
12	Lahere	0.5	0.79	0.3
13	Malik Fateh Khan Kili	0.28	0.45	
14	Khankai	0.24	0.38	
15	Kili Nali	0.2	0.32	
16	Tiari Kili	0.17	0.27	
17	Kili Abdul Ali		0.25	
18	Kili Haji Amin		0.18	
19	Malgai			
20	Kaza Mirzai			
21	Kotan Kili			
22	Kili Sahib Jan			
23	Kili Haji Sanzar Khan			
24	Khalifa Muhammad Nur			
25	Kalu Kili			
26	Ziarat Manjara			
27	Kili Maulvi Bakhtiar			
28	Zari Khotozai			
29	Kabir			
30	Diwan			
31	Qila Sher Ali Khan			

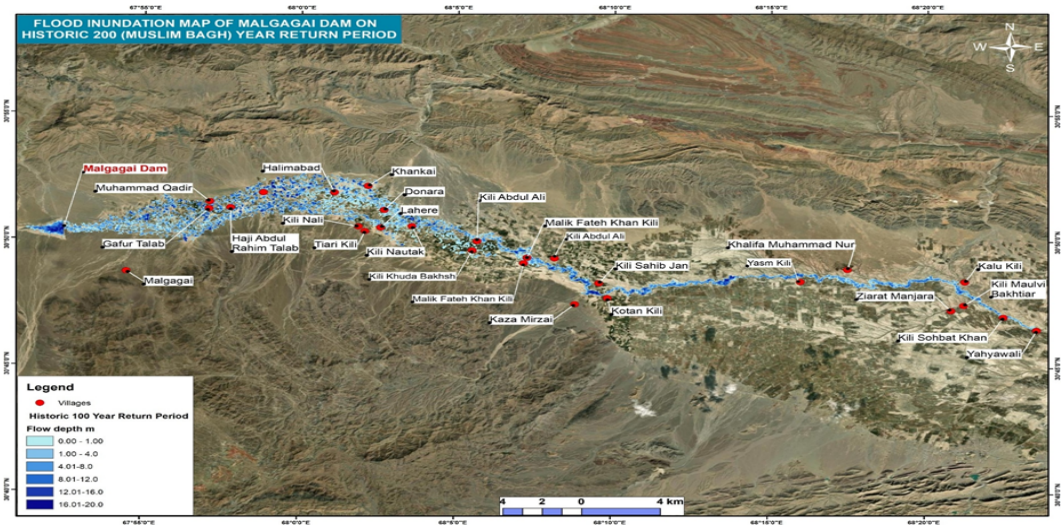

FIGURE 4.46: Flood Inundation Map of Historic 200-year Return period

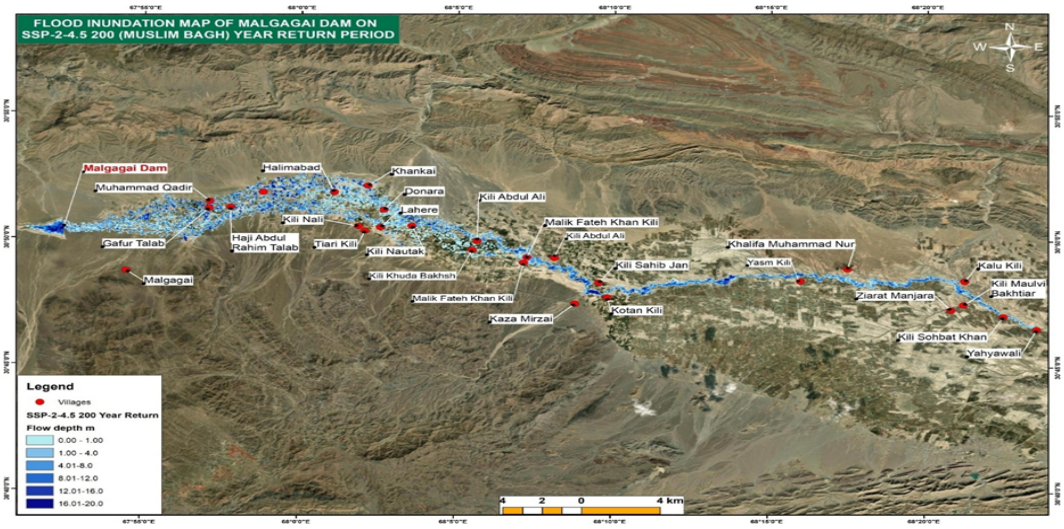

FIGURE 4.47: Flood Inundation Map of SSP 2-4.5 200-year Return period

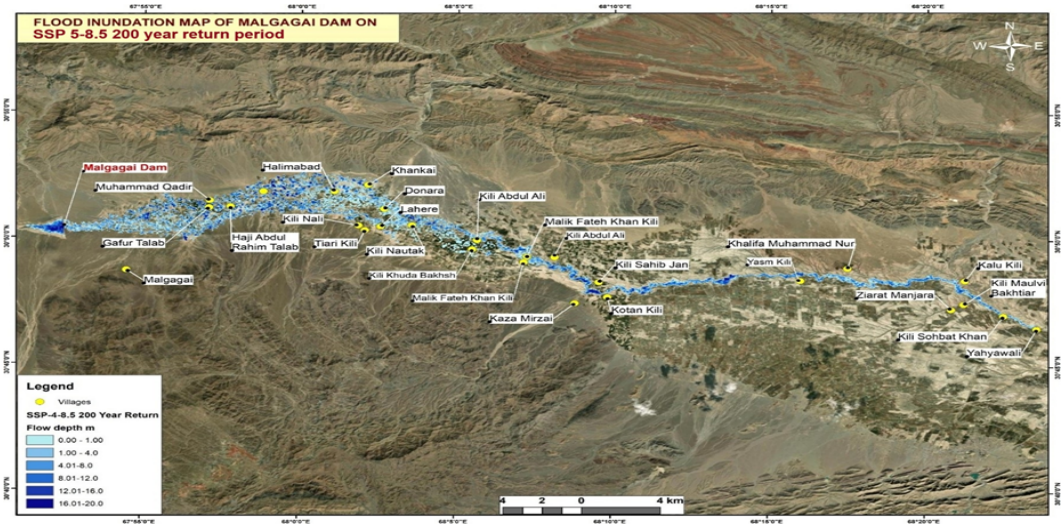

FIGURE 4.48: Flood Inundation Map of SSP 5-8.5 200-year Return period

Chapter 5

Conclusions and Recommendations

5.1 Conclusions

This study conducted a comprehensive flood risk assessment for an earthen dam, integrating historical climate data with projected future climate scenarios (SSP 2-4.5 and SSP 5-8.5). Using advanced hydrological and hydraulic modeling techniques, including the Gumbel Extreme Value Distribution, HEC-HMS for hydrological simulations, and HEC-RAS for dam breach analysis, the research evaluated the dam's performance and associated flood risks under varying climate conditions. These assessments provided detailed insights into potential future flood behaviors, dam safety vulnerabilities, and the broader impacts on downstream communities. The key conclusions drawn from the analysis are summarized as follows.

5.1.1 Increased Precipitation and Flood Intensity

Frequency analysis using the Gumbel Extreme Value Distribution revealed significant increases in precipitation intensity under future climate scenarios. The projected rainfall intensities, especially for higher return periods, showed substantial increases.

The study highlights that climate change has significantly increased the risk of dam failures due to extreme weather events, including intense and prolonged rainfall

events. Future climate scenarios (SSP 2-4.5 and SSP 5-8.5) suggest an increase in extreme precipitation, under the SSP 2-4.5 scenario, with projected increases ranging from 17% to 21% for the years 2026 to 2050, 21% to 23% for 2051 to 2075, and 21% to 26% for 2076 to 2100. Similarly, for the SSP 5-8.5 scenario, projected increases in precipitation range from 25% to 33% for the years 2026 to 2050, 28% to 41% for the years 2051 to 2075, and 24% to 28% for 2076 to 2100 making the dam safety planning at risk. Such intensified rainfall events directly contribute to elevated flood risks, placing greater demands on hydraulic infrastructure and increasing the likelihood of severe downstream flooding.

5.1.2 Impact of Climate Change Scenarios on Flood Magnitude

The study integrates future climate projections (SSP 2-4.5 and SSP 5-8.5) into hydrological models, showing that rainfall intensity is expected to increase leading to higher inflows and a greater probability of overtopping. This suggests that design parameters of existing dams are outdated and must be revised to accommodate future climate conditions.

The flood discharge simulations using HEC-HMS demonstrated that future flood events are likely to have higher peak flows and longer durations compared to historical conditions.

For instance, the 100-year return period flood discharge rises from 30,008 cusecs historically to 47,464.6 cusecs under SSP 2-4.5 and 56,130 cusecs under SSP 5-8.5. As compared to Historic flood the result shows increase of 58.17% under SSP 2-4.5 and 87.05% under SSP 5-8.5. These elevated flows surpass the design capacities of existing hydraulic structures, significantly increasing overtopping risks and posing substantial threats to dam safety and downstream areas.

5.1.3 Dam Breach Modelling Results

This study presents a detailed dam breach analysis under historical and future climate change scenarios (SSP2-4.5 and SSP5-8.5) for 100-year and 200-year return periods. The final breach width reached a consistent maximum of 151 meters

across all scenarios; however, the rate and timing of breach formation varied significantly. Under historical conditions, the breach initially widened to 75 m (100-year) and 105.11 m (200-year), while under SSP5-8.5, these increased to 104.64 m and 146.17 m, respectively, indicating more rapid structural failure under intensified inflow.

Breach velocities also increased under climate scenarios. Peak velocities were 2.24 m/s and 2.41 m/s for historical 100- and 200-year events, increasing to 2.47 m/s and 2.75 m/s under SSP2-4.5, and reaching 3.22 m/s and 3.81 m/s under SSP5-8.5 scenarios. These elevated velocities suggest more forceful outflows, leading to greater erosion and downstream hazard.

In terms of breach flow, peak discharges rose from 848.22 m^3/s (historical 100-year) and 1,035 m^3/s (historical 200-year), to 1,301.78 m^3/s and 1,368.32 m^3/s under SSP2-4.5, and further to 1,335.82 m/s and 1,597.86 m^3/s under SSP5-8.5. Similarly, total outflow values followed this trend, with the SSP5-8.5 200-year event exhibiting the highest peak of 1,589.09 m^3/s, about 19% higher than its 100-year counterpart.

These results clearly demonstrate that future climate scenarios significantly intensify breach parametersreducing breach onset time, increasing flow velocity, and enlarging flood volumes. Consequently, the study emphasizes the urgent need to integrate climate-resilient design standards, reinforce dam structures, improve reservoir management, and implement robust early warning and evacuation systems to mitigate the heightened flood risks posed to downstream communities.

5.1.4 Downstream Impact Assessment

The downstream flood risk assessment revealed greater inundation depths and an increased number of affected villages under future climate scenarios. The SSP 5-8.5 scenario presented the highest flood risk, potentially inundating up to 18 villages, with maximum flood depths reaching 7.35 meters, a 12.7% increase compared to historical conditions. These increased flood depths create critical conditions for downstream communities, highlighting significant vulnerability to climate-induced flooding.

5.2 Recommendation

Based on the conclusions of this study, the following recommendations are proposed to strengthen dam safety, enhance flood risk management, and improve community resilience:

5.2.1 Spillway Capacity Enhancement

- Upgrade spillway design capacities to safely accommodate projected increases in peak flood discharges under SSP5-8.5 and SSP2-4.5 scenarios.
- Conduct periodic spillway evaluations and modifications based on updated climate projections.

5.2.2 Dam Structural Improvements

- Reinforce embankments and incorporate erosion-resistant materials to withstand high breach velocities and intense flood conditions.
- Establish routine structural inspections and maintenance schedules to detect and mitigate vulnerabilities pro-actively.

5.2.3 Flood Management Strategies

- Integrate climate-adaptive reservoir operations, including dynamic storage management during high precipitation periods to mitigate flood risks.
- Develop and regularly update inundation mapping and risk assessment tools to aid in emergency preparedness and response.

5.2.4 Early Warning and Monitoring Systems

- Install real-time hydrological monitoring systems upstream and downstream of the dam to provide timely alerts and improve emergency response capabilities.

- Enhance community-based early warning systems to effectively communicate flood risks and evacuation procedures.

5.2.5 Climate Resilience and Adaptation Planning

- Incorporate bias-corrected climate data and updated flood risk assessments into local infrastructure planning and water resources management frameworks.
- Promote climate-resilient land-use planning downstream to minimize flood vulnerability.

5.2.6 The Need for Updated Dam Safety Regulations

Pakistans current dam safety protocols do not account for climate change-driven hydrological extremes. There is an urgent need to revise spillway design criteria; considering climate-inclusive flood estimates and enhancing early warning mechanisms to mitigate the risk of dam failures in future.

5.2.7 Vulnerability of Earthen Dams in Balochistan

Earthen dams in Balochistan, may highly be vulnerable/at risk due to overtopping due climate inclusive floods in future, therefore need to be studied in detail. 5.2.8 Community Preparedness and Education:

- Strengthen community awareness programs focusing on flood risks, safety protocols, and evacuation strategies.
- Facilitate regular training and simulation exercises for local authorities and residents.

By adopting these recommendations, authorities and stakeholders can proactively address future flood risks, enhance dam safety, and safeguard downstream communities against climate-induced flooding.

Bibliography

[1] Hoshyar Pakistan, "Worst rains and floods; 1128 people dead, more than 4 crore people homeless pakistan," *Hoshyar Pakistan*, Aug. 2022, accessed: Feb. 03, 2025. [Online]. Available: https://hoshyarpakistan.com/national/more-than-4-crore-people-homeless/

[2] Barron's, "Pakistan floods worst in countrys history, says pm sharif," *Barron's*, Aug. 2022, accessed: Feb. 03, 2025. [Online]. Available: https://www.barrons.com/news/pakistan-floods-worst-in-country-s-history-pm-sharif-01661870707

[3] The Express Tribune, "Floods have affected over 30 million in pakistan: minister," *The Express Tribune*, Aug. 2022, accessed: Feb. 03, 2025. [Online]. Available: http://tribune.com.pk/story/2373444/floods-have-affected-over-30-million-in-pakistan-minister

[4] M. Kugelman, "How bad governance exacerbated pakistans flooding," *Foreign Policy*, Sep. 2022, accessed: Feb. 03, 2025. [Online]. Available: https://foreignpolicy.com/2022/09/01/pakistan-flooding-crisis-climate-change-governance/

[5] National Disaster Management Authority, "Ndma floods (2022) sitrep - 2022 (daily sitrep no 158 dated 18th november, 2022)," *NDMA*, Nov. 2022, accessed: Feb. 03, 2025. [Online]. Available: https://cms.ndma.gov.pk/storage/app/public/situation-reports/November2022/N2n1eEarMt6q6Rb8ZYwn.pdf

[6] A. T. Sheikh, "Victims of climate change or bad governance?" *Dawn*, Sep. 2022, accessed: Feb. 03, 2025. [Online]. Available: https://www.dawn.com/news/1708344

[7] NPR, "How melting glaciers contributed to floods in pakistan," *NPR*, Sep. 2022, accessed: Feb. 03, 2025. [Online]. Available: https://www.npr.org/2022/09/04/1120952641/how-melting-glaciers-caused-by-climate-change-led-to-to-floods-in-pakistan

[8] Reuters, "Pakistan floods have affected over 30 million people: climate change minister," *Reuters*, Aug. 2022, accessed: Feb. 03, 2025. [Online]. Available: https://www.reuters.com/world/asia-pacific/pakistan-floods-have-affected-over-30-million-people-climate-change-minister

[9] Z. Abbas, "Pakistan declares emergency in the face of calamitous floods," *Dawn*, Aug. 2022, accessed: Feb. 03, 2025. [Online]. Available: https://www.dawn.com/news/1706862

[10] S. R. Abt, R. J. Wittier, A. Taylor, and D. J. Love, "Human stability in a high flood hazard zone," *AWRA Water Resour Bull*, vol. 25, no. 4, pp. 881–890, 1989.

[11] M. Kramer, K. Terheiden, and S. Wieprecht, "Safety criteria for the trafficability of inundated roads in urban floodings," *Int J Disaster Risk Reduct*, vol. 17, pp. 77–84, Aug. 2016.

[12] E. Martnez-Gomariz, C. Barbero, M. Sanchez-Juny, E. Forero-Ortiz, and M. Sanz-Ramos, "Dams or ponds classification based on a new criterion to assess potential flood damage to roads in case of failure," *Natural Hazards*, vol. 117, no. 1, pp. 625–653, May 2023.

[13] H. Chanson and R. Brown, "New criterion for the stability of a human body in floodwaters," *J Hydraul Res*, vol. 53, no. 4, pp. 540–541, Jul. 2015.

[14] A. Awal, U. Bhattarai, V. P. Pandey, and P. K. Bhattarai, "Downstream impacts of dam breach using hec-ras: a case of budhigandaki concrete arch

dam in central nepal," *Environmental Systems Research*, vol. 13, no. 1, pp. 1–16, Dec. 2024.

[15] F. Aureli, A. Maranzoni, and G. Petaccia, "Review of historical dam-break events and laboratory tests on real topography for the validation of numerical models," *Water (Switzerland)*, vol. 13, no. 14, Jul. 2021.

[16] Ministry of Water Resources, "Ministry of water resources," 2025, accessed: Feb. 03, 2025. [Online]. Available: https://mowr.gov.pk/Detail/YmVhMzI2NTQtNjM4Ni00ZjdjLThhNDMtZGI2ZTJlZTMxN2Vj

[17] "Rs2.4bn irregularities in dams construction in balochistan - pakistan - dawn.com," 2025, accessed: Feb. 03, 2025. [Online]. Available: https://www.dawn.com/news/1834416

[18] M. Ishfaque, S. Salman, K. Z. Jadoon, A. A. K. Danish, K. U. Bangash, and D. Qianwei, "Understanding the effect of hydro-climatological parameters on dam seepage using shapley additive explanation (shap): A case study of earth-fill tarbela dam, pakistan," *Water (Basel)*, vol. 14, no. 17, p. 2598, Aug. 2022.

[19] K. Sindhu and K. H. V. D. Rao, "Hydrological and hydrodynamic modeling for flood damage mitigation in brahmanibaitarani river basin, india," *Geocarto Int*, vol. 32, no. 9, pp. 1004–1016, Sep. 2017.

[20] P. Dornpunya *et al.*, "Reservoir inflow prediction of sirikit dam using artificial intelligence with machine learning: Extreme gradient boosting technique," 2021, unpublished.

[21] U. Manglore, A. U. Rahman, F. Marwat, T. Naz, S. Dilbar, and F. Khan, "Geospatial analysis of flood causes and extent of flood damages in swat valley, north pakistan," *Natural and Applied Sciences International Journal (NASIJ)*, vol. 5, no. 1, pp. 130–153, Jun. 2024.

[22] P. Y. Sandakov, A. A. Parshakov, A. V. Popov, E. N. Smirnova, and S. Y. Podtaev, "Features of neurogenic disorders and endothelial mechanisms of

vasoregulation in patients with neuropathic and neuroischemic forms of diabetic foot," *World Appl Sci J*, vol. 23, no. 7, pp. 887–891, 2013.

[23] F. Jafari, F. Salmasi, and J. Abraham, "Numerical investigation of granular filter under the bed of a canal," *Appl Water Sci*, vol. 9, no. 5, Jul. 2019.

[24] "Types of embankment dams — earth embankment dams — types of earth dams," 2025, accessed: Feb. 01, 2025. [Online]. Available: https://www.aboutcivil.org/embankment-dams-types.html

[25] A. Koskinas *et al.*, "Insights into the oroville dam 2017 spillway incident," *Geosciences (Switzerland)*, vol. 9, no. 1, Jan. 2019.

[26] "Gravity dam and eathen dam — pdf," 2025, accessed: Feb. 01, 2025. [Online]. Available: https://www.scribd.com/document/567283479/Gravity-Dam-and-Eathen-Dam

[27] H. Ma and F. Chi, "Major technologies for safe construction of high earth-rockfill dams," *Engineering*, vol. 2, no. 4, pp. 498–509, 2016.

[28] F. Salmasi and B. Mansuri, "Effect of homogeneous earth dam hydraulic conductivity ratio (kx/ky) with horizontal drain on seepage," *Indian Geotechnical Journal*, vol. 44, no. 3, pp. 322–328, 2014.

[29] B. Nourani, F. Salmasi, A. Abbaspour, and B. O. Bakhshayesh, "Numerical investigation of the optimum location for vertical drains in gravity dams," *Geotechnical and Geological Engineering*, vol. 35, no. 2, pp. 799–808, Apr. 2017.

[30] F. Salmasi, R. Norouzi, J. Abraham, B. Nourani, and S. Samadi, "Effect of inclined clay core on embankment dam seepage and stability through lem and fem," *Geotechnical and Geological Engineering*, vol. 38, no. 6, pp. 6571–6586, Dec. 2020.

[31] G. Ren *et al.*, "Historical and recent change in extreme climate over east asia," *Clim Change*, vol. 168, no. 3–4, Oct. 2021.

[32] Z. Zhang *et al.*, "Effect of soluble salt loss via spring water on irrigation-induced landslide deformation," *Water (Switzerland)*, vol. 12, no. 10, pp. 1–17, Oct. 2020.

[33] W. Hou, S. Zhang, J. Yin, and J. Huang, "Research on challenges and strategies for reservoir flood risk prevention and control under extreme climate conditions," *Water*, vol. 16, no. 23, p. 3351, Nov. 2024.

[34] D. Mirauda, R. Albano, A. Sole, and J. Adamowski, "Smoothed particle hydrodynamics modeling with advanced boundary conditions for two-dimensional dam-break floods," *Water (Switzerland)*, vol. 12, no. 4, Apr. 2020.

[35] E. Psomiadis, L. Tomanis, A. Kavvadias, K. X. Soulis, N. Charizopoulos, and S. Michas, "Potential dam breach analysis and flood wave risk assessment using hec-ras and remote sensing data: A multicriteria approach," *Water*, vol. 13, no. 3, p. 364, Jan. 2021.

[36] N. Al-Ansari, N. Adamo, S. Knutsson, J. Laue, and V. Sissakian, "Mosul dam: Is it the most dangerous dam in the world?" *Geotechnical and Geological Engineering*, vol. 38, no. 5, pp. 5179–5199, Oct. 2020.

[37] D. C. Froehlich and D. G. Diaz, "Dam safetyliving with the risk of failure," in *Lecture Notes in Civil Engineering*, 2022, vol. 205, pp. 417–429.

[38] V. P. Singh, *Dam Breach Modeling Technology*, 1996, vol. 17.

[39] "Causes of failures of earthfill dams," 2025, accessed: Feb. 01, 2025. [Online]. Available: https://test.theconstructor.org/water-resources/causes-failures-earthfill-dams/2287/

[40] J. Yang, P. Andreasson, P. Teng, and Q. Xie, "The past and present of discharge capacity modeling for spillways-a swedish perspective," *Fluids*, vol. 4, no. 1, Mar. 2019.

[41] O. N. Dhar, P. R. Rakhecha, B. N. Mandal, and R. B. Sangam, "The rainstorm which caused the morvi dam disaster in august 1979," *Hydrological Sciences Bulletin*, vol. 26, no. 1, pp. 71–81, 1981.

[42] S. V. Sivapriya and A. A. Sherin, "Causes and consequences of dam failurescase study," in *Lecture Notes in Civil Engineering*, 2022, vol. 179, pp. 155–159.

[43] M. Foster, R. Fell, and M. Spannagle, "The statistics of embankment dam failures and accidents," *Canadian Geotechnical Journal*, vol. 37, no. 5, pp. 1000–1024, 2000.

[44] Y. Xu, L. M. Zhang, and J. Jia, "Lessons from catastrophic dam failures in august 1975 in zhumadian, china," 2008, accessed: Feb. 01, 2025. [Online]. Available: http://repository.ust.hk/ir/Record/1783.1-20080

[45] "Teton dam (idaho, 1976) — case study — asdso lessons learned," 2025, accessed: Feb. 01, 2025. [Online]. Available: https://damfailures.org/case-study/teton-dam-idaho-1976/

[46] "The sardar sarovar project-a failure of two bottom lines, uncertainty looms over the third," 2025, accessed: Feb. 01, 2025.

[47] "The failure of embankment dams due to overtopping," 2025, accessed: Feb. 01, 2025.

[48] W. J. Graham, "Major u.s. dam failures: Their cause, resultant losses, and impact on dam safety programs and engineering practice," in *Proceedings of the History Symposium of the World Environmental and Water Resources Congress 2009: Great Rivers History*, vol. 344, 2009, pp. 52–60.

[49] "Camar dam (brazil, 2004) — case study — asdso lessons learned," 2025, accessed: Feb. 01, 2025. [Online]. Available: https://damfailures.org/case-study/camara-dam-brazil-2004/

[50] M. Wang, Y. F. Chen, R. Hu, W. Liu, and C. B. Zhou, "Coupled hydro-mechanical analysis of a dam foundation with thick fluvial deposits: A case study of the danba hydropower project, southwestern china," *European Journal of Environmental and Civil Engineering*, vol. 20, no. 1, pp. 19–44, Jan. 2016.

[51] C. Guerra, "The government was warned that the oroville dam emergency spillway was unsafe. it didnt listen." Feb. 2017, accessed: Feb. 01, 2025.

[52] "Whaley bridge dam collapse: Evacuation over toddbrook reservoir fears," 2025, accessed: Feb. 01, 2025. [Online]. Available: https://www.bbc.com/news/uk-england-derbyshire-49189955

[53] B. Wang *et al.*, "Empirical and semi-analytical models for predicting peak outflows caused by embankment dam failures," *J Hydrol (Amst)*, vol. 562, pp. 692–702, Jul. 2018.

[54] L. M. Albu, A. Enea, M. Iosub, and I. G. Breaban, "Dam breach size comparison for flood simulations. a hec-ras based, gis approach for drcani lake, sitna river, romania," *Water*, vol. 12, no. 4, p. 1090, Apr. 2020.

[55] "Raising san vicente dam: Why and how," 2025, accessed: Feb. 01, 2025. [Online]. Available: https://www.hydroreview.com/world-regions/north-america/raising-san-vicente-dam-why-and-how/

[56] "Dam-break risk analysis and mitigation at pidekso dam, wonogiri regency, central java, indonesia," 2025, accessed: Feb. 01, 2025. [Online]. Available: https://www.chijournal.org/C521

[57] "Numerical analysis of manifold: A case study of phukot karnali hydroelectric project," 2025, accessed: Feb. 01, 2025.

[58] S. Ahmad *et al.*, "Gis-based identification and analysis of optimal evacuation areas and routes in flood-prone zones of swabi district, pakistan," *Journal of Engineering (United Kingdom)*, vol. 2024, 2024.

[59] D. Rincn, U. T. Khan, and C. Armenakis, "Flood risk mapping using gis and multi-criteria analysis: A greater toronto area case study," *Geosciences (Switzerland)*, vol. 8, no. 8, Aug. 2018.

[60] . B. Peker, S. Glbaz, V. Demir, O. Orhan, and N. Beden, "Integration of hec-ras and hec-hms with gis in flood modeling and flood hazard mapping," *Sustainability*, vol. 16, no. 3, p. 1226, Feb. 2024.

[61] "Hydrologic modeling system hec-hms users manual cpd-74a," 2006.

[62] A. Bharath, A. V. Shivapur, C. G. Hiremath, and R. Maddamsetty, "Dam break analysis using hec-ras and hec-georas: A case study of hidkal dam, karnataka state, india," *Environmental Challenges*, vol. 5, p. 100401, Dec. 2021.

[63] M. Kiwanuka *et al.*, "Dam breach analysis of kibimba dam in uganda using hec-ras and hec-georas," *Environmental Systems Research*, vol. 12, no. 1, Dec. 2023.

[64] Y. Xiong, "A dam break analysis using hec-ras," *J Water Resour Prot*, vol. 3, no. 6, pp. 370–379, 2011.

[65] W. W. Zin *et al.*, "Flood hazard assessment of bago river basin, myanmar," *Journal of Disaster Research*, vol. 13, no. 1, pp. 14–21, Feb. 2018.

[66] P. Lan, B. Lin, Y. Zhang, and H. Chen, "Probable maximum precipitation estimation using the revised km-value method in hong kong," *J Hydrol Eng*, vol. 22, no. 8, Aug. 2017.

[67] A. P. Phyo, H. Yabar, and D. Richards, "Managing dam breach and flood inundation by hec-ras modeling and gis mapping for disaster risk management," *Case Studies in Chemical and Environmental Engineering*, vol. 8, p. 100487, Dec. 2023.

[68] M. S. Lodhi and D. K. Agrawal, "Dam-break flood simulation under various likely scenarios and mapping using gis: Case of a proposed dam on river yamuna, india," *J Mt Sci*, vol. 9, no. 2, pp. 214–220, Apr. 2012.

[69] A. Tariq, F. Mumtaz, M. Majeed, and X. Zeng, "Spatio-temporal assessment of land use land cover based on trajectories and cellular automata markov modelling and its impact on land surface temperature of lahore district pakistan," *Environ Monit Assess*, vol. 195, no. 1, 2023.

[70] D. Sarkar and P. Mondal, "Flood vulnerability mapping using frequency ratio (fr) model: a case study on kulik river basin, indo-bangladesh barind region," *Appl Water Sci*, vol. 10, no. 1, 2020.

[71] J. A. Ormiston and J. M. White, "The polyzene-f stent coating improves healing and outcomes preclinically, but is it effective clinically?" *Cardiovascular Revascularization Medicine*, vol. 41, pp. 81–82, Aug. 2022.

[72] E. Taskaya, G. Bombar, and G. Tayfur, "Experimental investigation of sediment movement as a result of homogeneous earth-fill dam overtopping break over a simplified urban area," *J Hydrol (Amst)*, vol. 617, p. 128924, Feb. 2023.

[73] Z. han Du *et al.*, "Experimental analysis on breaching mechanism of earth-rock dam induced by landslide generated waves," *Eng Geol*, vol. 346, Feb. 2025.

[74] "Typhoon ninabanqiao dam failure — 1975 banqiao dam disaster, chinese history — britannica," 2025, accessed: Feb. 01, 2025. [Online]. Available: https://www.britannica.com/event/Typhoon-Nina-Banqiao-dam-failure

[75] A. Koskinas *et al.*, "Insights into the oroville dam 2017 spillway incident," *Geosciences (Switzerland)*, vol. 9, no. 1, Jan. 2019.

[76] "Oroville dam (california, 2017) — case study — asdso lessons learned," 2025, accessed: Feb. 01, 2025. [Online]. Available: https://damfailures.org/case-study/oroville-dam-california-2017/

[77] M. J. Harris, "Failure of dams due to overtopping a historical prospective," in *Dam Protections against Overtopping and Accidental Leakage - Proceedings of the 1st International Seminar on Dam Protections Against Overtopping and Accidental Leakage*, 2015, pp. 73–81.

[78] A. Miniussi, R. Merz, L. Kaule, and S. Basso, "Identifying discontinuities of flood frequency curves," *J Hydrol (Amst)*, vol. 617, Feb. 2023.

[79] I. A. Alvi and I. S. Alvi, "Why dams fail: a systems perspective and case study," *Civil Engineering and Environmental Systems*, vol. 40, no. 3, pp. 150–175, 2023.

[80] M. Ho, D. OShea, C. Wasko, R. Nathan, and A. Sharma, "The impact of climate change on dam overtopping flood risk," 2025.

[81] R. P. Allan and B. J. Soden, "Atmospheric warming and the amplification of precipitation extremes," *Science (1979)*, vol. 321, no. 5895, pp. 1481–1484, sep 2008.

[82] G. Dharmarathne, A. O. Waduge, M. Bogahawaththa, U. Rathnayake, and D. P. P. Meddage, "Adapting cities to the surge: A comprehensive review of climate-induced urban flooding," *Results in Engineering*, vol. 22, jun 2024.

[83] F. AlZaatiti, J. Halwani, and M. R. Soliman, "Climate change impacts on flood risks in the abou ali river basin, lebanon: A hydrological modeling approach," *Results in Engineering*, vol. 25, p. 104186, mar 2025.

[84] M. Rummukainen, "Changes in climate and weather extremes in the 21st century," *Wiley Interdiscip Rev Clim Change*, vol. 3, no. 2, pp. 115–129, 2012.

[85] J. Wang, C. Hu, B. Ma, and X. Mu, "Rapid urbanization impact on the hydrological processes in zhengzhou, china," *Water (Switzerland)*, vol. 12, no. 7, jul 2020.

[86] J. Lehmann, D. Coumou, and K. Frieler, "Increased record-breaking precipitation events under global warming," *Clim Change*, vol. 132, no. 4, pp. 501–515, oct 2015.

[87] I. S. Astuti, K. Sahoo, A. Milewski, and D. R. Mishra, "Impact of land use land cover (lulc) change on surface runoff in an increasingly urbanized tropical watershed," *Water Resources Management*, vol. 33, no. 12, pp. 4087–4103, sep 2019.

[88] Z. Kalantari, C. S. S. Ferreira, R. P. D. Walsh, A. J. D. Ferreira, and G. Destouni, "Urbanization development under climate change: Hydrological responses in a peri-urban mediterranean catchment," *Land Degrad Dev*, vol. 28, no. 7, pp. 2207–2221, oct 2017.

[89] S. E. hyd E. Soomro *et al.*, "How does the climate change effect on hydropower potential, freshwater fisheries, and hydrological response of snow on water availability?" *Appl Water Sci*, vol. 14, no. 4, pp. 1–31, apr 2024.

[90] B. Arheimer, C. Donnelly, and G. Lindstrm, "Regulation of snow-fed rivers affects flow regimes more than climate change," *Nat Commun*, vol. 8, no. 1, dec 2017.

[91] K. E. Hale, K. S. Jennings, K. N. Musselman, B. Livneh, and N. P. Molotch, "Recent decreases in snow water storage in western north america," *Commun Earth Environ*, vol. 4, no. 1, dec 2023.

[92] M. Q. H. S. M. M. H. M. I. Y. K. Abbass, "A review of the global climate change impacts adaptation, and sustainable mitigation measures," *Environ Sci Pollut Res*, vol. 29, pp. 42 539–42 559, 2022.

[93] G. Dharmarathne, A. O. Waduge, M. Bogahawaththa, U. Rathnayake, and D. P. P. Meddage, "Adapting cities to the surge: A comprehensive review of climate-induced urban flooding," *Results in Engineering*, vol. 22, p. 102123, jun 2024.

[94] M. Kondolf and J. Yi, "Dam renovation to prolong reservoir life and mitigate dam impacts," *Water*, vol. 14, no. 9, p. 1464, may 2022.

[95] M. Muller, "Managing current climate variability can ensure water security under climate change," in *African Handbook of Climate Change Adaptation: With 610 Figures and 361 Tables*, jan 2021, pp. 2311–2337.

[96] Y. Zhang and G. Tayfur, "Sediment transport modelling in densly populated urban areas due to earthfill dam break," *Journal of Ecohydraulics*, 2024.

[97] K. Larco, G. M. Mosquera, S. R. Jacobs, I. Cardenas, and P. Crespo, "Factors controlling the temporal variability of streamflow transit times in tropical alpine catchments," *J Hydrol (Amst)*, vol. 617, feb 2023.

[98] S. Dai *et al.*, "Numerical study of impact pressure and force of cascading dam-break floods on the downstream dam," *J Hydrol (Amst)*, vol. 648, feb 2025.

[99] Y. Liu, S. Li, Z. Liao, and K. Liu, "Physical and numerical modeling of random wave transformation and overtopping on reef topography," *Ocean Engineering*, vol. 220, Jan. 2021.

[100] L. Y. Zhang, W. L. Xu, F. X. Zhang, W. M. Zhang, W. R. Wei, and X. L. Zhang, "Improved general unit hydrograph model for dam-break flood hydrograph," *J Hydrol (Amst)*, vol. 635, May 2024.

[101] M. Abdelgawad and A. R. Fayek, "Risk management in the construction industry using combined fuzzy fmea and fuzzy ahp," *J Constr Eng Manag*, vol. 136, no. 9, pp. 1028–1036, Sep. 2010.

[102] J. R. Ribas, J. C. R. Severo, L. F. Guimarães, and K. P. C. Perpetuo, "A fuzzy fmea assessment of hydroelectric earth dam failure modes: A case study in central brazil," *Energy Reports*, vol. 7, pp. 4412–4424, Nov. 2021.

[103] G. Antzoulatos *et al.*, "Flood hazard and risk mapping by applying an explainable machine learning framework using satellite imagery and gis data," *Sustain*, vol. 14, no. 6, p. 3251, Mar. 2022.

[104] F. Alcrudo and J. Mulet, "Description of the tous dam break case study (spain)," *J Hydraul Res*, vol. 45, no. 1, pp. 45–57, 2007.

[105] A. O. Turkel, H. Zaifoglu, and A. M. Yanmaz, "Probabilistic modeling of dam failure scenarios: a case study of kanlikoy dam in cyprus," *Natural Hazards*, vol. 120, no. 11, pp. 10 087–10 117, Sep. 2024.

[106] J. S. R. Murthy, "Gradual dam breach flow routing," *ISH J Hydraul Eng*, vol. 4, no. 2, pp. 30–38, 1998.

[107] I. Ahmad, M. Waseem, A. Ashraf, M. K. Leta, S. Ahmad, and H. Wahab, "Hydrological risk assessment for mangla dam: compound effects of instant flow and precipitation peaks under climate change, using hec-ras and hec-georas," *SN Appl Sci*, vol. 5, no. 12, pp. 1–21, Dec. 2023.

[108] M. Pilotti, A. Maranzoni, M. Tomirotti, and G. Valerio, "1923 gleno dam break: Case study and numerical modeling," *Journal of Hydraulic Engineering*, vol. 137, no. 4, pp. 480–492, Apr. 2011.

[109] I. R. Karim, Z. F. Hassan, H. H. Abdullah, and I. A. Alwan, "2d-hec-ras modeling of flood wave propagation in a semi-arid area due to dam overtopping failure," *Civil Engineering Journal (Iran)*, vol. 7, no. 9, pp. 1501–1514, 2021.

[110] M. Pilotti, L. Milanesi, V. Bacchi, M. Tomirotti, and A. Maranzoni, "Dam-break wave propagation in alpine valley with hec-ras 2d: Experimental cancano test case," *Journal of Hydraulic Engineering*, vol. 146, no. 6, 2020.

[111] D. Abdessamed and B. Abderrazak, "Coupling hec-ras and hec-hms in rainfallrunoff modeling and evaluating floodplain inundation maps in arid environments: case study of ain sefra city, ksour mountain sw of algeria," *Environ Earth Sci*, vol. 78, no. 19, pp. 1–17, 2019.

[112] V. Atashi, R. Barati, and Y. H. Lim, "Distributed muskingum model with a whale optimization algorithm for river flood routing," *Journal of Hydroinformatics*, vol. 25, no. 6, pp. 2210–2222, 2023.

[113] S. A. Hosseinzadeh-Tabrizi, M. Ghaeini-Hessaroeyeh, and M. Ziaadini-Dashtekhaki, "Numerical simulation of dam-breach flood waves," *Appl Water Sci*, vol. 12, no. 5, 2022.

[114] E. Psomiadis, L. Tomanis, A. Kavvadias, K. X. Soulis, N. Charizopoulos, and S. Michas, "Potential dam breach analysis and flood wave risk assessment using hec-ras and remote sensing data: A multicriteria approach," *Water (Switzerland)*, vol. 13, no. 3, 2021.

[115] A. R. Refaiy, N. M. AboulAtta, M. A. Gad, and D. A. El-Molla, "Modeling the successive failure of complex dams systems: A necessity in the light of climatic shifts in extreme storms," *Ain Shams Engineering Journal*, vol. 15, no. 11, p. 103033, 2024.

[116] Y. . Frank and . Xiong, "A dam break analysis using hec-ras," *J Water Resour Prot*, vol. 3, no. 6, pp. 370–379, 2011.

[117] V. Bellos, V. K. Tsakiris, G. Kopsiaftis, and G. Tsakiris, "Propagating dam breach parametric uncertainty in a river reach using the hec-ras software," *Hydrology 2020, Vol. 7, Page 72*, vol. 7, no. 4, p. 72, 2020.

[118] B. H. Tessema, A. Y. Gebremedhn, and Y. S. Getahun, "Dam breach analysis and flood inundation mapping of dire dam, using hec-hms and hec-ras models," *Sustain Water Resour Manag*, vol. 10, no. 2, pp. 1–16, 2024.

[119] M. S. Lodhi and D. K. Agrawal, "Dam-break flood simulation under various likely scenarios and mapping using gis: Case of a proposed dam on river yamuna, india," *J Mt Sci*, vol. 9, no. 2, pp. 214–220, 2012.

[120] A. P. Phyo, H. Yabar, and D. Richards, "Managing dam breach and flood inundation by hec-ras modeling and gis mapping for disaster risk management," *Case Studies in Chemical and Environmental Engineering*, vol. 8, p. 100487, 2023.

[121] M. Zarei, O. Bozorg-Haddad, S. Baghban, M. Delpasand, E. Goharian, and H. A. Loiciga, "Machine-learning algorithms for forecast-informed reservoir operation (firo) to reduce flood damages," *Sci Rep*, vol. 11, no. 1, p. 24295, 2021.

[122] M. Wieland, "Seismic hazard and seismic design and safety aspects of large dam projects," *Geotechnical, Geological and Earthquake Engineering*, vol. 34, pp. 627–650, 2014.

[123] "4. construction and design criteria earthen dams.pptx," Online, 2025. [Online]. Available: https://www.slideshare.net/slideshow/4-construction-and-design-criteria-earthen-damspptx/255130900

[124] A. L. Learned, "Regular operation, maintenance, and inspection of dams is important to the early detection and prevention of dam failure. — lessons learned — asdso lessons learned," Online, 2025.

[125] B. of Reclamation, "Bureau of reclamation," Online, 2025. [Online]. Available: https://www.usbr.gov/

[126] D. Devi, A. Baruah, and A. K. Sarma, "Characterizing dam induced flood at downstream of a hydel project," 2021.

[127] J. Daramola, T. M. Ekhwan, J. Mokhtar, K. C. Lam, and G. A. Adeogun, "Estimating sediment yield at kaduna watershed, nigeria using soil and water assessment tool (swat) model," *Heliyon*, vol. 5, no. 7, 2019.

[128] J. Fluix-Sanmartn, L. Altarejos-Garca, A. Morales-Torres, and I. Escuder-Bueno, "Review article: Climate change impacts on dam safety," *Natural Hazards and Earth System Sciences*, vol. 18, no. 9, pp. 2471–2488, 2018.

[129] L. Altarejos-Garca, I. Escuder-Bueno, A. Serrano-Lombillo, and M. G. de Membrillera-Ortuo, "Methodology for estimating the probability of failure by sliding in concrete gravity dams in the context of risk analysis," *Structural Safety*, vol. 36–37, pp. 1–13, 2012.

[130] K. Arnbjerg-Nielsen and et al., "Impacts of climate change on rainfall extremes and urban drainage systems: A review," *Water Science and Technology*, vol. 68, no. 1, pp. 16–28, 2013.

[131] F. Azadi, P. S. Ashofteh, and H. A. Loiciga, "Reservoir water-quality projections under climate-change conditions," *Water Resources Management*, vol. 33, no. 1, pp. 401–421, 2019.

[132] A. Ferdowsi, F. Piadeh, K. Behzadian, S.-F. Mousavi, and M. Ehteram, "Urban water infrastructure: A critical review on climate change impacts and adaptation strategies," *Urban Clim*, vol. 58, p. 102132, 2024.

[133] "The hazard classification of a dam can change over time (hazard creep). — lessons learned — asdso lessons learned," 2025. [Online]. Available: https://damfailures.org/lessons-learned/the-hazard-classification-of-a-dam-can-change-over-time-hazard-creep/

[134] "Dam failure — undrr," 2025. [Online]. Available: https://www.undrr.org/understanding-disaster-risk/terminology/hips/tl0009

[135] "Towards a probabilistic performance-based approach for dam safety," 2025.

[136] E. Blad and et al., "Iber: herramienta de simulacin numrica del flujo en ros," *Revista Internacional de Metodos Numericos para Calculo y Diseno en Ingenieria*, vol. 30, no. 1, pp. 1–10, 2014.

[137] J. I. Barredo, "Normalised flood losses in europe: 1970-2006," *Natural Hazards and Earth System Science*, vol. 9, no. 1, pp. 97–104, 2009.

[138] "Dam safety: Technical problems of aging embankment dams," 2025.

[139] "Fema releases 2015 national household survey results on preparedness findings," 2025.

[140] "Water resources reform and development act (wrrda) of 2014," 2025. [Online]. Available: https://www.usace.army.mil/Missions/Civil-Works/Project-Planning/Legislative-Links/wrrda2014/

[141] D. Chang, R. Boulanger, S. Brandenberg, and B. Kutter, "Fem analysis of dynamic soil-pile-structure interaction in liquefied and laterally spreading ground," *Earthquake Spectra*, vol. 29, no. 3, pp. 733–755, 2013.

[142] "Dams at increasing danger of collapse due to climate change and conflict - world — reliefweb," 2025. [Online]. Available: https://reliefweb.int/report/world/dams-increasing-danger-collapse-due-climate-change-and-conflict

[143] Y. M. K. Alla and L. Liu, "Impacts of dams on the environment: A review," *International Journal of Environment, Agriculture and Biotechnology*, vol. 6, no. 1, pp. 064–074, 2021.

[144] S. S. Aqilah, K. Z. Karmilla, K. Tamanna, Z. Ali, and N. Mat, "Assessing socio-economic and environmental losses of dam-failure flood risk: A review on sustainable framework," *J Sustain Sci Manag*, vol. 19, no. 1, pp. 171–195, 2024.

[145] R. Kidson and K. S. Richards, "Flood frequency analysis: Assumptions and alternatives," *Prog Phys Geogr*, vol. 29, no. 3, pp. 392–410, 2005.

[146] F. Zamir, F. Hanif, and S. Naz, "Extreme rainfall frequency analysis for balakot, pakistan, using gumbels distribution," *Arabian Journal of Geosciences*, vol. 14, no. 13, 2021.

[147] J. M. Lzaro, J. . S. Navarro, A. G. Gil, and V. E. Romero, "Flood frequency analysis (ffa) in spanish catchments," *J Hydrol (Amst)*, vol. 538, pp. 598–608, 2016.

[148] A. Mehmood, S. Jia, M. Masood, A. Lv, R. Mahmood, and W. Zhu, "Impact of climate change on extreme floods under high-end warming scenario rcp8.5 for the kabul river basin in pakistan," *Arabian Journal of Geosciences*, vol. 15, no. 23, 2022.

[149] (2025) Faster, more intense, with more devastating impacts: New ipcc report lays out the scientific basis of the climate emergency citytalk. Accessed: Feb. 02, 2025.

[150] C. Buizert *et al.*, "Gas transport in firn: Multiple-tracer characterisation and model intercomparison for neem, northern greenland," *Atmospheric Chemistry and Physics*, vol. 12, no. 9, pp. 4259–4277, 2012.

[151] (2025) Global warming of 1.5 c. Accessed: Feb. 02, 2025. [Online]. Available: https://www.ipcc.ch/sr15/

[152] P. Brohan *et al.*, "Uncertainty estimates in regional and global observed temperature changes: A new data set from 1850," *Journal of Geophysical Research: Atmospheres*, vol. 111, no. 12, 2006.

[153] B. D. Beckley *et al.*, "Assessment of the jason-2 extension to the topex/-poseidon, jason-1 sea-surface height time series for global mean sea level monitoring," *Marine Geodesy*, vol. 33, no. SUPPL. 1, pp. 447–471, 2010.

[154] M. Meinshausen *et al.*, "The shared socio-economic pathway (ssp) greenhouse gas concentrations and their extensions to 2500," *Geoscientific Model Development*, vol. 13, no. 8, pp. 3571–3605, 2020.

[155] Z. Micovic *et al.*, "Sensitivity and uncertainty analyses for stochastic flood hazard simulation," in *Sensitivity Analysis in Earth Observation Modelling*. Elsevier, 2017, pp. 213–234.

[156] F. Hooimeijer *et al.*, "Integrated urban flood design in the united states and the netherlands," in *Coastal Flood Risk Reduction: The Netherlands and the U.S. Upper Texas Coast*. Elsevier, 2022, pp. 241–254.

[157] "Chapter 10 reservoir sizing," *Developments in Water Science*, vol. 51, no. C, pp. 555–612, 2003.

[158] M. I. K, "Hydrological modeling of upper indus basin using hec -hms," *Journal of Mechanics of Continua and Mathematical Sciences*, vol. 14, no. 3, 2019.

[159] (2025) Application of scs-cn method and hec hms model in the estimation of runoff of machhu river basin, gujarat, india. Accessed: Feb. 02, 2025.

[160] . Kocaer and A. Yarar, "Experimental and numerical investigation of flow over ogee spillway," *Water Resources Management*, vol. 34, no. 13, pp. 3949–3965, 2020.

[161] M. M. Akhtar *et al.*, "Correction to: Water resources of balochistan, pakistana review (arabian journal of geosciences, (2021), 14, 4, (289), 10.1007/s12517-021-06502-y)," *Arabian Journal of Geosciences*, vol. 14, no. 7, 2021.

[162] ——, "Water resources of balochistan, pakistana review," *Arabian Journal of Geosciences*, vol. 14, no. 4, 2021.

[163] M. R. Chaudhry. (2025) Water management in baluchistan. Accessed: Feb. 03, 2025. [Online]. Available: https://www.fao.org/4/y3690e/y3690e09.htm

[164] E. M. Michailidi *et al.*, "Timing the time of concentration: shedding light on a paradox," *Hydrological Sciences Journal*, vol. 63, no. 5, pp. 721–740, 2018.

[165] K. J. Beven, "A history of the concept of time of concentration," *Hydrology and Earth System Sciences*, vol. 24, no. 5, pp. 2655–2670, 2020.

[166] M. Beza *et al.*, "Dam breach modeling and downstream flood inundation mapping using hec-ras model on the proposed gumara dam, ethiopia," *Advances in Civil Engineering*, vol. 2023, 2023.

[167] (2025) Usace publications - engineer manuals. Accessed: Feb. 03, 2025. [Online]. Available: https://www.publications.usace.army.mil/usace-publications/engineer-manuals/

[168] P. D. P. O. Peramuna *et al.*, "Novel approach to the derivation of dam breach parameters in 2d hydrodynamic modeling of earthquake induced dam failures," *Science of The Total Environment*, vol. 927, p. 171505, 2024.

[169] N. N. W. S. U. D. of Commerce, "The 3-tiered approach to keeping you alerted to severe weather," 2025.

[170] B. Feinberg *et al.*, "Reclamations empirical method for estimating life loss due to dam failure," in *E3S Web of Conferences*, vol. 7, 2016.